Thermal analysis of an industrial brine chilling system for the review of control and operating philosophies, with a survey of some heat transfer correlations for refrigerant evaporation.

Mark Pettigrew BEng CEng MIMecheE MinstR

Energy Systems Research Unit,
Department of Mechanical Engineering
University of Strathclyde

A thesis submitted as part of the degree of Master of Science
Energy Systems and the Environment
2005

Acknowledgments

I would like to thank the following people:

Mr Craig McLean of the Department of Mechanical Engineering, University of Strathclyde for his early guidance and discussions in formulating the work contained in this dissertation.

David Findlay (senior) and David Findlay (junior) of Latent refrigeration Ltd for their assistance in setting up the test procedures and taking measurements from the field instruments during the test runs.

The operations staff across all shifts in the Utilities area of DSM Nutritional Products Ltd, Dalry, Ayrshire, Scotland, for their assistance in setting up and operating the test runs.

Abstract

Operations personnel made observations on the control and operating philosophies of a large-scale brine chilling system in the energies facility of a large-scale chemical manufacturing site. These observations suggested that that the system was not being operated in the most efficient manner. The system consisted of four chillers with low load capacity running facilities and ammonia as the primary refrigerant.

A model was constructed which allowed first and second laws of thermodynamics analysis of the system for each possible combination of running the four chillers to meet process cooling demand. A number of correlations for heat transfer coefficients were modelled in the evaporators to identify the combinations which best modelled the overall heat transfer coefficient. Correlations for brine transient and turbulent flow conditions were considered, together with the boiling correlations developed by, Bromley, Chen, Cooper and Mostinski.

Tests were conducted on the real system to obtain the data for input to the model. For each running combination with real plant, measurements were taken on the brine and ammonia sides of the chillers.

The analyses showed that the best mode of operation was the lowest number of chillers running at the highest loading. For modelling the overall heat transfer coefficient the best combination of correlations for low refrigerating loads was the heat transfer coefficient for transition brine flow with Mostinski's correlation for ammonia boiling. For higher refrigerating loads the best combination was turbulent brine flow conditions with Bromley's coefficient for ammonia.

It was concluded that the control and operating philosophies in place should be retained. Future modelling work on heat transfer correlations is recommended to facilitate cost effective design of heat exchangers using alternative refrigerants.

Table Of Contents

Illustrations

page

List of figures

List Of tables

Nomenclature

A	surface or cross-sectional area (m^2)
c_p	specific heat capacity at constant pressure ($Jkg^{-1}k^{-1}$)
COP	coefficient of performance
COSP	coefficient of system performance
F	correction factor for log mean temperature difference
	Chen correlation factor
h	specific enthalpy ($kJkg^{-1}$)
I	irreversibility (kJ)
i	specific irreversibilty ($kJkg^{-1}$)
k	thermal conductivity ($Wm^{-1}K^{-1}$)
l	length (m)
$\dot{m}$	mass flow rate (kgs^{-1})
M	atomic mass
Nu	Nusselt number
P	pressure (Nm^{-2})
Pr	Prandtl number
P_R	Pressure ratio
Re	Reynolds number
Q	heat transfer (kW)
T	temperature (^oC, K)
U	overall heat transfer coefficient ($Wm^{-2}K^{-1}$)
u	velocity (ms^{-1})
r	radius of tube (m)
S	suppression factor
s	specific entropy ($kJkg^{-1}k^{-1}$)
S_D	diagonal tube pitch
S_T	transverse tube pitch
V	volume (m3)
V_i	volume ratio
W	work (kJ)
x	entry length (m)
x	dryness fraction
X	Martinelli parameter

Greek Letters

α_o	boiling heat transfer coefficient on outer surface of tube ($Wm^{-2}K^{-1}$)
α_i	heat transfer coefficient on inner surface of tube ($Wm^{-2}K^{-1}$)
γ	ratio of specific heats
ε	surface roughness, effectiveness
ϕ	heat flux (kWm^{-2})
Ψ	availability (kJ)
η	efficiency
λ	specific latent heat ($kJkg^{-1}$)
μ	dynamic viscosity ($kgs^{-1}m^{-1}$)
π	pressure ratio
ρ	density (kgm^{-3})
σ	surface tension (N/m)

Subscripts

act	actual
b	bulk
c	critical
comp	compressor
e	entry
e,t	entry, thermal
evap	evaporator
D	discharge
d_i	diameter internal
d_o	diameter external
fc	forced convection
fg	liquid to gas saturation conditions
g	gas
H	high
i	internal
L	low
l	liquid
nb	nucleate boiling
o	external
rev	reversible
S	suction
sat	saturated
TP	two phase
v	vapour

w	wall
II	second law

1.0 Introduction

1.1 Chapter summary

The reasons for modelling and analysing the performance of four industrial chillers are explained. A background to industrial scale refrigeration is given. The main subject of the subsequent chapters is outlined.

1.2 Introduction

It had been observed that for a particular array of four industrial chillers, there may have been potential to make energy savings through maximising the number of chillers on line for a given heat load. This was based on the observation that the total absorbed power from running four compressors appeared less than the total power absorbed by running three. The helical screw compressors installed in each chilling unit have low load capacity running facilities which reduce the electrical power demand on the motors at lower refrigerating loads Plant operations personnel made the observations from the supervisory DCS (distributed control system).

The chillers in question were retrofitted to an existing secondary refrigeration system at a bulk chemical manufacturing plant. The chillers were installed using an alternative primary refrigerant, namely ammonia or R717, as part of the global exercise in removing CFC refrigerants from use. The secondary refrigerant used was a 27.5 % $CaCl_2$ calcium chloride in water brine solution. The equipment is described in detail in chapter 4.0.

The existing internal (evaporator) and external (process distribution) circulation pumps were retained. This presented problems in the early days of design and commissioning, as the brine flow through the evaporators was considered to potentially be approaching laminar or was transitional. This impacted on the effectiveness of the evaporators and therefore refrigerating effect of the chillers.

The objectives of this study are detailed in chapter 2.0. In chapter 3.0 the development of understanding of the heat transfer and thermodynamic principles required for the design and analysis of industrial scale refrigeration plant is outlined.

A large number of refrigeration applications use secondary or indirect refrigerants to transfer heat from the parts of the system to be cooled to the evaporator of the primary refrigeration system or chiller. These systems can vary in complexity from ice making machines to large industrial process cooling systems where a number of exothermic processes are occurring, all at different conditions and durations.

It is obvious therefore that for a system containing a large number of transient processes some means of ensuring secondary refrigeration system stability would be desirable. If a system can be modelled with acceptable accuracy, it may be possible to review the system for additional capacity, over and above a static heat load model. In addition, it may be possible to review the energy consumption from electrical drives on both primary and secondary systems for different reaction rates or process conditions within such a system.

Traditionally, secondary refrigerants have been water where the temperature does not fall below 2^{o}C, air that is blown across the evaporator surfaces then onto the body to be cooled, and brines. Brines are solutions of salts dissolved in water and can operate at temperatures well below the freezing point of water. Other common secondary refrigerants are ethylene glycol, propylene glycol, methanol and glycerine. These secondary refrigerants possess different chemical and thermodynamic characteristics, which must be taken into account in modelling.

Secondary refrigerant systems can be modelled mathematically. Applying appropriate bounded conditions to the systems can give useful outputs from the model. This thesis demonstrates how a series of mathematical models can be linked together to form a composite model for a given system.

This work is based on a chemical process site, where refrigeration systems working on the Megawatt scale are employed. Often these systems become unstable particularly when exothermic processes input rapid high heat loads to the system. This of course can have a number of consequences, from yield losses in processes using cooling elsewhere in the process, to excessive electrical power demand on pumps and compressors.

Most of the previous work done in modelling of refrigeration plant and processes appears to have concentrated on the food industry and on cold storage of food products or on detailed modelling of chillers. This work attempts to demonstrate a sound methodical approach to building a model and to provide the building blocks to do so.

The model developed considered heat transfer correlations applied to the evaporators of the chillers. It was also used to analyse the refrigeration cycles of the chillers and to conduct thermodynamic performance measures including a second law analysis. The model is developed in chapter 5.0. The model was constructed using a Microsoft Excel spreadsheet.

A series of performance tests were conducted with relevant measurements taken or values calculated for properties of the primary and secondary refrigerants at various states. The test procedures are described in detail in chapter 4.0 and results are presented in chapter 6.0.

The results are discussed in chapter 7.0 with conclusions presented in chapter 8.0.

In addition, some chapters have keywords identified to assist the reader in identifying areas of interest.

2.0 Objectives

The purpose of this study was to investigate the thermal performance of the possible running combinations of an industrial brine chilling plant comprising four chillers working on a vapour compression refrigeration cycle. Evaluation of this would allow a review of operational and control philosophy for this equipment.

The specific areas of interest were to:

- identify the combination of heat transfer correlations which best describe the heat transfer behaviour in the evaporators of the chillers
- apply a first law of thermodynamics analysis of the system for each running condition to evaluate the optimum combination based on coefficient of performance of the plant
- apply a second law of thermodynamics analysis to the system to evaluate the areas of greatest irreversibility in the systems
- propose an optimum operating philosophy for the chiller plant.

3.0 Literature Review

3.1 Chapter summary

A detailed review of the literature was conducted. An historical picture was built prior to reviewing a body of contemporary papers and works. Modelling of chillers and liquid thermal storage systems was evaluated. Suitable heat transfer correlations for modelling and analysis of heat exchangers were reviewed. For further thermodynamic evaluation of system performance, techniques for both first and second law analysis were investigated. The properties of ammonia as a refrigerant and its safe handling and application were commented upon.

Keywords: refrigeration, thermal storage, heat transfer, second law of thermodynamics, ammonia.

3.2 Overview

Analysis and modelling of refrigeration systems has evolved over time. In vapour compression cycles, improved understanding heat transfer behaviour in evaporators and condensers has been critical. Greater understanding of two-phase flow phenomena has facilitated developments in the field. A significant body of literature exists in the study of heat transfer and refrigeration.

J G Leidenfrost in 1756, attempted to understand the mechanism of water evaporation in the first real study of two-phase flow in his treatise “De Aquaea Communis Nonnulis Qualitatibus Tracitus”.

Although Newcomen, Smeaton and Watt each advanced performance in the steam engine during the 18th century, understanding of two-phase flow was still limited. Jacob Perkins obtained a patent for a vapour compression cycle refrigerating machine using ether as the refrigerant in 1834.

During the 19th and more so through the 20th century, great strides were made in understanding both boiling and condensing phenomena. Focussed research into these processes allowed others to explore heat transfer in refrigeration cycles.

Modelling or analysis of any complex system requires knowledge of a number of important elements. In the case of modelling an industrial scale refrigeration system, these elements include the behaviour of the primary refrigeration system or chiller, the interactions of the secondary refrigerant with the chiller, the fluid dynamics of the system and the heat transfer processes between the secondary refrigerant and consumer units in the external system that use the cooling. These relationships may on occasion be represented by elemental models or by lumped parameter models.

To improve understanding of each of these main components of a model, it is useful to review previous work in the field. Models where a secondary refrigerant is considered, irrespective of the fluid were examined. An understanding of their effectiveness and the suitability of the techniques applied are explored.

Moving next to review modelling of chillers and evaporators, the critical interactions between primary and secondary refrigerants were examined. If an overall model is to provide meaningful results that acceptably match the real system, this component must be described adequately. A number of heat transfer correlations from the literature were reviewed.

Thermal storage capacity in a secondary refrigeration system is vital to its performance. If the system has low thermal storage capacity, the system will undoubtedly become 'unstable' and the chiller or chillers will modulate and consume more energy than should be required to provide cooling. Modelling techniques used in this area were reviewed and consideration was given to population balance models for residence times within a system.

A review of suitable linear differential and algebraic equations for modelling of heat exchange equipment was undertaken. Particular focus is necessary in establishing the overall heat transfer coefficient in heat exchangers since accuracy here will contribute significantly to the successful modelling of a system.

Real systems are not perfect and as such will demonstrate irreversibility and losses. Some work has been carried out to describe these ireversibilities and entropy production in refrigeration process. The principle of entropy production is explained in a number of engineering thermodynamics and physics texts. The second law of thermodynamics provided techniques for further analysis of systems. Some techniques available from the second law were reviewed. Such analyses can indicate areas where system energy performance can be improved. These may not be obvious under first law analysis.

The aim of this literature review was to establish the extent to which modelling of large scale, industrial secondary refrigerant systems have been successfully attempted. A review of various approaches to mathematical modelling, in particular of refrigeration systems is intended to build a library of techniques, which may be adapted to a refrigeration system model.

Major components in refrigeration plant include heat exchangers, mainly evaporators, condensers and coolers. The other significant component is the compressor. The literature was reviewed for relevant detail on these components. This included mathematical models.

3.3 Developments in two-phase flow modelling and boiling heat transfer correlations

A vast array of literature is available on the analysis of two-phase flow and boiling heat transfer correlations. A number of textbooks were reviewed together with published papers.

In terms of general texts, Carey (1992) covers the field in detail. Following a thorough review of the thermophysical background required for underpinning knowledge, pool boiling and relevant correlations were explained in detail.

Incropera and de Witt (1985) and Welty (1974) offered useful details on the phenomena. Whalley (1996) presented the subject mater in a distilled format, which was most useful. Bergles et al (1981) was the most comprehensive work reviewed on the subject.
Most of the above texts contained the standard correlations found in other literature. Chen; Forster-Zuber; Mostinski; Cooper; Rohsenow etc. were covered in detail. The generalised nature of some correlations was demonstrated by the regression analysis applied to scatter plots. This helps to explain the difficulty in universally applying correlations to various substances.

The literature contained a significant body of work on boiling heat transfer. Several papers identified the low Reynolds number problem in two-phase flow. Kandlikar et al (2003) conducted a series of experiments using water, to determine the effects of surface roughness on low Reynolds number heat transfer and flow regimes. They were able to demonstrate that surface roughness and pipe diameter did indeed have an effect. The scope of the study was fairly limited and they identified a need to expand this work further.

Kandlikar and Bahasubramanian (2003) investigated the applicability of flow boiling correlations in micro channels. Experimental data from third parties for R134a and

HCFC 123 were compared to the predicted results from correlations. The results indicated that refining of the correlations was required for most conditions to more closely match the measured results.

Both of the above papers considered internal or channel flow. Webb et al (1989) employed the Chen correlation with Forster-Zuber for external two-phase flow over a shell and tube evaporator. The results of their experiments yielded low Reynolds numbers. The authors concluded that the Chen correlation was not universally applicable to low Reynolds number external tube flow.

3.4 Internal flow conditions

The standard heat transfer texts such as Incropera and de Witt (1985) and Welty (1974) cover hydrodynamic and thermal boundary layer theory. They consider the general conditions for incompressible flow and convective heat transfer.

More detailed analyses of entrance conditions for internal tube flow have been conducted. Kandlikar (2002) explored the effects of entrance conditions on the entrance length and pressure gradient variation in the entry region. The fluid considered was an oil at 24 ^{o}C. Such a study should be regarded as quite specific to the fluid studied since its physical properties will necessarily determine the results.

However, of particular interest were the findings for the transition flow regime from laminar to turbulent conditions. For severely disturbed entrance conditions, it was speculated that transitional flow may exist over the entire length of the channel. This would increase the complexity of any calculations of heat transfer coefficients.

The Langhaar entry length of 0.05ReD was validated for the testing.

The experiment incorporated a turbulator as means of modifying flow conditions. Turbulators are frequently used to enhance heat transfer. Kalinin and Dreitser (1998), described the influence of the Reynolds and Prandtl numbers on heat transfer for internal flow. They reviewed the effects of the turbulator shape on heat transfer. The turbulator greatly impacts on the Reynolds number.

They concluded that as the Prandtl number increases. The heat transfer enhancement efficiency also increased. Additionally, they concluded that little is known about the mechanisms for heat transfer in the transition and weakly turbulent flow regimes.

Kreith (1984), provides a number of correlations and techniques for developing heat transfer coefficients. Conditions in the laminar, turbulent and transition flow regimes re covered. The inherent uncertainty in the transition range is once more highlighted. This is attributed to the instability of the flow pattern.

However, the correlation presented for the transition flow heat transfer coefficient is useful and can be applied elsewhere. It must be cautioned that the correlation is based on specific test data and may not be suitable for application in all other conditions.

3.5 Modelling of Chillers and Evaporators

A number of papers have been produced detailing modelling techniques for cold stores and freezing or cooling of bodies. This work has tended to concentrate on food products.

Cleland (1983) describes a method for simulating industrial refrigeration systems with several independent variables. The system is described as a series of ordinary differential and algebraic equations. By numerically integrating the system differential equations with respect to time, various processes in the system can be simulated.

The model is based on food freezing where the secondary refrigerant is air and demonstrates an ability to handle time-variable heat loads. An example for simulation is chosen which comprises five types of refrigeration applications. The model described how air temperature changes with time in each application and the effects of this on the rate of product freezing or chilling.

Hasse et al (1996) propose a top-down modelling approach to dynamic modelling of cold-storage plants. Their aim is to provide simple equations that sufficiently describe the system to describe all major dynamic features of a system. The model is based on mass and energy balances with simple assumptions made on heat and mass transfer. By using a modular approach to combine the subsystems in the model (room structure, goods, evaporator, fan, air change etc) with their interactions through heat and mass transfer.

A simulation of the model was executed using a software package (MATLAB). Reasonable results were achieved when comparing the model predictions with experimental readings. The basic aim of the model was to develop control system algorithms requiring a minimal amount of data. However with lower levels of complexity, less accurate control systems are almost inevitable.

Gordon et al (1997) provide a generalised finite time model for reciprocating compressor chillers. Browne and Bansal (1998) offer a steady-state model of vapour-compression centrifugal liquid chillers, which is intended as an aid to design engineers. Both offer methods for characterising the performance of chiller systems.

Browne and Bansal (1998), constructed their model based on three different centrifugal liquid chiller models and considered thermodynamic activity in the condenser, expansion device, evaporator, compressor suction line (where the refrigerant was considered to be slightly superheated) and centrifugal compressor.

Capacity control of the chiller is considered as an arbitrary throttling process. A linear relationship was assumed to determine the degree of throttling based on the set point temperature of the chilled water secondary refrigerant.

Heat transfer correlations were employed for the condenser and evaporator and heat transfer models developed. The procedures used to calculate heat transfer coefficients are provided and lead to overall coefficients for both condenser and evaporator. The authors chose to ignore fouling resistances since the chillers were cleaned once per year. In many applications such cleaning has been shown to be either ineffective or not carried out.

Experimental data were measured and recorded for two water chiller systems over a number of days. The temperature of chilled water leaving the evaporator was recorded; the corresponding evaporator refrigeration capacity, compressor electrical work output and coefficient of performance were then measured, calculated and recorded.

The model was then applied for the conditions recorded and the values predicted for evaporator refrigeration capacity, compressor electrical work output and coefficient of performance. These values were plotted against the actual values. In general the model predictions were within plus or minus ten percent of the actual values.

Gordon et al (1997), focus on the efficiency losses from a chiller system through dissipation from their principal components. The paper develops a characteristic curve for the chiller that relates the inverse of the coefficient of performance as a function of the inverse of the cycle-average rate of heat absorption at the evaporator or cooling rate.

$$\frac{1}{COP}+1=\frac{\dfrac{T_{cond}^{in}X_{cond}(mCE)_{cond}}{Q_{evap}}\left[\Delta S_{\text{int}}-X_{evap}(mCE)_{evap}-\dfrac{T_{cond}^{in}\Delta S_{\text{int}}X_{evap}(mCE)_{evap}}{Q_{evap}}\right]}{X_{cond}(mCE)_{cond}+X_{evap}(mCE)_{evap}-\Delta S_{\text{int}}+\dfrac{T_{cond}^{in}\Delta S_{\text{int}}X_{evap}(mCE)_{evap}}{Q_{evap}}\left[\Delta S_{\text{int}}-X_{cond}(mCE)_{cond}\right]}$$

COP = Coefficient of Performance
T_{cond}^{in} = condenser coolant inlet temperature
X_{cond} = fraction of cycle time that refrigerant is in the condenser (dimensionless)
Q_{evap} = cycle - average rate of heat absorption at the evaporator = cooling rate (W K^{-1})
m = coolant mass flow rate (kg s^{-1})
C = coolant specific heat (J kg^{-1} K^{-1})
E = heat exchanger inventory constant
ΔS_{int} = cycle - average total internal entropy production (W K^{-1})
X_{evap} = fraction of cycle time thet refrigerant is in the evaporator (dimensionless)

In order to match predicted values to real values, an 'intrusive' approach is adopted. Here, it is attempted to optimise chiller configurations by thermodynamically modelling key components in the chiller system and allocating time to each component during the cycle.

Willatzen et al (1998) for evaporators in vapour compression refrigeration plant propose a general dynamic simulation model. The proposal is presented in two parts, firstly, moving-boundary formulation of two-phase flow with heat exchange, and secondly, simulation and control of an evaporator.

The proposed general lumped moving-boundary model equations for two phase flow are derived from the conservation principles of mass and energy and Newton's second law. The assumption is that all fluids in such models are Newtonian (i.e. that shear stress in the fluid is proportional to the time rate of strain). The system is thus described in terms of the Navier Stokes equations for conservation of mass, energy and momentum.

The model reduces the complexity of the system down from three dimensional, to a one-dimensional description of fluid flow in a straight section of horizontal tube. Pressure drop along the tube is considered as negligible.

The model developed was for a domestic refrigeration system and deals with three zones, liquid, two phase and vapour phase, in the evaporators and condensers. This model whilst rigorously describing the primary refrigerant system, may be rather complex for inclusion in a secondary refrigerant system model.

Several comparative studies comparing alternative refrigerants have been produced.

Grace and Tarsou (2001), produced a model that compared the performance of a number of refrigerants as alternatives to R22 (which will be phased out of use by 2015). This produced results showing the refrigerants with the best cooling capacities. However, the use of these alternatives as drop in replacements for R22 does not appear to be straight forward with modifications to plant required for some.

Domanski (1995) theoretically compared 38 refrigerants applied to the Rankine cycle and three modified vapour compression cycles. The analysis was comprehensive, although entirely theoretical with no experimental back up. The data remains useful but caution is required in applying the findings without fieldwork.

3.6 Compressor modelling

The literature covers refrigeration screw compressors with a number of useful references available. There are a number of studies and models developed for compressors, some of which are not readily applicable to chiller modelling.

The most useful papers relate to helical screw compressors as applied to refrigerating plant. A number of papers refer to the models used in that analysis. The models range from classical adiabatic or polytropic behaviour.

The simplest model applied by Marshall and James (1975), assumed that the indicated power could be used to evaluate the enthalpy increase during compression. A simple relationship between volumetric efficiency and pressure ratio was used to derive the mass flow rate allowing the enthalpy rise to be calculated. A similar approach was employed by Cleland (1983).

3.7 Secondary refrigeration systems and thermal storage

López and Lacarra (1999) outline a method for mathematical modelling of thermal storage systems in the food industry, where chilled water is the secondary refrigerant. The authors recognised that a model must be capable of handling time-varying loads. The importance of determining the real heat load profile to achieve a suitable design of the refrigeration system and the thermal storage system is acknowledged.

In addition to determining the amount of heat to be removed from process systems, the additional heat sources such as distribution pumps, stirring devices and thermal losses in the thermal storage and refrigeration systems are considered.

A useful model for the secondary refrigerant holding or buffer tank which divides the tank into a hot and cold zone was developed. This is a very useful tool for modelling thermal storage holding or buffer tanks. Many large-scale installations use such storage tanks to buffer out the effects of heat loads and to smooth the response of the system and to maintain stability of the system.

These equations were developed to model the temperature differences between the two tank zones and could be used to model similar buffer tank systems. In multiple chiller systems, there are “internal” pumps between the evaporator and the buffer tank and “external” pumps between the buffer tank and the users of the cooling. This can be complicated when the suction line to the external pumps is the discharge line from the internal pumps. In such cases a flow balance must be built into the equation.

The equations applied to the holding tank zones are shown below.

$$\frac{dT_{11}}{dt} = \frac{1}{(M_1.C_{pw})}\left[m_{b1}C_{pw} \bullet \left(T_{weo} - T_{11}\right) + m_{b2} \bullet C_{pw} \bullet \left(T_{12} - T_{wto}\right)\right]$$

$$\frac{dT_{12}}{dt} = \frac{1}{(M_2.C_{pw})}\left[m_{b1}C_{pw} \bullet \left(T_{11} - T_{wei}\right) + m_{b2} \bullet C_{pw} \bullet \left(T_{wti} - T_{12}\right)\right]$$

and if $M = M_1 + M_2$ and $T = (T_{11} + T_{12})/2$

$$\frac{dT}{dt} = \frac{1}{M \bullet C_{pw}}\left[m_{b1}C_{pw} \bullet \left(T_{weo} - T_{wei}\right) + m_{b2} \bullet C_{pw} \bullet \left(T_{wti} - T_{wto}\right)\right]$$

where c_p = specific heat capacity $(J/kg\ K)$
m = mas flow rate (kg/s)
M = mass (kg)
T = temperature $(\text{K or } ^oC)$
Subscripts e = evaporator
w = water
wei = water at evaporator inlet
weo = water at evaporator outlet
wti = water at holding tank inlet
wto = water at holding tank outlet

Richards (1979), demonstrates population balance models. Here transport phenomena based models may be complimented by using population balance, or age distribution models. This method can be particularly useful for mixing type processes and inflowoutflow models. The method is considered to be particularly suitable for non-ideal behaviour such as channelling and dead space.

Such models may enable a unit to be divided into a lumped parameter perfectly mixed vessel in series or in parallel with a plug flow section. The thermal storage and transport behaviour of the secondary refrigerant may be modelled in such a manner.

The 'age' of an element of fluid in a vessel at a time t (the elapsed time since the element entered the vessel) is defined as the elapsed time since entry to vessel and time t. An age distribution function I(t) is defined such that the fraction of fluid elements having ages between t +Δt is given by I(t)Δt. The sum of all such fractions is unity , i.e.

$$\int_0^\infty I(t)dt = 1$$

A residence time distribution function E(t), is defined such that the fraction of elements of fluid leaving the vessel having ages between t and t +Δt. This function gives the age distribution of the fluid elements at time t prior to leaving the vessel. Again, the sum of all such fractions is unity,

$$\int_0^\infty E(t)dt = 1$$

These functions I(t) and E(t), are related to each other and to a third function Λ(t). This function is the intensity function, defined as that fraction of the fluid which will leave the vessel between time t and t +Δt. The continuity equation is then applied to these functions to establish the relationships for a constant volume and flow rate.

By determining the response of flow processes to a step input and impulse input of inert tracers, curves are found known as the F and C curves respectively. These are plotted against a dimensionless time base θ

$\theta = \frac{t}{\bar{t}}$ where $\bar{t}$ = mean residence time

It is therefore possible to incorporate population balance into a mathematical model of a system. This is important if a useful flow model is required and may involve conducting experimental work using tracers in a real system. If this information can be gathered, the flow data can be applied to the heat equations used in a model, with the hope of providing a useful model.

Lovatt et al (1998) compared three refrigeration simulation environments to simulate the performance of two large meat processing refrigeration systems. They identified weaknesses in the systems' abilities to effectively simulate the thermal storage capacities of room walls in such environments, which previously have tended only to consider their thermal resistance.

In all of the simulation programmes, which modelled the two systems, represented the compressors and pipelines as algebraic equations thus assuming them to be time-invariant. This somewhat ignores the dynamic tendencies of refrigeration systems which can in reality see variations in load. With a secondary refrigeration system which uses a liquid secondary refrigerant with a holding or buffer tank, or has multiple coolant users, time-variance must be considered.

3.8 Heat exchanger modelling

A vast number of texts exist outlining classical theory in heat transfer from one fluid to another via heat exchange equipment. Incropera and De Witt (1985) provide a sound basis for progress in the analysis of heat exchange equipment. Covering the modes of heat transfer (conduction, convection and radiant heat transfer) from first principles, through the more complex boiling and condensing processes to heat exchangers. The material covered includes two-phase flow as found in evaporators in primary refrigeration cycles. This material may be useful as part of a chiller model.

In order to develop an effective heat transfer model, accurate core data is essential. Physical properties of materials and fluid within the system are relatively readily available. However, depending on the geometry of the heat exchange equipment establishing an overall heat transfer coefficient can be difficult.

For a secondary refrigerant system, a wide variety of heat transfer equipment can be found. These range from standard heat exchanger types; shell and tube, plate, carbon block, with varying geometries and configurations. Heat exchangers also demonstrate a number of flow patterns; cross flow, counter flow and parallel flow. Add to this the differing number of passes on one side or the other of the heat exchanger and the possible number of configurations becomes very large.

For heat exchangers the general equation for heat transfer is

$$q = UA\Delta T_m$$

where q = heat transfer rate (W)

U = overall heat transfer coefficient $(W/m^2 K)$

A = surface area for heattransfer (m^2)

ΔT_m = the mean temperature difference

The overall heat transfer coefficient U, is found by using the forced convection relations to find the film coefficients of convection on both the hot and cold fluid sides of the heat exchanger and the thermal conductivity of the separating material(s).

The preferred measure of temperature difference is the log mean difference. Incropera and De Witt (1985) offer a range of heat exchanger calculation methods including log mean temperature difference (LMTD), correction factors for use with the LMTD and the

effectiveness-NTU (Number of Transfer Units) method. The effectiveness-NTU method is used in situations where only the inlet temperatures for a given configuration are known. The relationships between effectiveness and NTU are tabulated and graphed.

3.9 Second law perspectives

Inefficiencies in any real thermodynamic system contribute to rendering that system irreversible. A secondary refrigerant process cannot be reversible since, having taken place it cannot be reversed and leave no change either to the system or its surroundings.

The main factors which make a process irreversible are; friction, unrestrained expansion, heat transfer through a finite temperature difference and mixing of two different substances. Many other factors contribute to irreversibilities such as combustion; hysteresis and i^2R effects in electrical circuits render processes irreversible.

Most of the approaches to modelling of refrigeration systems that were reviewed did not appear to consider entropy production or irreversible thermodynamics as affecting the performance of the systems being modelled. However, Chau et al (1997) focussed very clearly on entropy production and develop a model for absorption systems that relates the COP of a plant to the total internal entropy production per cycle. Gordon Et al (1997) propose that by considering the practical constraints on chillers, maximising COP and minimising entropy production can be regarded as equivalent.

Thermodynamics texts such as van Wylen et al (1994) explain the concept of entropy production for irreversible processes, from the basis that the change in entropy for an irreversible process will be larger than that for a reversible process.

$$dS = \frac{\delta Q}{T} + \delta S_{gen}$$

provided the last term is positive $\delta S_{gen} \geq 0$

Where S = entropy *(kJ/K)*
Q = heat transfer *(W)*
T = temperature *(K)*

δS_{gen} is the amount of entropy production due to irreversibilities in the system.

Entropy change of a control mass can be either positive or negative, since the entropy can be increased by internal entropy generation, and either increased or decreased depending on the direction of heat transfer in or out of the system.

It can be shown that the entropy change of a solid or liquid between two states 1 and 2 is:

$$s_1 - s_2 = C \ln \frac{T_2}{T_1}$$

Where s = specific entropy *(kJ/kg K)*
C = specific heat capacity *(kJ/kg K)*

For many applications, C can be considered as a constant.

For an ideal gas, where air for example is the secondary refrigerant, there are several possibilities for calculating the change in entropy, some of which are shown below. The first two cases can be shown, where specific heat is taken as a constant.

$$s_2 - s_1 = C_{p0} \ln \frac{T_2}{T_1} - R \ln \frac{P_2}{P_1}$$

$$s_2 - s_1 = C_{v0} \ln \frac{T_2}{T_1} - R \ln \frac{v_2}{v_1}$$

where R = gas constant *(kJ/kg K)*
P = Pressure *(N/m^2)*
v = specific volume *(m^3/kg)*

If the specific heat is not taken as a constant then equation (2.6.3) can be modified by integrating the results of calculations from statistical thermodynamics from a reference temperature T_o to any temperature T.

$$s_T^0 = \int_{T_0}^{T} \frac{C_{po}}{T} dT$$

The entropy change between any two states is then given as

$$s_2 - s_1 = (s_{T2} - s_{T1}) - R \ln \frac{P_2}{P_1}$$

3.10 Properties and Analysis of Anhydrous Ammonia (R 717)

The merits of the application of ammonia as a refrigerant are widely recognised and are covered extensively in the literature. The primary factors are the excellent heat transfer and thermodynamic properties of ammonia. Ammonia is a relatively low cost refrigerant compared to other refrigerants, and increased production levels due to demand from the agricultural fertilizer sector increase its attractiveness. This attractiveness is however reduced somewhat by the flammability of its vapour in air.

The thermodynamic properties of ammonia were investigated and documented by Haar and Gallagher (1978) in the first comprehensive review since a document known as NBS Circular 142 "Tables of Thermodynamic Properties of Ammonia" published in 1923. This document is an excellent reference for properties required in modelling and analysis of ammonia heat transfer processes.

From the construction of a Helmholtz free energy function for the entire temperature and density range of the correlation, effectively a thermodynamic surface was developed at selected states. From the Helmholtz function F (the energy free to do work in a reversible process) where

$$F = U - TS$$

U = internal energy
T = temperature
S = entropy

By expressing this function in derivative form it is possible to calculate the other thermodynamic properties.

The properties of Ammonia in the critical region are discussed by Haar and Gallagher (1978) in relation to their calculations. Specific analysis of the thermodynamic properties of ammonia in the critical region was carried by Edison and Sengers (1999). The ability to accurately model thermodynamic behaviour in the vicinity of the critical point is raised by Haar and Gallagher (1978) and Edison and Sengers (1999) make comparison with their results.

Edison and Sengers (1999) approach the problem of transition from points in the critical region and those further away from the critical point by a strenuous mathematical analysis. Both the papers above identify the existence of varying data for ammonia in the critical region in previous literature.

The results calculated by Edison and Sengers came to within 0.1% of experimental pressure data.

It is unlikely that values in the critical region would be required for analysis of a vapour compression refrigeration cycle as the state of the refrigerant at elevated temperatures would be as a superheated vapour. In the critical region the refrigerant could exist as a liquid. The cycle would not work as the phase change from gas to liquid across the condenser would not occur and the heat from the evaporation and compression processes could not be removed. Liquid phase refrigerant in the compressor could seriously damage the compressor. Dossat (1997) recommends avoiding superheat in the compressor suction as this can lead to very high temperatures in the discharge. Such temperatures can increase the cooling requirements for the compressor and the required size of condenser. Dossat does not state that high temperatures may force the ammonia towards the critical range.

A vapour compression refrigeration cycle relies on two-phase flow in both the evaporator and condenser and where installed in flash economisers. The low surface tension properties of ammonia are frequently quoted in the literature. Ammonia is readily boiled off and condensed. This makes it an ideal refrigerant.

MacLaine-Cross (1999) conducted a survey of replacement refrigerants for water chillers. In comparing the performance and properties of nine alternatives he concluded that ammonia possessed the best thermodynamic and transport properties. Chillers using ammonia could potentially produce COP's of up to 20% higher than the alternatives. This work gives a useful and straightforward critique of refrigerant performance, less mathematical and more operator orientated than some of the papers produced.

Dossat (1997) states that ammonia has the best refrigerating effect per kilogram of an refrigerant. The environmental and economic benefits of ammonia are also mentioned.

Whilst the global environmental benefits of using R717 are extolled by Dossat (1997). The hazards and risks of use are also important factors. Useful research into the combustion of ammonia-air mixtures was conducted by Fenton et-al (1995). The review concluded that whilst useful data for many areas of use are available, more work on refrigeration use is required. Specific areas of concern were in droplet, spray and lubricating oil effects on ammonia combustion characteristics.

Experimental work on ammonia-air flammability limits was documented by Khan et-al (1995). However the conclusions were rather open in that the size and nature of energy sources available was large and the available data far from complete. Both this and the previous paper do suggest that if ammonia is the best option for the long-term replacement of CFC refrigerants then further work on characterisation of combustion and flammability limits is required.

The literature suggests that the thermodynamic and heat transfer properties of ammonia point to a successful re-birth as a refrigerant. The engineering consequences of this are not discussed, such as the requirement for flameproof equipment or sophisticated interlocked detection/shutdown systems to maintain safe plant conditions. The code of practice from the Institute of Refrigeration (2002) details how such installations should be designed, installed, operated and maintained.

There is little evidence in the literature of the move towards critical charge systems using plate rather than conventional shell and tube heat exchangers. This reduces the quantities of ammonia required for good refrigeration performance. The pressure vessel design is also much simplified.

4.0 System description and test procedures

4.1 Chapter summary

A number of test procedures were applied to an industrial cooling system comprising 4 calcium chloride brine chiller units. Eleven procedures running all possible combinations of two, three and four chillers were observed. Sufficient details were recorded to allow full refrigeration cycle performance evaluation for each set of test procedures. The chillers employed shell and tube heat exchangers for evaporation, condensing and oil cooling. The compressors were of the twin helical screw type with oil cooling and flash gas port injection from an economiser. The measurements taken were mainly by manual recording from local instrumentation. A minimal amount of the data was recorded or trended electronically. However the results indicated reasonable accuracy and were sufficient for further analysis.

Keywords: chiller performance, test procedures, manual observation and recording

4.2 Objectives of the test procedures

The main objectives of the test procedures were-

- To observe the performance of the chillers when different combinations of 2, 3 and 4 chillers were on-line.
- To record data which would allow detailed analysis of the thermodynamic and heat transfer performance of the chillers.

4.3 Equipment and hardware

A schematic of the main components on the brine (secondary refrigerant) side of the system is shown on figure 4.3.1. The secondary refrigerant used was a 27.5 % $CaCl_2$ calcium chloride in water brine solution. The chiller array is intended to supply chilled brine at a temperature of –24 ^{o}C to process coolant users.

The system consists of four off chiller units with a design heat removal capacity of 1340kW. Warm brine returns from process coolant users to the chiller units and is pumped through the evaporators via dedicated centrifugal pumps rated at 450 m^3/h. These pumps were previously used as internal pumps to four completely different chiller units. The motors have kW transducers installed that will allow comparisons of relative flows from the pumps by interpretation from the pump performance curves.

Four off external brine pumps rated at 350 m^3/h supply cool brine to the process coolant users controlled by pressure drop as control valves open on consumer equipment to increase flow. A 50m^3 capacity buffer tank is positioned between the internal and external pump circuits.

The pipework configuration of the system is such that since the total flow rate of the four internal brine pumps is greater than the four external pumps, any excess of cool brine will circulate through the buffer tank and return to the chillers cooling heated brine returning from the consumers. The consumer units in the chemical process area of the plant are of various heat exchanger types e.g. jacketed reaction vessels, plate heat exchangers, shell and tube heat exchangers etc. Controlling the internal temperature regulates heat removal from the process side of the exchangers; this is achieved by varying the flow of cool brine on the external side of the exchanger.

A header tank located in one of the production buildings ensures that all consumer equipment remains flooded with coolant.

A schematic of the chiller package system is shown on figure 4.3.2. The system consists of four identical chiller packages which as described above provide chilled 27.5 % $CaCl_2$ calcium chloride brine solution for a chemical processing plant. The original design basis was for three chillers to be on line with a fourth chiller available as an installed spare unit, allowing planned or breakdown maintenance of any one unit without compromising the requirement for cool brine to process users.

The chillers have R717 (Anhydrous Ammonia) as their primary refrigerant and have a charge of approximately 1966 kg each. Due to the high toxicity and explosive limits of R717, a sophisticated gas detection system is employed for personnel protection and as a control measure against explosion since not all electrical equipment in the chiller room is compatible with a hazardous gas atmosphere. Since the plant is operated remotely via a Distributed Control System (DCS) with occasional occupation for inspection and maintenance activities, gas leaks in the zone around the detectors will trigger an alarm at a concentration of 25 ppm. A concentration of 1%v/v will trip all non-hazardous area rated electrical equipment.

The evaporator is a shell and tube heat exchanger consisting of 792 tubes with six passes of brine and a single shell pass of ammonia. There is no direct level control in the evaporator; both the economiser and condenser have level control valves. There are three vapour accumulators on the top surface, each with demister pads at the bottom to ensure that only saturated vapour enters the compressor suction line, the suction line is intended to supply saturated vapour to the compressor.

The compressor is a rotary screw type with an internal slide valve for capacity control. Thus, at lower loads the compressor can run with lower absorbed electrical power. With the compressor fully loaded the slide valve is in the closed position. As unloading commences the slide valve moves away from the valve stop, reduces the effective length of the compressor and progressively creates an opening through which suction gas can pass back to the inlet port of the compressor, since there is negligible work transferred to the gas at this stage, very little loss is incurred. The valve can reduce the compressor capacity down to around 10% of full load. Slide valve actuation is by hydraulics and is initiated by temperature or pressure of the suction gas. A fixed speed water-cooled 3.3kV 700kW electrical drive powers the compressor. The compressor also has a variable volume ratio control which adjusts the compression ratio dependent upon operating conditions.

Hot compressed gas is passed from the compressor to the oil separator, hot gas then passes onto the shell and tube condenser, which consists of 438 tubes with eight passes on the water side and single pass on the shell side. Cooling water is supplied via a forced draught cooling tower system supplying various other consumers on the plant.

The refrigerant expansion process is carried out in two stages with an inter-stage flash economiser between the two expansion valves, which also regulate liquid levels in the condenser, and economiser respectively. Flash vapour from the first expansion stage is fed back to the compressor. However, this vapour is not passed through the compressor suction but at an inlet in a later stage of the compressor. Saturated liquid refrigerant is then passed through a second stage of expansion. From here the very wet ammonia is fed to the evaporator where it picks up heat from the brine circuit and recommences the cycle.

The oil separator is an impingement type, where oil-laden vapour passes through coalescing filters that collect the oil droplets together. The oil drops by gravity to the bottom of the vessel, where it is then passed through an oil cooler which uses cooling tower water to remove heat from the oil and passes the clean, cool oil back to the compressor inlet.

Figure 4.3.3 (also in Appendix F), a pressure-enthalpy diagram, shows the thermodynamic cycle for the chiller at design loads. At state point 1 (also corresponding to point 1 on figure 4.2.2), dry saturated vapour from the evaporator enters the compressor via the suction line; there is minimal superheat in the vapour.

At state point 2, compressed superheated vapour approaches the coalescing filters, dropping off oil in the filters. The oil is pushed through the oil cooler and returned to the compressor where it lubricates the bearings, seals the compressor screw clearances and significantly cools the ammonia being compressed. From state point 3, condensation ensues until state point 4 is reached. Here there has been a slight pressure drop across the condenser where the vapour has undergone a phase change to saturated liquid.

Isenthalpic expansion takes the liquid refrigerant to lower pressure and temperature in the flash economiser at state point 5. During the expansion process some of the refrigerant has flashed off as vapour at state point 6, by removing this vapour the refrigerating effect from the evaporator is increased since gas in the evaporator will reduce the potential for heat removal from the brine. This vapour is expanded further then fed back to the compression process from state point 7 to state point 7'.

As a result of removing the flash vapour, the liquid in the economiser at state point 6 cools to state point 8. This liquid goes through a second isenthalpic expansion thus lowering its temperature further giving the necessary temperature gradient for heat transfer from the brine. At state point 9 the refrigerant enters the evaporator as a two-phase mixture with 6.25% of the mixture being vapour.

The ammonia removes heat from the returning brine in the evaporator by boiling off. This vapour then returns to state point 1 with increased enthalpy where it is once again compressed. A slight pressure drop occurs across the evaporator.

As described above the evaporator is a shell and tube design with a single shell pass and six tube passes. There are 792 bare tubes with a length of 5486.4mm, outside diameter

31.75mm, nominal thickness is 2.159mm. The pitch pattern is TEMA 30 (equilateral triangular, staggered) with a pitch of 39.6875mm. The material grade is carbon steel ASTM/ASME A/SA 175-A/214-90A. The volumetric flow rate of brine is given as 450m^3/h. The heat transfer performance of the evaporators is a key component of this study.

During the chiller load trials, the method of measurement and measuring instrument or techniques applied are detailed below.

- Temperature probes measured brine inlet and outlet temperatures in the evaporators with the readings displayed on the chiller microprocessors local to the machines. The brine flow rate was determined from the pump performance curve using the kW transducers installed on each pump drive; these values were displayed on the system DCS (Distributed Control System) located in a central control room.
- Brine system temperatures at the buffer tank were measured using temperature probes; brine external flow was measured using an in-line flow meter with the readings displayed on the DCS.
- Ammonia side temperatures were measured using temperature probes; pressures were measured using pressure transducers. Again these figures were displayed on the chiller microprocessors.
- The compressor slide valve positions were measured from installed potentiometers repeating to the chiller microprocessors.

4.4 Commentary on test procedures

4.4.1 Chiller characterisations

For the evaporators, the brine inlet, brine outlet temperatures and the internal brine pump absorbed power were recorded. The ammonia (shell) side pressure and temperature were recorded.

The compressor suction pressure, suction temperature, slide valve position, volume ratio and motor absorbed power were recorded.

The condenser temperature and pressure on the ammonia (shell) side were recorded.

The temperature and pressure of after first stage expansion, flash evaporation and second stage expansion were recorded.

The following parameters were then calculated or derived from available data. The enthalpies at relevant locations around the chiller circuit, the quality or dryness fraction after first stage and second stage expansion. These figures allow the basic system performance to be evaluated for each chiller. Further properties of ammonia, required for application to the model described in chapter 5, section 5.2 were constructed from various sources detailed below. The values are tabulated in Appendix D.

Properties of ammonia were obtained from, Carey (1992), Haar and Gallagher (1978), and the CATT2 software package. Values were then obtained for points of interest by linear interpolation. Properties of brine were obtained from user data and tabulated as described in Appendix C.

4.4.2 Procedures: varying the number of chillers on-line

The following procedures were conducted using the combinations of chillers detailed below. Firstly with only two chillers from four on line, then three from four, and finally all four chillers on line. The tests were applied to operational industrial chillers, therefore the heat load on the system was variable due to varying process coolant users on the system. 20 to 30 minutes were normally allowed between trials to reduce the impact of the pervious test procedure on the next.

Procedure1- Chillers No.1 and 2 on line.
Procedure 2- Chillers No.1 and 3 on line.
Procedure 3- Chillers No.1 and 4 on line.
Procedure 4- Chillers No.2 and 3 on line.
Procedure 5- Chillers No.2 and 4 on line.
Procedure 6- Chillers No.3 and 4 on line.
Procedure 7- Chillers No.1, 2 and 3 on line.
Procedure 8- Chillers No.1, 3 and 4 on line.
Procedure 9- Chillers No.1, 2 and 4 on line.
Procedure 10- Chillers No.2, 3 and 4 on line.
Procedure 11- ChillersNo.1,2,3 and 4 on line.

This yielded 29 data sets including the design values, for analysis and application to the model. The development of the model is shown in chapter 5.0.

4.5 Discussion

The instruments used to measure the performance of the chillers were, where possible, calibrated in advance of the tests. However, due to the nature of the equipment, its scale and the fact that the plant was in use, the readings were subject to some error as the means of recording was by up to four people recording the key data by reading from the package control panels. The readings were the best average observed as there were often minor fluctuations in the values.

The measurement sheets in Appendix A, show the measurements to the resolution available. This meant that some readings are to no, one, or two decimal places. Calculated values associated with the tests such as enthalpy and quality or dryness fraction of the ammonia are included.

Since the plant was in normal operation, the chillers were subject to transient heat loads from the process users. It was therefore impossible to maintain the same cooling load for each of the test procedures.

In addition, the flow rates from internal brine pumps, which circulated the brine through the evaporators had kW transducers that read to only whole numbers. The flow rates were then taken from the pump performance curve.

As such the potential for errors in the readings is significant. However, this is the reality in many industrial chiller plants where the cost of more elaborate instrumentation cannot be justified.

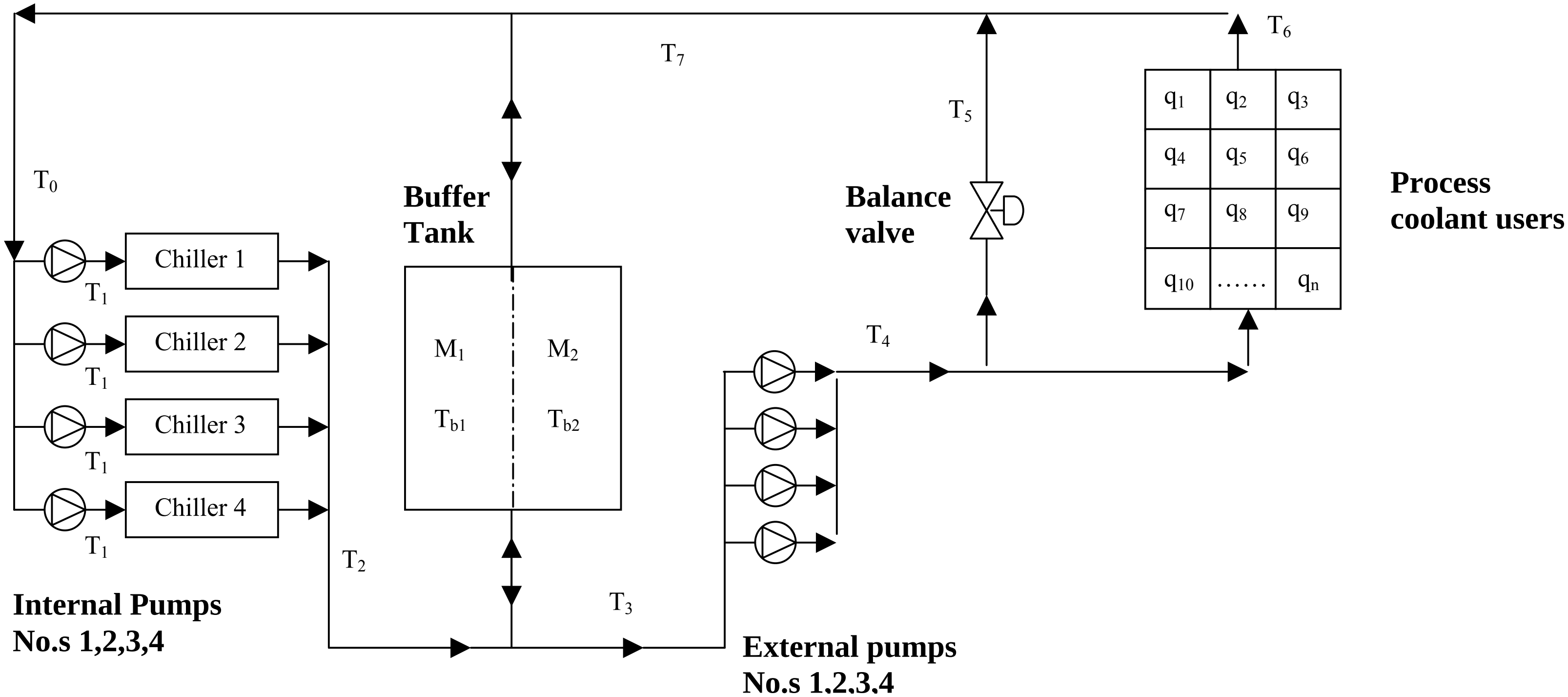

Secondary refrigerant temperature T_n (^oC), n=0…..7 at points on the thermal circuit shown.

Heat sources from the process plant are described as q_k (kW), k=1…..n

$$Q = \sum_{k=1}^{n} q_k$$

Where Q is the total heat load from the process coolant users

Figure 4.3.1 Secondary refrigerant system

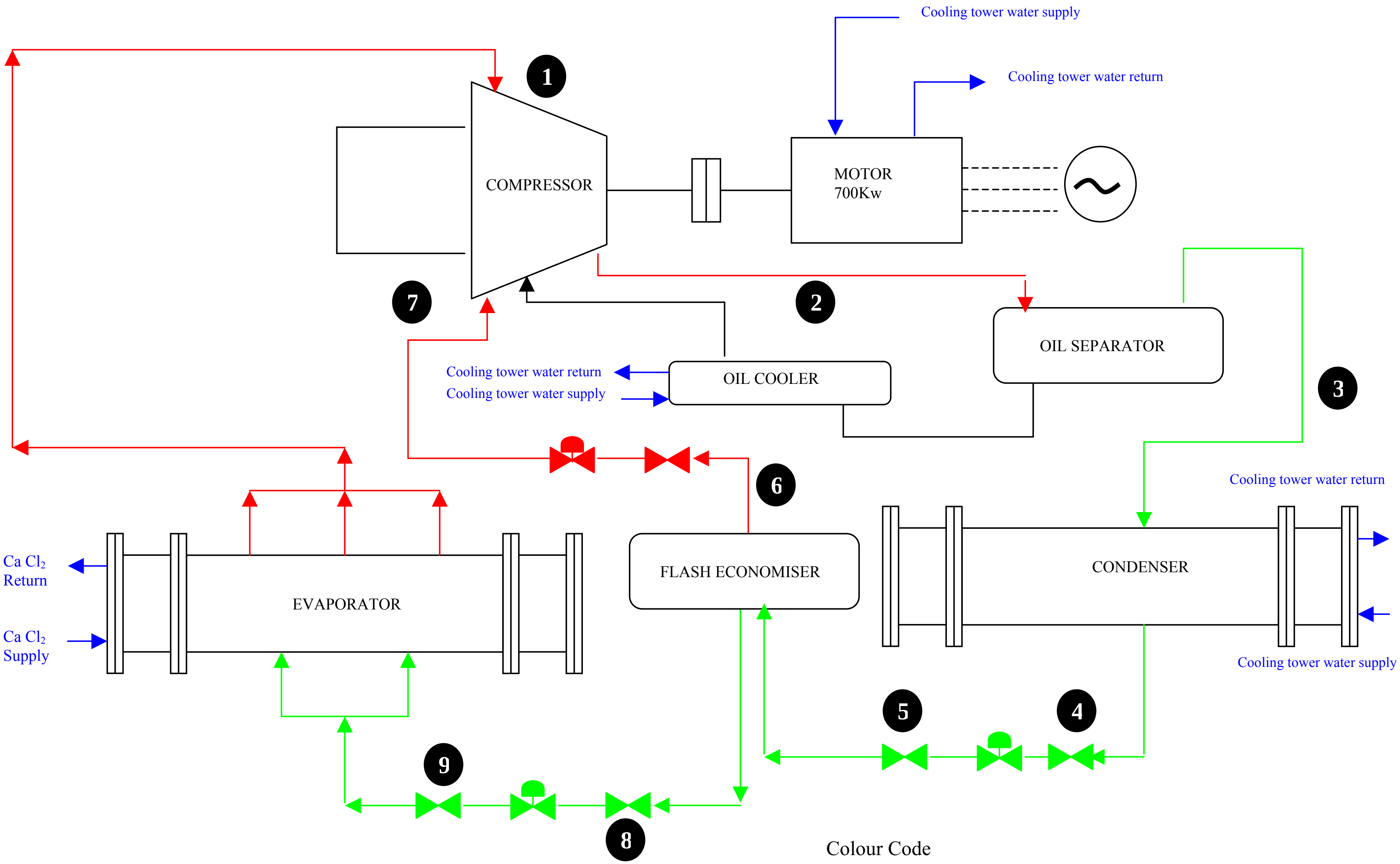

Colour Code

Liquid ammonia

Ammonia vapour/oil

Cooling water/brine

Figure 4.3.2 Chiller Schematic

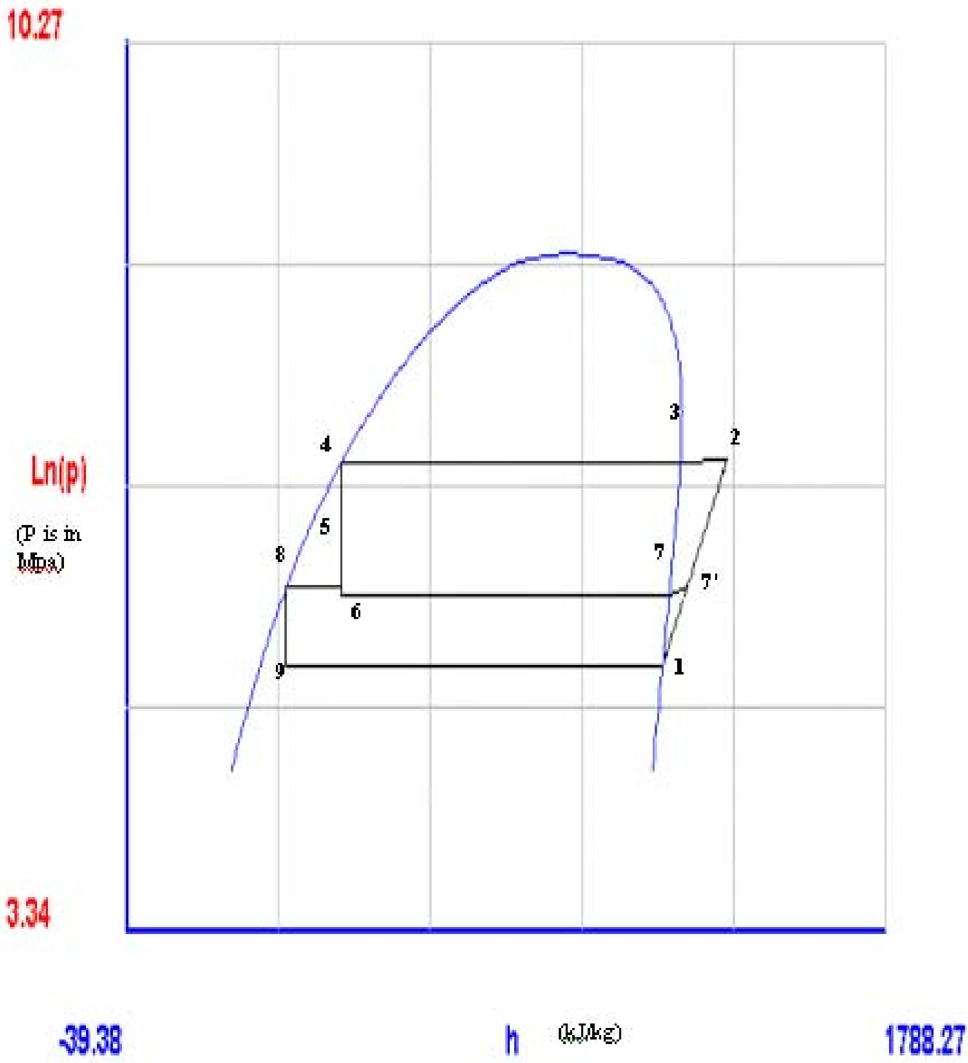

Figure 4.3.3 Pressure-enthalpy diagram for the chillers at design conditions

5.0 Component Correlations and Applications at Design Conditions

5.1 Chapter summary

The chiller system described in Chapter 4.0 was broken down to component level. After evaluation, appropriate correlations were selected which allowed the system to be analysed. This analysis ranged from heat transfer coefficient analysis of the evaporator, including internal convective and external two-phase flow heat transfer across the tube bundle, to thermodynamic cycle analysis. The energy performance of the system was modelled allowing a first law analysis to be conducted. The model then extended to a detailed second law analysis

Keywords: coefficient of heat transfer, coefficient of performance, second law analysis

5.2 Component modelling and correlations applied

It is useful to predict the performance of the system using design data for comparison with actual performance of the system. The correlations applied to the chiller model are detailed below. The design conditions are applied and the calculations are shown in section

Calculation of the heat transfer (kW) from the chilled brine passing through the evaporator is found using-

$$Q = \dot{m} c_p (T_{ei} - T_{eo}) \qquad \text{- 5.2.1}$$

In analysing the heat transfer behaviour of the system a simple calculation can be carried out to find the brine side overall heat transfer coefficient U from the following

$$Q = UFA\Delta T_m \qquad \text{- 5.2.2}$$

The correction factor for a phase change component is equal to one, since the temperature of ammonia in the exchanger is considered to be constant.

The overall heat transfer coefficient from the brine side of the tube can also be calculated by combining the three thermal resistance components. Some correlations are applied to evaluate the relative components.

$$U_i = \frac{1}{1/\alpha_i + [r_o \ln(r_o / r_i)]/k + r_i / r_o \alpha_o} \qquad \text{- 5.2.3}$$

Some correlations are applied to evaluate the relative components. Only the thermal conductivity of the tube wall is known from tables (Bolton 1999) at this point.

The analysis of the evaporator is then carried out using appropriate correlations for heat transfer on the brine side and then on the ammonia side. Taking the brine side first, the type of flow in the tubes is evaluated by calculating the Reynolds number, where Re< 2300 is considered as laminar.

$$\mathrm{Re} = \frac{\rho u l}{\mu} \qquad \text{- 5.2.4}$$

Once the flow is identified as laminar the tube entry conditions must be established to determine the length along the tube whereby the velocity profile becomes invariant with axial position using the Langhaar equation.

$$x_e = (0.05)\,\mathrm{Re}_{d_i}\, d_i \qquad - 5.2.5$$

The thermal entry length for fully developed flow is given by

$$x_{e,t} = (0.05)\,\mathrm{Re}_{d_i}\,\mathrm{Pr}\, d_i \qquad - 5.2.6$$

The Prandtl number Pr is given by the following-

$$\mathrm{Pr} = \frac{c_p \mu}{k} \qquad - 5.2.7$$

For developing thermal profile and developed velocity profile the Hausen equation can be used to establish the average Nusselt number from which the convective heat transfer coefficient can be calculated.

$$\overline{Nu} = \frac{\overline{\alpha}_i L}{k} \qquad - 5.2.8$$

And

$$\overline{Nu} = 3.66 + \frac{0.0668(d_i / L)\,\mathrm{Re}_{d\,i}\,\mathrm{Pr}}{1 + 0.04[(d_i / L)\,\mathrm{Re}_{di\,i}\,\mathrm{Pr}]^{2/3}} \qquad - 5.2.9$$

This allows the internal convective flow heat transfer coefficient to be calculated for fully developed flow. If x_e < L, that is, significantly less than the overall tube, length, we can assume a fully developed velocity profile.

In the region where 2300<*Re*<4000, the flow is normally considered to be in the transition region between laminar and turbulent flow. This is an extremely unreliable area for calculation. However, the following correlation shall be applied.

$$Nu\,\mathrm{Pr}_b^{-0.2}\left(\frac{\mu_w}{\mu_b}\right)^{0.14} = 0.0067\,\mathrm{Re} \qquad - 5.2.10$$

In order to apply this correlation, certain assumptions on the temperature of the brine at the tube wall are made. Assuming that the wall temperature is equal to the outlet temperature of the brine leaving the evaporator, allows dynamic viscosity values to be entered.

For turbulent flow normally, Re>4000. The correlation applied to turbulent flow is

$$Nu = 0.26\,\mathrm{Re}^{0.6}\,\mathrm{Pr}^{0.33} \qquad - 5.2.11$$

The external heat transfer coefficient on the ammonia side of the tube can be calculated from a number of correlations for pool boiling conditions. Two conditions are considered.

Film boiling conditions arise where a vapour film develops on the outer surface of the tube. In stable film conditions the vapour blanket on the heated tube surface is conducted through the vapour and the liquid evaporates at the phase interface. The most appropriate must be judged on the values calculated for each.

Bromley (Incropera and DeWitt 1985) developed the correlation that suggests the coefficient of heat transfer is given by

$$\alpha_o = 0.62\left[\frac{k_v^{\,3}\rho_v(\rho_l - \rho_v)g(h_{fg} + 0.4c_{pv}\Delta T)}{d_o\mu_v(T_o - T_{sat})}\right]^{1/4} \qquad - 5.2.12$$

In this instance $\Delta T = T_o - T_{sat}$, where T_o is the tube outer surface temperature. This is evaluated from the bulk temperature of the brine T_b and the heat transfer across the wall of the tube. This is calculated from the heat flux using

$$T_o - T_b = -\frac{q}{2\pi kL}\ln\frac{r_o}{r_i} \qquad \text{- 5.2.13}$$

For the more likely nucleate boiling regime, ignoring surface effects which are not known for sure, two correlations are applied. Firstly, the Mostinski correlation (Whalley 1996) which gives

$$\alpha_o = 0.106 p_c^{0.69} \phi^{0.7} f(p_R) \qquad \text{- 5.2.14}$$

Where $f(p_R) = 1.8 p_R^{\ 0.17} + 4 p_R^{\ 1.2} + 10 p_R^{\ 10}$ - 5.2.15

And $p_R = p / p_c$ - 5.2.16

$p_c =$ critical pressure and $\phi =$ heat flux

Cooper's correlation gives

$$\alpha_o = A p_R^{(0.12 - \log_{10}\varepsilon)} (-\log_{10} p_R)^{-0.55} M^{-0.5} \phi^{2/3} \qquad \text{- 5.2.17}$$

The Chen correlation for boiling heat transfer considers the boiling process as a combination of flow and nucleate boiling. Here two components of heat transfer are considered, a nucleate component and a forced convection component.

$$\alpha_o = \alpha_{nb} + \alpha_{fc} \qquad \text{- 5.2.18}$$

Various correlations for α_{nb} can be applied, in this case the chosen correlation is that proposed by Forster-Zuber (Webb et al 1996),

Where $\alpha_{nb} = \dfrac{S0.00122\Delta T_{sat}^{0.24}\Delta P_{sat}^{0.75}C_{pl}^{0.45}\rho_l^{0.49}k_l^{0.79}}{\sigma^{0.5}\lambda^{0.24}\mu_l^{0.29}\rho_g^{0.24}}$ - 5.2.19

And $\alpha_{fc} = \alpha_l F$ - 5.2.20

Where

$$\frac{\alpha_l d}{k_l} = 0.0023\,\mathrm{Re}_l^{0.8}\,\mathrm{Pr}_l^{0.4} \qquad \text{- 5.2.21}$$

Due to the fact that the ammonia is in the two-phase condition, the quality of the substance is factored into Re to ensure that only the liquid phase is considered in the calculation.

$$\mathrm{Re}_l = \frac{\rho u_{\max}(1-x)d_o}{\mu} \qquad \text{- 5.2.22}$$

To calculate $u_{\max}$ the approach suggested by Incropera and DeWitt for external flow across a tube bank is applied. The downstream velocity is considered to be that across the area immediately in front of the first row of tubes. The mass flow rate is calculated from the heat load removed from the brine and the enthalpy rise across the evaporator.

The maximum velocity across the tube bank is calculated for a staggered tube bank. The following modification is used, which accounts for the geometry of the bank. S_T Is the transverse tube pitch and S_D is the diagonal tube pitch. But from TEMA pattern 30 the pitches are equal.

$$u_{\max} = \frac{S_T}{2(S_D - d_o)} u \qquad \text{- 5.2.23}$$

So

$$\mathrm{Re}_l = \frac{\rho \frac{S_T}{2(S_D - d_o)} u(1-x) d_o}{\mu} \qquad \text{- 5.2.24}$$

The forced convection component of Chen's correlation given in 4.3.19 above. F Is the two-phase heat transfer coefficient multiplier and is found from the chart (Whalley p 65) after the Martinelli parameter X is found, by comparing F to $\frac{1}{X}$.

Where

$$X = \left(\frac{1-x}{x}\right)^{0.9} \left(\frac{\rho_g}{\rho_l}\right)^{0.5} \left(\frac{\mu_l}{\mu_g}\right)^{0.1} \qquad \text{- 5.2.25}$$

This allows the two-phase Reynolds number to be found, where

$$\mathrm{Re}_{TP} = \mathrm{Re}_l F^{1.25} \qquad \text{- 5.2.26}$$

The suppression factor S is then found from the chart (Whalley p65), by comparing Re_{TP} to S.

Component modelling and correlations applied to the compressor

The compressor performance is represented mathematically assuming adiabatic compression. The relevant relationships for analysis of the compressor are given below.

Referring to figure 4.2, from mass continuity the total mass flow rate of refrigerant around the system can be calculated. The total mass flow rate leaving the compressor is $\dot{m}$. The flash economiser removes vapour equivalent to the dryness fraction, or quality at the conditions in the economiser. This means that the mass flow rate of vapour leaving the economiser is $\dot{m}x$ and the mass flow of liquid leaving is $\dot{m}(1-x)$.

The mass flow rate of refrigerant through the evaporator can be found from

$$Q = \dot{m}(1-x)(h_1 - h_9) \qquad \text{- 5.2.27}$$

So

$$\dot{m} = \frac{Q}{(1-x)(h_1 - h_9)} \qquad \text{- 5.2.28}$$

The heat input from the compressor (excluding the heat removed by the lubricating oil) can then be calculated from the following-

$$W = \dot{m}(1-x)(h_2 - h_1) + \dot{m}x(h_2 - h_7) \qquad \text{- 5.2.29}$$

Volume ratio of the compressor is the ratio of the trapped gas pocket immediately after it opens to the discharge port, to the volume immediately before, given by.

$$V_i = \frac{V_s}{V_d} \qquad \text{- 5.2.30}$$

Compression ratio of the compressor

$$\pi_i = \frac{p_2}{p_1} \qquad \text{- 5.2.31}$$

From known compressor inlet and outlet pressures

$$V_i = \pi_i^{1/\gamma} \qquad \text{- 5.2.32}$$

The compressor performance can then be evaluated against the motor amps and performance curves supplied by the manufacturer, figure 4.3. Since the compressor is a variable volume ratio design, V_i can be calculated for any given pressure ratio. The maximum Vi value is 5.0, thus the condensing pressure acts back to the discharge pressure of the compressor.

The coefficient of performance of the chiller is calculated considering the absorbed power of the compressor from the ammonia thermodynamic cycle, from the following-

$$COP = \frac{Q_{evap}}{W_{comp}} \qquad \text{- 5.2.33}$$

Critically here, the compressor work includes the heat input to the system plus the heat removed from the compressor by the injection of lubrication oil. This heat removal has a great impact on the COP of the chiller. Thus the COP is given by

$$COP = \frac{\dot{m}(1-x)(h_9 - h_1)}{Q_{oil} + \dot{m}(1-x)(h_2 - h_1) + \dot{m}x(h_2 - h_7)} \qquad \text{- 5.2.34}$$

The heat transferred to the lubricating oil in the compressor is given by

$$Q_{oil} = \dot{m}_{oil} Cp_{oil} (T_{oil_e} - T_{oil_i}) \qquad - 5.2.35$$

The mass flow rate is found for each set of running conditions by referencing the design conditions against each actual compressor discharge pressure. The geometry of the pipework from the compressor, through the oil separator and oil cooler back to the compressor is fixed. The compressor acts as a pump, therefore the following can be applied.

$$\dot{m}_{oil_n} = \dot{m}_{oil_{design}} \left(\frac{P_{2_{design}}}{P_{2_n}} \right)^{1/2} \qquad - 5.2.36$$

However in reality, there is a significant energy input to the chiller from the internal brine pump, thus the net work should include this component, so-

$$COSP = \frac{Q_{evap}}{W_{comp} + W_{pump}} \qquad - 5.2.37$$

Where COSP is the Coefficient of System Performance.

Second law analysis of the system

In order to conduct a full thermodynamic analysis of a chiller system, a second law analysis is required. This involves reviewing the irreversibilities, or losses in each component of the system.

For the chosen systems there are six main components for analysis. There are three heat exchangers in the system, the condenser, flash economiser and evaporator. There are three throttling processes, the first and second stages of liquid expansion and the expansion of flash vapour from the economiser to the compressor. Additionally the compressor suction pipework, inter-device pipework and oil filter would be analysed in a complete system analysis. However, only the six main components will be considered here.

The chiller is a heat engine, with heat transfer from the hot brine to the cool ammonia. This means that the availability produced is in the evaporator, and the work used is in the compressor and in the pump. The power consumed by other auxiliary devices can be ignored for this analysis.

The cycle irreversibility is given as-

$$I = Q_L \left(\frac{1}{COP_{act}} - \frac{1}{COP_{Carnot}} \right) \qquad \text{- 5.2.38}$$

Where COP_{Carnot} is given by

$$COP_{Carnot} = \frac{1}{\frac{T_H}{T_L} - 1} \qquad \text{- 5.2.39}$$

Therefore the irreversibility for the refrigeration cycle is expressed as

$$I_{cycle} = Q_L \left(\frac{1}{COP_{act}} - \frac{1}{\frac{T_H}{T_L} - 1} \right) \qquad \text{- 5.2.40}$$

The maximum conversion of heat to work in the heat engine will occur if the engine is completely reversible. The lower temperature reservoir is considered to be the surrounding environment. The reversible work is defined as-

$$W_{rev} = Q - Q_0 \qquad \text{- 5.2.41}$$

$$\frac{Q}{T} = \frac{Q_0}{T_0} \qquad \text{- 5.2.42}$$

This means that the reversible work in the heat engine is given by

$$W_{rev} = Q\left(1 - \frac{T_0}{T}\right) \qquad \text{- 5.2.43}$$

This is the open system availability Ψ, the maximum amount of reversible work that can be extracted from the system.

For the main components in the system, the irreversibilites are calculated from-

$$I = \dot{m}T_o\left[\left(s_e - s_i\right) + \frac{q_k}{T_k}\right] \qquad \text{- 5.2.44}$$

The summation of all component irreversibilities should be equal to the value for the cycle found from 5.2.38 above. The sign of convention of negative heat transfer or work into the system and positive for work or heat transfer is applied. T_k is the temperature of the heat source or sink for the particular heat transfer.

The adiabatic efficiency of the compressors is another measure of the irreversibilites in those particular devices. For the compressor, the adiabatic efficiency is given by-

$$\eta_c = \frac{W_s}{W_{act}} \qquad - 5.2.45$$

Due to the flash economiser this is stated in the following form.

$$\eta_c = \frac{\dot{m}(1-x)(h_{2s} - h_1) + \dot{m}x(h_{2s} - h_5)}{Q_{oil} + \dot{m}(1-x)(h_2 - h_1) + \dot{m}x(h_2 - h_5)} \qquad - 5.2.46$$

The second law efficiency is defined as-

$$\eta_{II} = \frac{W_{rev}}{W_{act}} \qquad - 5.2.47$$

Where the fictitious reversible work is given by-

$$W_{rev} = I + W_{act} \qquad - 5.2.48$$

The three work values can then be compared. Similarly, the adiabatic and second law efficiencies also be compared.

The second law effectiveness for the chillers is defined as-

$$\varepsilon_{II} = \frac{availability\ produced}{work\ used} \qquad - 5.2.49$$

5.3 Analysis of the system at design conditions

The system performance was predicted using the given design conditions, see Appendix A. The results are detailed in Appendix B. Physical and thermodynamic properties of brine and ammonia are found in Appendices C and D respectively.

The heat transferred in the evaporator given by equation 5.2.1 is.

$$Q = 166.85 \times 2.7341 \times [-21 - (-24)] = 1368.56\,\text{kW}$$

From equation 5.2.2 the overall heat transfer coefficient U is evaluated.

Where the area for heat transfer, the outer surface area of the 792 tubes was given by

$$A = \pi d_o L = \pi \times 0.03175 \times 5.4864 = 433.4173\,\text{m}^2$$

And the log mean temperature difference was given by

$$\Delta T_{lm} = \frac{\Delta T_a - \Delta T_b}{\ln\left(\frac{\Delta T_a}{\Delta T_b}\right)} \quad \text{Where} \quad \begin{aligned} \Delta T_a &= T_{e_i} - T \\ \Delta T_b &= T_{e_o} - T \end{aligned}$$

Thus

$$\Delta T_{lm} = \frac{7.7 - 4.7}{\ln\left(\frac{7.7}{4.7}\right)} = 6.0771$$

Therefore

$$U = \frac{1361.59 \times 1000}{433.4173 \times 6.0771} = 518.28 \text{ Wm}^{-2} K^{-1}$$

To compare the value above with the appropriate heat transfer correlations, some manipulations were required.

Using equation 5.2.3, basing the overall heat transfer coefficient on the internal tube surface, values for the internal convective heat transfer coefficient and boiling heat transfer coefficient are required. Therefore the following are calculated-

Where the velocity of the brine was calculated for the number of tubes per pass

$$u = \frac{166.85}{132 \times \pi \times \left(\frac{0.0274^2}{4}\right) \times 1277.43} = 1.6742 \text{ms}^{-1}$$

Giving

$$\text{Re} = \frac{1277.43 \times 1.6742 \times 0.027432}{13.0193 \times 10^{-3}} = 4506.24$$

Normally, this would suggest turbulent flow. However, since laminar flow has been observed at values up to 50000 for Re (Douglas et al p100), the laminar and transition regimes may also be considered.

$$\text{Pr} = \frac{2734.109 \times 13.0193 \times 10^{-3}}{0.4996} = 71.2494$$

The hydrodynamic and thermal entry lengths are calculated.

$$x_e = 0.05 \times 4506.24 \times 0.0274 = 6.174\,\text{m}$$

$$x_{e,t} = 0.05 \times 4506.24 \times 71.2494 \times 0.0274 = 439.86\,\text{m}$$

However, since the velocity profile is developing (x_e>L), but the tube wall temperature will vary with length, a suitable correlation for laminar flow is not available.

For flow in the transition regime, equation 5.2.10 is applied, by substituting for Nu.

$$\overline{\alpha_i} = \frac{0.0067 \times 4509.5 \times 0.4996}{71.2494^{-0.2}\left[\dfrac{13.8708}{13.0193}\right]^{0.14} \times 0.0274} = 1281.68\,\text{Wm}^{-2}\text{K}^{-1}$$

For flow in the turbulent regime, equation 5.2.11 is applied by substituting for Nu.

$$\overline{\alpha_i} = \frac{0.26 \times 4509.50^{0.6} \times 71.2494^{0.33} \times 0.4996}{0.0274} = 3016.84\,\text{Wm}^{-2}\text{K}^{-1}$$

The four external heat transfer coefficients on the ammonia side proposed above yield the following possible values.

Bromley's correlation from equation 5.2.12 is applied. However, a value for the tube outer wall temperature is required. This is found using average values for the brine temperature and assuming that this is the same as the inner wall temperature. Applying the solution for a single layer cylinder to Fourier's law for conduction, and re-arranging to find T_o.

$$T_o = \frac{-\phi \ln\left(\frac{r_o}{r_i}\right)}{2\pi kL} + T_i$$

So

$$T_o = \frac{-3149.6354 \times \ln\left(\frac{0.015875}{0.013716}\right)}{2\pi \times 40 \times 5.4864} - 22.5 = -22.83^{\circ} C$$

Bromley's correlation is thus applied where $\Delta T = T_o - T_{sat}$, giving

$$\alpha_o = 0.62\left[\frac{0.01921^3 \times 1.1008(675.6757 - 1.1008) \times 9.81 \times (1355.95 + 0.4 \times 2.201 \times 5.866)}{0.03175 \times (9.3879 \times 10^{-6}) \times 5.866}\right]^{1/4}$$

So

$$\alpha_o = 49.369 \text{ Wm}^{-1}\text{K}^{-1}$$

Next, applying Mostinski from equation 5.2.14.

$$p_R = \frac{1.28}{112.9} = 0.0113$$

The pressure ratio function is

$$f(p_R) = 1.8(0.0113)^{0.17} + 4(0.0113)^{1.2} + 10(0.0113)^{10} = 0.859$$

Thus

$$\alpha_o = 0.106 \times 112.9^{0.69} \times 3149.6354^{0.7} \times 0.859011 = 667.4967 \text{ Wm}^{-2}\text{K}^{-1}$$

For Cooper's correlation using a surface roughness figure from (Welty, p183), applying equation 5.2.17.

$$\alpha_o = 55 \times 0.0113^{0.12 - \log_{10} 0.127} \times (-\log_{10} 0.0113)^{-0.55} \times 17.0304^{-0.5} \times 3149.6354^{2/3}$$

$$= 20.94 \text{ Wm}^{-2}\text{K}^{-1}$$

However, the more common range of values for ε, is given by Webb et al as 0.3- 0.5. So applying the value of 0.5, we have a more realistic $298.967 \text{ Wm}^{-2}\text{K}^{-1}$.

Chen's correlation applied to the design conditions requires a detailed series of calculations.

Firstly, the Reynolds number for the liquid phase is required. The effective area approaching the first row of tubes is calculated to be 3.603 m^2. The other required values are taken from the tables of properties in Appendix D The mass flow rate is 1.06 kgs^{-1}, which gives an upstream velocity of-

$$u = \frac{1.06}{675.6757 \times 3.603} = 4.354 \times 10^{-4} \text{ ms}^{-1}$$

In equation 5.2.24 the tube pitch is 39.6875 mm, so

$$\text{Re}_l = \frac{675.6757 \times \dfrac{39.6875}{2(39.6875 - 31.75)} \times 4.354 \times 10^{-4} \times (1 - 0.06493) \times 0.03175}{269.181 \times 10^{-6}}$$

$$\mathrm{Re}_l = 80.773$$

The Martinelli parameter X is found from equation 5.2.25-

$$X = \left(\frac{1-0.06493}{0.06493}\right)^{0.9}\left(\frac{1.008}{675.6757}\right)^{0.5}\left(\frac{269.181}{9.3879}\right)^{0.1} = 0.5958$$

So

$$\frac{1}{X} = 1.6782$$

From the chart the two-phase heat transfer coefficient is 3.7. The two-phase Reynolds number is found from equation 5.2.26-

$$\mathrm{Re}_{TP} = 94.12 \times 3.7^{1.25} = 414.492$$

The best estimate from the chart of S versus Re_{TP}, gives a suppression factor of 0.95. Applying this to the Forster-Zuber correlation in equation 5.2.19 and using $\Delta P_{sat} = 40{,}200\ \mathrm{kNm^{-2}}$, gives

$$\alpha_{nb} = \frac{0.95 \times 0.0012 \times 5.886^{0.24} \times 40{,}200^{0.75} \times 4489^{0.49} \times 675.6757^{0.49} \times 0.6057^{0.79}}{0.03293^{0.5} \times 1{,}357{,}210^{0.24} \times \left(269.181 \times 10^{-6}\right) \times 1.008^{0.24}}$$

$$\alpha_{nb} = 460.925\ \mathrm{Wm^{-2}K^{-1}}$$

From equations 5.2.20 and 5.2.21 h_{fc} is found.

$$\Pr_l = \frac{\left(270.337\times10^{-6}\right)\times 4489}{0.6057} = 2.003$$

So

$$\alpha_{fc} = \frac{3.7\times0.0023(80.773)^{0.8}\times6.852^{0.4}\times0.6057}{0.03175} = 7.194\ \text{Wm}^{-2}\text{K}^{-1}$$

So from equation 5.2.18

$$\alpha_o = 460.8387\ \text{Wm}^{-2}\text{K}^{-1}$$

The overall heat transfer function can now be calculated using the different possible combinations of heat transfer coefficients and the tube thermal conductivity for comparison with the log mean temperature difference method. These are shown below after insertion into equation 5.2.3.

Firstly, for laminar brine flow and applying Bromley, Mostinski, Cooper and lastly Chen.

$$U_i = \frac{1}{\dfrac{1}{1358.447} + \left[\dfrac{0.015875\ln\left(\dfrac{0.015875}{0.013716}\right)}{40}\right] + \dfrac{0.013716}{0.015875\times49.354}} = 54.6434\ \text{Wm}^{-2}\text{K}^{-1}$$

$$U_i = \frac{1}{\frac{1}{1358.447} + \left[\frac{0.015875\ln\left(\frac{0.015875}{0.013716}\right)}{40}\right] + \frac{0.013716}{0.015875\times 662.311}} = 476.491\ \mathrm{Wm^{-2}K^{-1}}$$

$$U_i = \frac{1}{\frac{1}{1358.447} + \left[\frac{0.015875\ln\left(\frac{0.015875}{0.013716}\right)}{40}\right] + \frac{0.013716}{0.015875\times 298.969}} = 271.438\ \mathrm{Wm^{-2}K^{-1}}$$

$$U_i = \frac{1}{\frac{1}{1358.447} + \left[\frac{0.015875\ln\left(\frac{0.015875}{0.013716}\right)}{40}\right] + \frac{0.013716}{0.015875\times 468.119}} = 378.812\ \mathrm{Wm^{-2}K^{-1}}$$

Secondly, for transition brine flow and applying Bromley, Mostinski, Cooper and lastly Chen.

$$U_i = \frac{1}{\frac{1}{1265.095} + \left[\frac{0.015875\ln\left(\frac{0.015875}{0.013716}\right)}{40}\right] + \frac{0.013716}{0.015875\times 49.354}} = 54.482\ \mathrm{Wm^{-2}K^{-1}}$$

$$U_i = \frac{1}{\frac{1}{1265.095} + \left[\frac{0.015875 \ln\left(\frac{0.015875}{0.013716}\right)}{40}\right] + \frac{0.013716}{0.015875 \times 662.311}} = 464.470 \text{ Wm}^{-2}\text{K}^{-1}$$

$$U_i = \frac{1}{\frac{1}{1265.095} + \left[\frac{0.015875 \ln\left(\frac{0.015875}{0.013716}\right)}{40}\right] + \frac{0.013716}{0.015875 \times 298.969}} = 267.494 \text{ Wm}^{-2}\text{K}^{-1}$$

$$U_i = \frac{1}{\frac{1}{1265.095} + \left[\frac{0.015875 \ln\left(\frac{0.015875}{0.013716}\right)}{40}\right] + \frac{0.013716}{0.015875 \times 468.119}} = 371.174 \text{ Wm}^{-2}\text{K}^{-1}$$

Lastly, for turbulent brine flow and applying Bromley, Mostinski, Cooper and lastly Chen.

$$U_i = \frac{1}{\frac{1}{2993.251} + \left[\frac{0.015875 \ln\left(\frac{0.015875}{0.013716}\right)}{40}\right] + \frac{0.013716}{0.015875 \times 49.354}} = 448.452 \text{ Wm}^{-2}\text{K}^{-1}$$

$$U_i = \frac{1}{\frac{1}{2993.251} + \left[\frac{0.015875\ln\left(\frac{0.015875}{0.013716}\right)}{40}\right] + \frac{0.013716}{0.015875 \times 662.311}} = 589.406\ \text{Wm}^{-2}\text{K}^{-1}$$

$$U_i = \frac{1}{\frac{1}{2993.251} + \left[\frac{0.015875\ln\left(\frac{0.015875}{0.013716}\right)}{40}\right] + \frac{0.013716}{0.015875 \times 298.969}} = 304.689\ \text{Wm}^{-2}\text{K}^{-1}$$

$$U_i = \frac{1}{\frac{1}{2993.251} + \left[\frac{0.015875\ln\left(\frac{0.015875}{0.013716}\right)}{40}\right] + \frac{0.013716}{0.015875 \times 468.119}} = 457.643\ \text{Wm}^{-2}\text{K}^{-1}$$

Applying the design conditions to the compressor model gave the following results. In order to establish the mass flow rate of ammonia through the compressor, the two streams must be evaluated.

From equation 5.2.28 the mass flow rate was found.

$$\dot{m} = \frac{1353.391}{(1 - 0.1431)(1406 - 138.6)} = 1.23\ \text{kgs}^{-1}$$

This figure was inserted into equation 5.2.29 to establish the compressor heat input (at this stage, the heat removed by the lubricating oil is not dealt with, this was considered at the COP calculation).

$$W = 1.23(1-0.1431)(1407.5-1625.7)+1.23\times 0.1431(1433.5-1625.7) = -263.297\text{ kW}$$

The volume ratio of the compressor was found from equation 5.2.32

$$V_i = \left(\frac{12.03}{1.26}\right)^{\frac{1}{1.69}} = 3.81$$

From the chart shown in *Appendix H*, the compressor load was found to be 76%.

The chiller performance was next evaluated using equation 5.2.34 to find the COP. In this instance the oil heat removal must be included since this is heat input from the compressor, which is removed during compression. The COP is found from equation 5.2.34 with the oil heat removal calculated from equation 5.2.35 first.

$$Q_{oil} = 3.7\times 2.02(86.6-48.9) = 281.35\text{ kW}$$

So the COP is given as-

$$COP = \frac{-1.23(1-0.1431)(138.6-1406)}{281.35+1.23(1-0.1431)(1625.7-1407.5)+1.23\times 0.1431(1625.7-1433)} = 2.46$$

The COSP, including the brine internal pump power of 46.1 kW in the denominator, which gives a value of 2.27.

The second law analysis applied to the design conditions gave the results detailed below. It was found that the COP required manipulation to accommodate the specific value of irreversibility (kJ/kg). From the previous calculation to determine the mass flow rate of ammonia via the flash economiser and the evaporator to the compressor, a mass ratio was calculated. This allows the irreversibility to be calculated for 1 kg of ammonia traversing the system. The modified COP was then calculated maintaining the same oil cooling effect. The mass ratio split the ammonia flow 0.8618 kg through the evaporator to 0.1382 kg from the flash economiser. The modified COP was calculated to be 2.203.

The Carnot COP was then calculated from equation 5.2.39.

$$COP_{Carnot} = \frac{1}{\left(\frac{295.15}{252.15} - 1\right)} = 5.8640$$

This allowed the irreversibility to be calculated. The refrigerating effect was divided by 1.23 to give the specific value per kilogram. Thus the irreversibility for 1 kg of ammonia was calculated from equation 5.2.40.

$$i = 1267.40\left(\frac{1}{2.2023} - \frac{1}{5.8640}\right) = 359.3642\ \text{kJkg}^{-1}$$

The individual component irreversibilities were then calculated for the main components using equation 5.2.44.

For the evaporator

$$i = 289.15\left[(5.7670 - 0.5713) + \frac{1267.40}{252.15}\right] = 48.961\,\text{kJkg}^{-1}$$

For the compressor

$$i = \frac{289.15\left[\left(1.06 \times (5.4430 - 5.7670) + \frac{281.35}{295.15}\right) + \left(0.17 \times (5.4430 - 5.5410) + \frac{281.35}{295.15}\right)\right]}{1.23} = 125.319\text{kJkg}^{-1}$$

For the condenser

$$i = 289.15\left[(1.2020 - 5.4430) + \frac{1302.7}{295.15}\right] = 49.933\,\text{kJkg}^{-1}$$

For the throttle processes

$$i = 289.15(1.255 - 1.2020) = 15.325\,\text{kJkg}^{-1}$$

$$i = 289.15(5.5410 - 5.5460) = 21.433\,\text{kJkg}^{-1}$$

$$i = 289.15(0.5713 - 0.5546) = 4.929\,\text{kJkg}^{-1}$$

The total of these irreversibilities was 265.889 kJkg^{-1})

There is a large difference in the irreversibility calculated for the cycle using the two methods. Since the most complex component was the compressor, the difference was attributed to the compressor. This gives a revised compressor irreversibility of 218.784 $kJkg^{-1}$.

This assumption is made based on the straightforward reversibility calculations applied to the evaporator, condenser and throttling processes. The flash economiser is regarded as reversible since the mixture of liquid and vapour is equal to entropies of the two phases.

The availability of the chillers was calculated as the reversible work in the heat engine defined by equation 5.2.43.

$$\Psi = 1343.44\left(1 - \frac{289.15}{252.15}\right) = 197.13\,\text{kW}$$

The adiabatic efficiency of the compressor was calculated from equation 5.2.46.

$$\eta_c = - = 0.483$$

The reversible work for the compressor was found from equation 5.2.48.

$$W_{rev} = 218.748 - 545.317 = -326.553\,\text{kJkg}^{-1}$$

This allowed a second law efficiency to be calculated from equation 5.2.47.

$$\eta_{II} = \frac{-326.553}{-545.317} = 0.599\,.$$

The second law effectiveness of the chiller was calculated from equation 5.2.49.

$$\varepsilon_{II} = \frac{-197.153}{-545.317} = 0.3615$$

5.4 Discussion

The correlations described above allow a detailed thermodynamic and heat transfer analysis of the chiller to be conducted. However a more refined approach to the evaluating the heat transfer coefficients could be applied by breaking the evaporator into elements for each tube pass through it.

It is possible to estimate the temperature of brine leaving each tube pass of the evaporator using the heat exchanger effectiveness or NTU (Number of Transfer Units) method. The NTU is defined as the ratio of the temperature change of one of the fluids divided by the mean driving force between the fluids.

The heat exchanger effectiveness is calculated as

$$\varepsilon = \frac{q}{q_{\max}}$$

Where $q_{\max}$ is defined as

$$q_{\max} = C_c (T_i - t_i)$$

For vapour boiling conditions the effectiveness is given from

$$\varepsilon = 1 - e^{-NTU}$$

Where NTU is given by

$$NTU = \frac{U_i A_i}{C_{\min}}$$

Thus having obtained the effectiveness of the heat exchanger, from

$$q_{\max} = C_c (T_i - T_o)$$

The temperature of the brine at the outlet of the tube pass can be calculated, and the cumulative calculation to the outlet of the sixth pass can be compared to the figure calculated from 5.2.1 above.

An average overall coefficient of heat transfer value for the evaporator can be calculated from internal flow and external boiling correlations and the thermal conductivity of the tube material.

The analysis above primarily models the primary refrigerant and its interface with the secondary refrigerant in the evaporator. The brine secondary refrigerant system thermal storage tank is used to buffer the effects of temperature changes in the brine caused either as a result of additional or reduced coolant user loads. The impact of this is observed when comparing the differential flow rate totals between the internal chiller pump array and the external brine system pump array.

The dynamics of the thermal storage tank are modelled using the principle of conservation of energy across the boundaries of the tank.

$$E_{out} = E_{in} + E_{generated} + E_{consumption} + E_{accumulation}$$

Depending upon the origination of flow to the tank the result will be a temperature rise or fall. A more extensive analysis of the system would encompass the secondary refrigerant system. However, that was beyond the scope of this study.

More detailed discussion of the applicability of the models is contained in Chapter 6.0, which reviews the results of the test procedures conducted in Chapter 4.0.

6.0 Results

6.1 Chapter summary

Employing the test procedures detailed in Chapter 4.0, the heat transfer performance of four chillers was analysed using a number of correlations explained in chapter 5.0. The results of the various combinations of heat transfer correlations giving the overall coefficient of heat transfer were identified. The energy performance of the system was reviewed for various combinations of running chillers. A second law analysis of each running condition was conducted. The complexity of the compressors led to problems in identifying irreversibilities in those parts of the chillers. This was overcome by using the Carnot COP method to identify the cycle irreversibilities.

Keywords: heat transfer coefficient, COP, energy performance, second law analysis

6.2 Comparison of overall heat transfer coefficients

The models described in Chapter 5.0 were applied using the measured and inferred data from the test procedures outlined in Chapter 4.0. The results of the calculations for each procedure are shown in *Appendix B.*

The first result in figure 6.2.1, shows the case for laminar brine flow, with boiling heat transfer coefficients calculated using Bromley's (U_{11}), Mostinski's (U_{12}), Cooper's (U_{13}) and Chen's (U_{14}) correlations. Each correlation is compared to the overall heat transfer coefficient (U_{lm}) calculated using the log mean temperature difference and refrigerating capacity. The results are plotted from left to right for each chiller in each test procedure in ascending order.

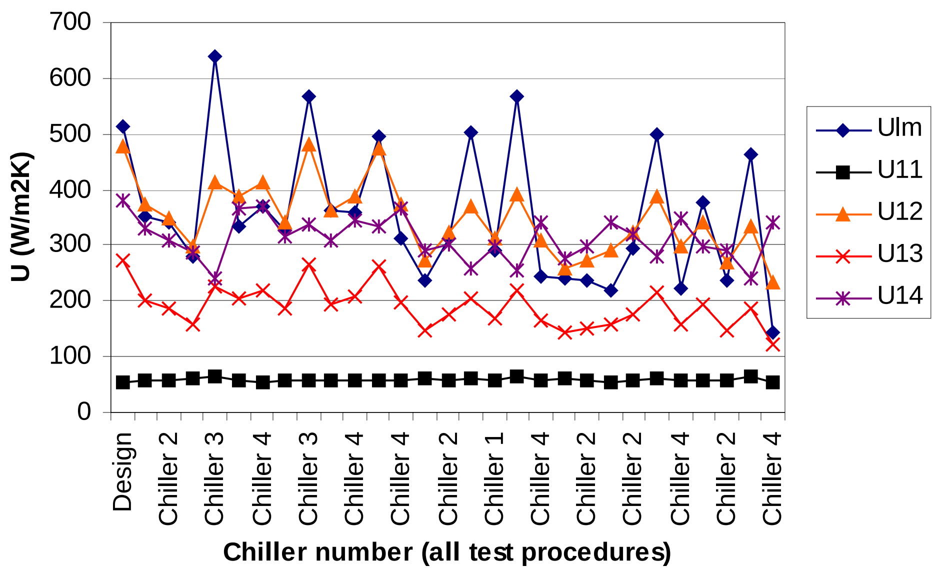

Figure 6.2.1 Comparison of calculated overall heat transfer coefficients for laminar brine flow

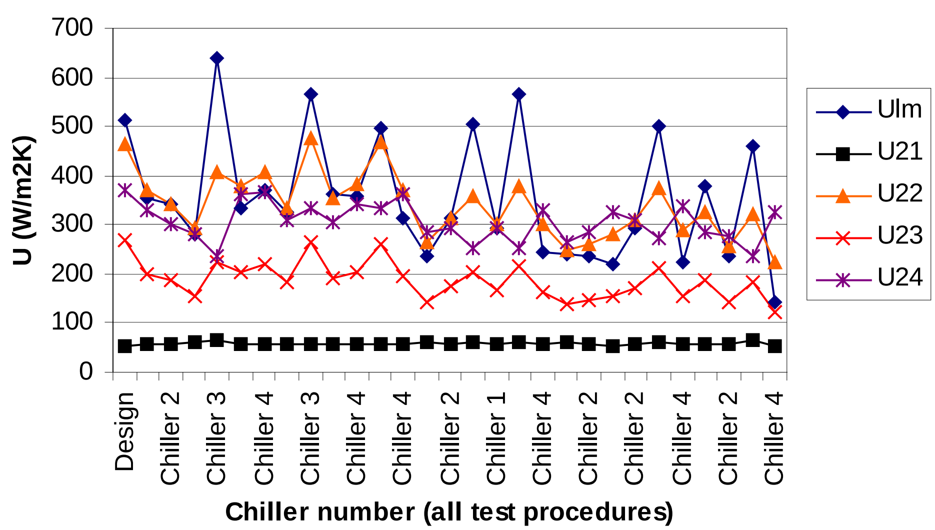

Figure 6.2.2 Comparison of calculated overall heat transfer coefficients for transition brine flow

The results plotted on figure 6.2.2, show the case for brine flow in the transition region between laminar and turbulent flow. As for laminar flow, the four boiling heat transfer correlations, Bromley's (U21), Mostinski's (U22), Cooper's (U23) and Chen's (U24) were applied to the model.

The third case is for brine flow in the turbulent region. The results applying the four correlations as before Bromley's (U31), Mostinski's (U32), Cooper's (U33) and Chen's (U44), are shown in figure 6.2.3.

The model was intended to analyse laminar flow where applicable. In order to evaluate the case with laminar flow, the model was applied assuming fully developed flow. Although the results of the model showed the calculated entry length to be in excess of the actual tube length, the correlation for fully developed laminar flow. Equation 5.2.9 for Nu was applied.

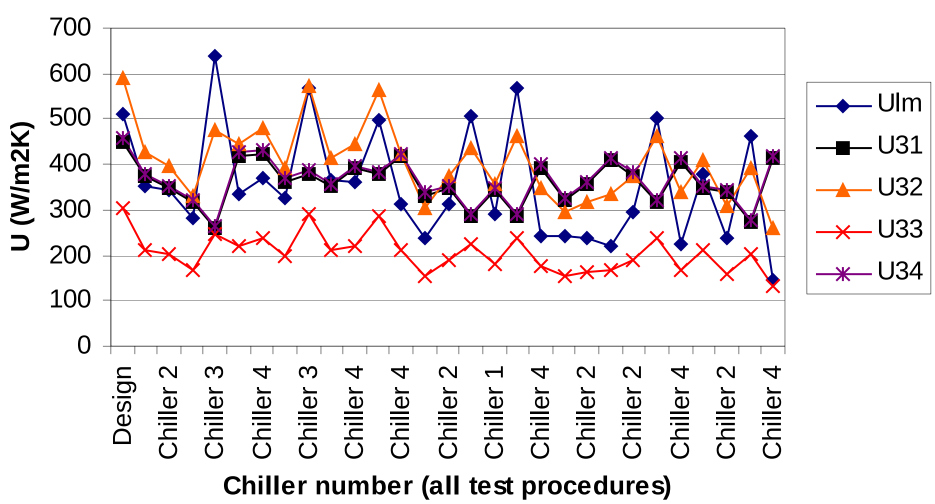

Figure 6.2.3 Comparison of calculated overall heat transfer coefficients for turbulent brine flow

Deviation from the expected value of U for each the combinations is analysed in table 6.2.1 below.

Table 6.2.1. Deviation statistics for all heat transfer coefficient correlation combinations

Overall Heat Transfer Coefficient Combination U_{nn}	Maximum –ve Deviation from U_{lm} (%)	Maximum +ve Deviation from U_{lm} (%)	Median Deviation from U_{lm} (%)	Mean Deviation from U_{lm} (%)
U_{11}	-89.77	-62.12	-75.95	81.67
U_{12}	-35.38	60.97	12.80	16.34
U_{13}	-64.46	-14.91	-36.69	43.39
U_{14}	-52.76	150.88	49.06	31.85
U_{21}	-89.71	-62.45	7 6.08	81.77
U_{22}	-36.21	55.2	9.50	15.15
U_{23}	-64.72	-16.55	-40.14	44.42
U_{24}	-53.2	137.15	41.98	29.78
U_{31}	-47.57	206.4	79.42	45.43
U_{32}	-25.56	81.77	28.11	25.71
U_{33}	-61.88	-9.43	35.56	39.13
U_{34}	-46.77	212.58	82.91	47.37

It is apparent that for all cases other than design conditions, values of U_{lm} above 500 and below 200 $Wm^{-2}K^{-1}$, had very large deviations between the correlated U value and Ulm. Filtering out these "extreme" values the trend lines for correlated values follow the Ulm values much more closely. For the transition and turbulent brine flow cases, the results are shown in figure 6.2.4 and 6.2.5 respectively. Here the best combinations are transition brine flow with Mostinski and Chen.

For turbulent brine flow conditions the best combination is with Mostinski. The combinations with Bromley, Cooper and Chen have relatively larger deviations.

Table 6.2.2 shows the deviation statistics with "extreme" values filtered out. The Laminar flow case is not now considered, since the values of Re in the tests was above the typical values of below 2000. This meant that al of the data from chiller No.3 was filtered out.

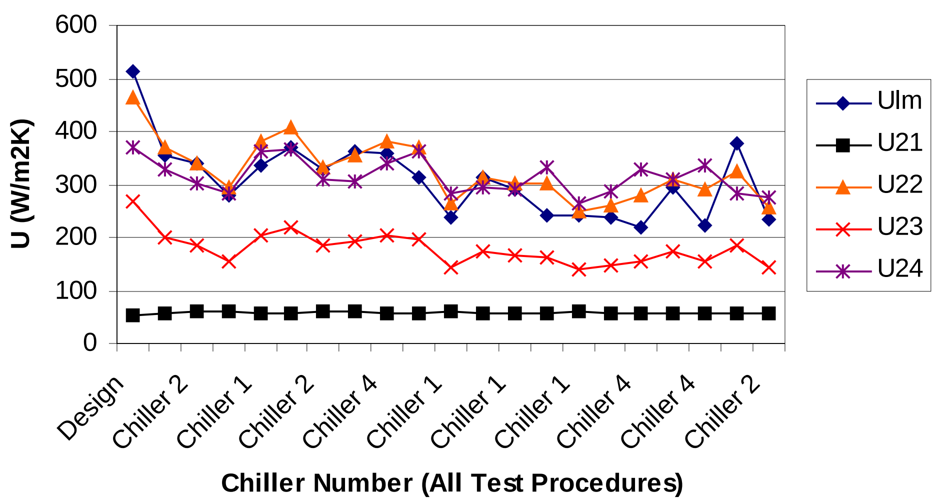

Figure 6.2.5 Comparison of calculated overall heat transfer coefficients for turbulent brine flow
with extremities filtered out

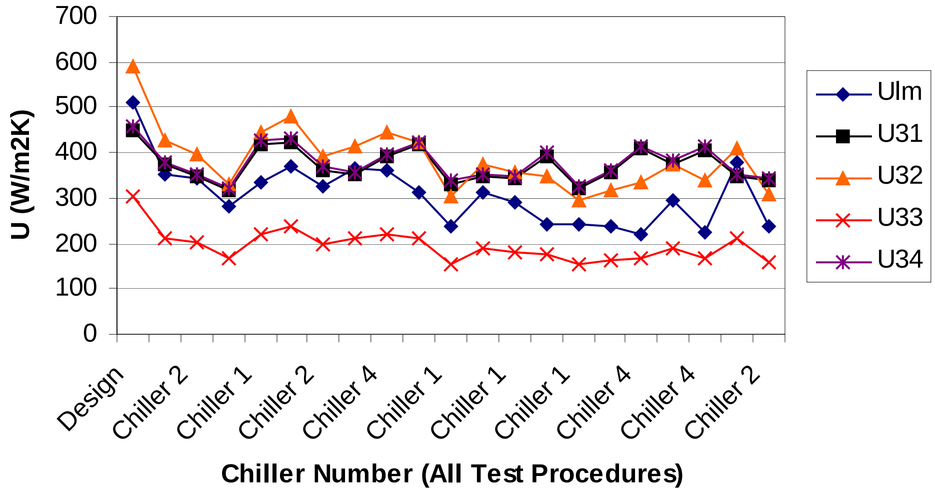

Figure 6.2.4 Comparison of calculated overall heat transfer coefficients for transition brine flow with extremities filtered out

Table 6.2.2. Deviation statistics for all heat transfer coefficient correlation combinations with extremities filtered out

Overall Heat Transfer Coefficient Combination U_{nn}	Maximum –ve Deviation from U_{lm} (%)	Maximum +ve Deviation from U_{lm} (%)	Median Deviation from U_{lm} (%)	Mean Deviation from U_{lm} (%)
U_{21}	-89.37	-74.92	82.15	84.49
U_{22}	-14.18	29.93	7.88	10.44
U_{23}	-50.61	-29.96	-40.29	43.29
U_{24}	-15.55	63.47	23.96	22.58
U_{31}	6.93	109.29	58.11	45.37
U_{32}	8.79	52.45	30.62	28.47
U_{33}	-40.76	24.04	32.4	37.55
U_{34}	8.91	103.95	56.43	48.30

6.3 Thermodynamic performance of the chillers

For each of the performance tests conducted the Coefficient of Performance (COP) was calculated. This compared the refrigerating capacity with the equivalent heat input to the compressor. In addition the Coefficient of System Performance (COSP) was calculated for each chiller. This compared the refrigerating effect of the chiller with the total electrical power consumed by the compressor and pump. From a cost perspective COSP gives a better indication of the system's energy performance.

The refrigerating effect versus COP for each chiller in the two, three and four chiller combinations are shown in figures 6.3.1, 6.3.2 and 6.3.3 below.

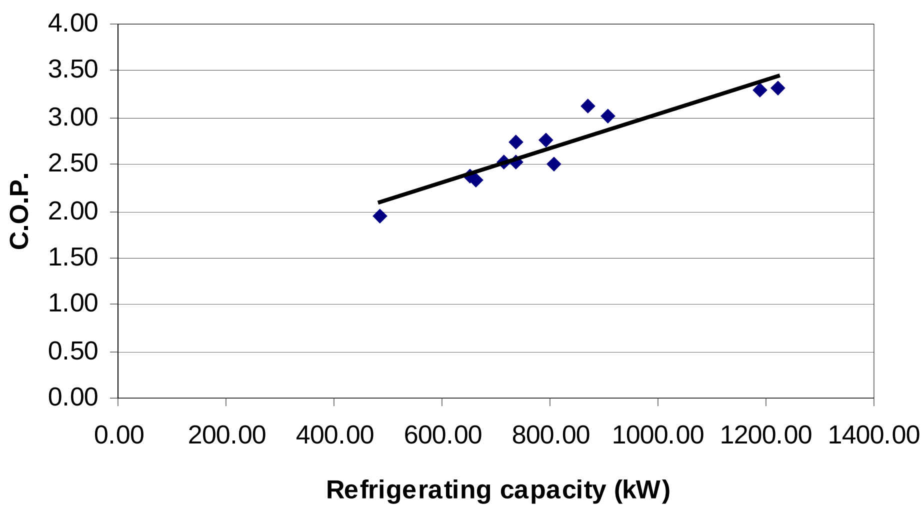

Figure 6.3.1 Refrigerating capacity versus C.O.P. for combinations of two chillers

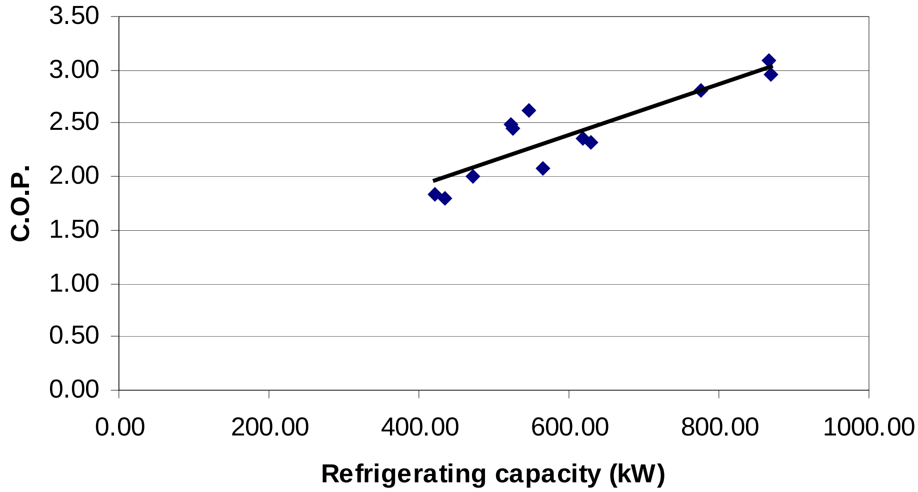

Figure 6.3.2 Refrigerating capacity versus C.O.P. for combinations of three chillers

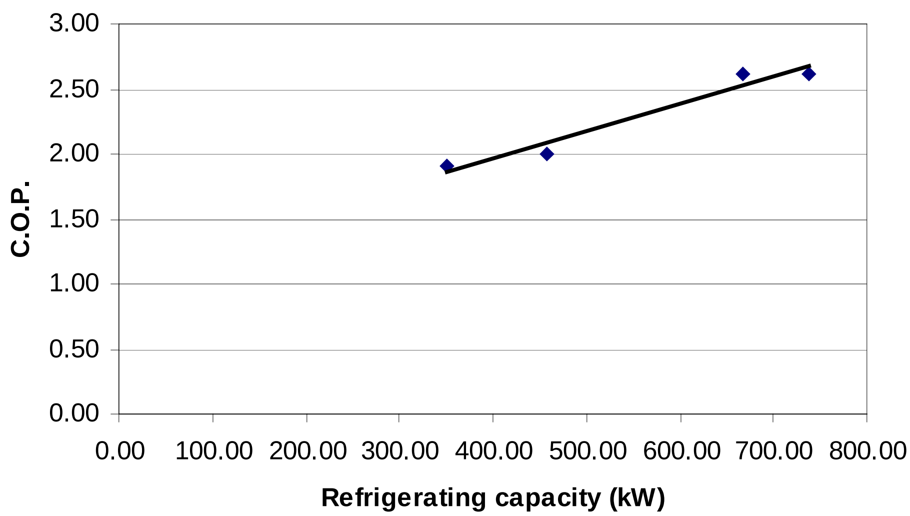

Figure 6.3.3. Refrigerating capacity versus C.O.P. for combination of four chillers

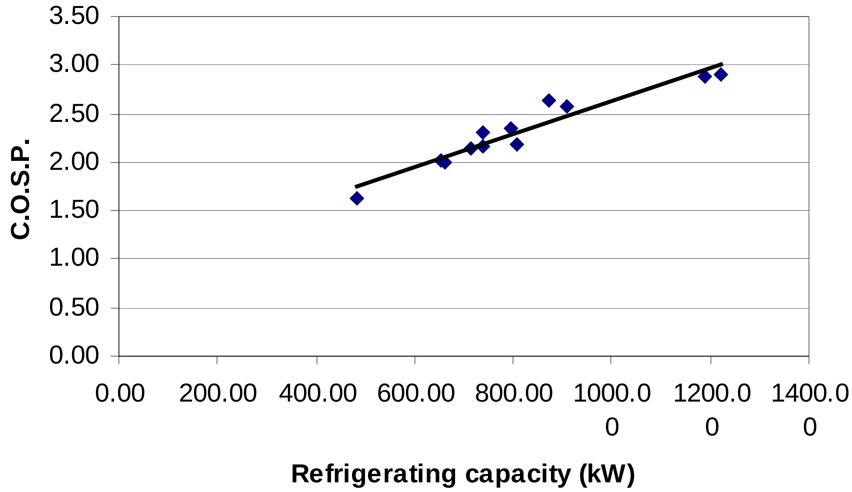

Figure 6.3.4 Refrigerating capacity versus C.O.S.P. for combinations of two chillers

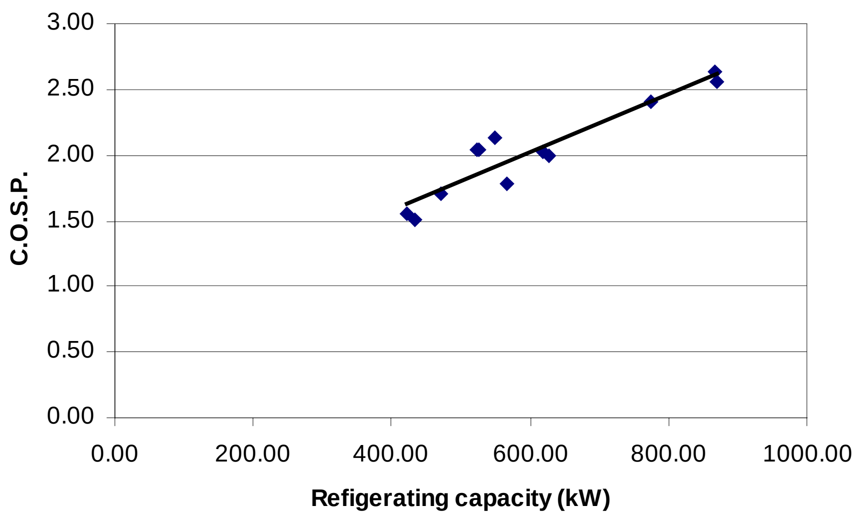

Figure 6.3.5 Refrigerating capacity versus C.O.S.P. for combinations of three chillers

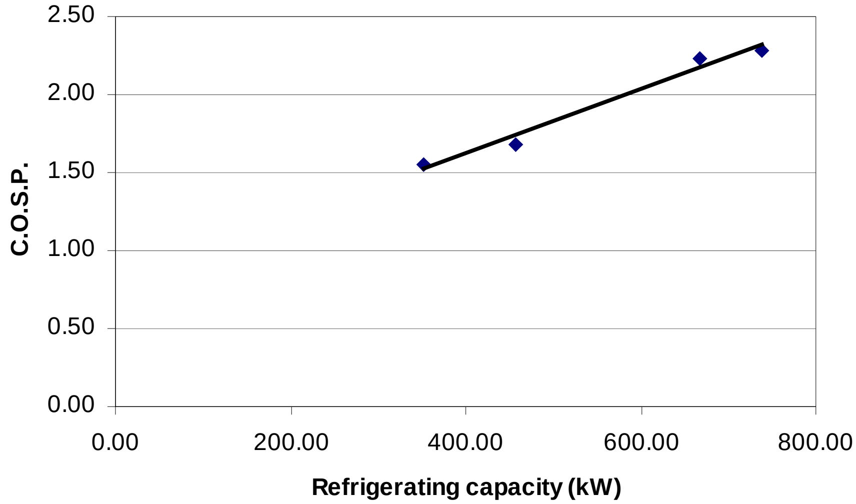

Figure 6.3.6 Refrigerating effect versus C.O.S.P. for combination of four chillers

6.4 Compressor Performance

From the performance tests, the pressure ratio and hence the volume ratio of the compressors was calculated. This allowed the loading of the compressors to be derived from the chart shown in figure H1 in *Appendix H*. A plot of refrigerating effect versus percentage of compressor capacity is shown in figure 6.4.1 below.

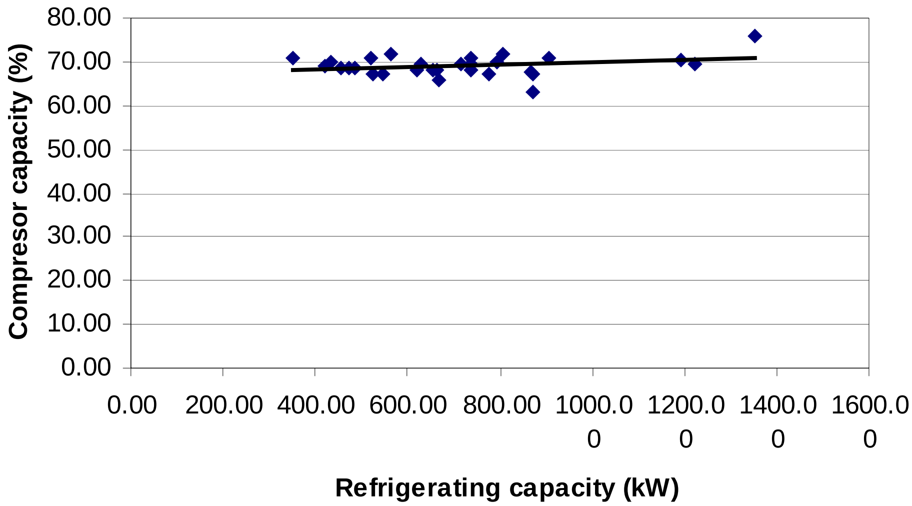

Figure 6.4.1 Refrigerating capacity versus compressor capacity

6.5 Second law analysis

Using the test data collected and applying the model for a second law analysis, a number of results were calculated.

Figure 6.5.1 below tabulates the results for actual, isentropic and reversible work for each compressor in each test procedure. As before the compressors are plotted ordinally for each procedure from left to right. This applies to all the plots shown below.

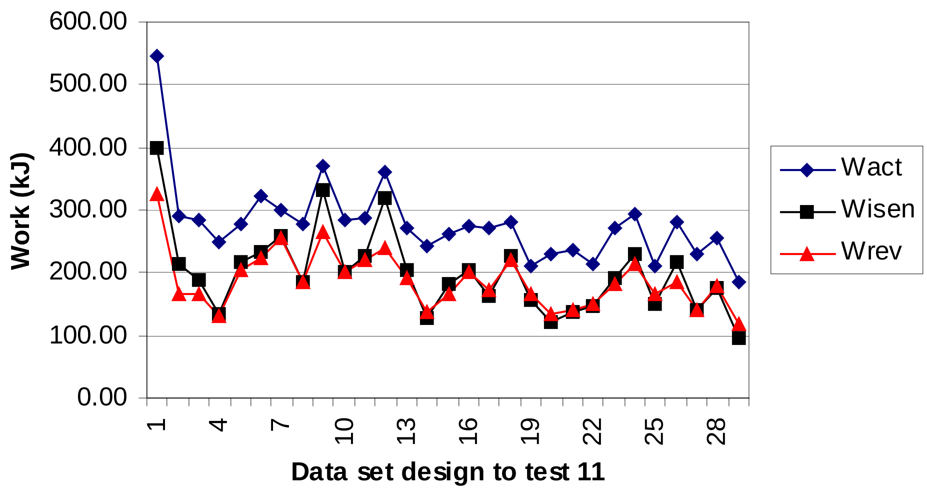

Figure 6.5.1 Comparison of compressor actual work with isentropic and reversible work

Figure 6.5.2 shows the comparison of individual irreversibilities calculated for each chiller with the Carnot COP method for the cycle. Figure 6.5.3 shows the plot of Carnot COP's versus refrigerating capacity. Figure 6.5.4 compares the second law efficiencies and effectiveness. Lastly, figure 6.5.5 shows the plot of heat engine availability for each chiller in each test procedure.

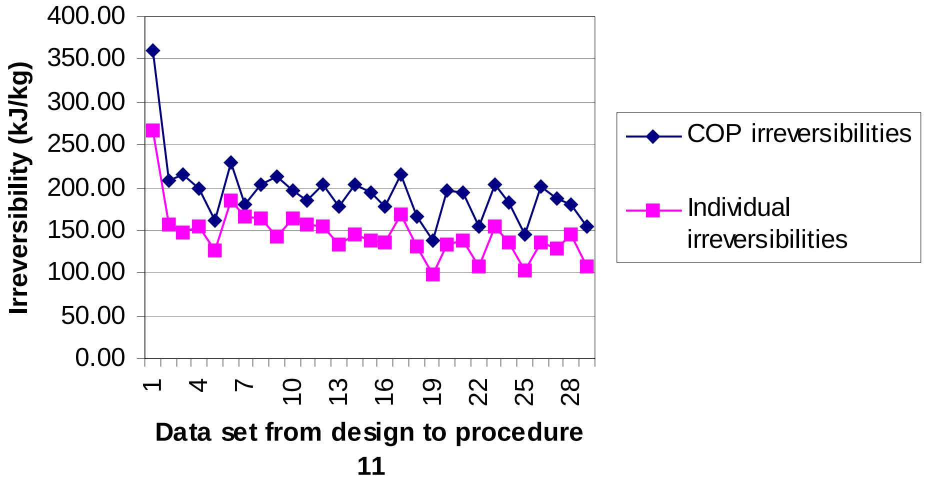

Figure 6.5.2 Comparison of cycle irreversibilities from COP and individual methods

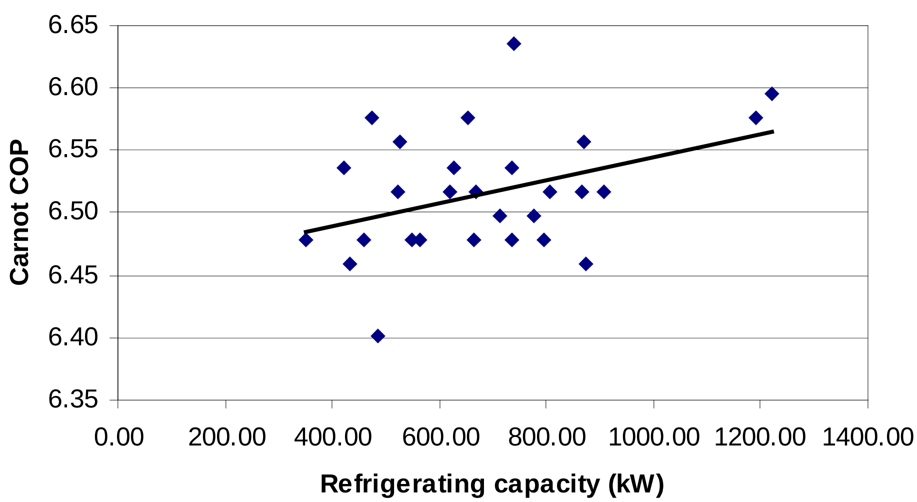

Figure 6.5.3 Carnot COP versus refrigerating capacities

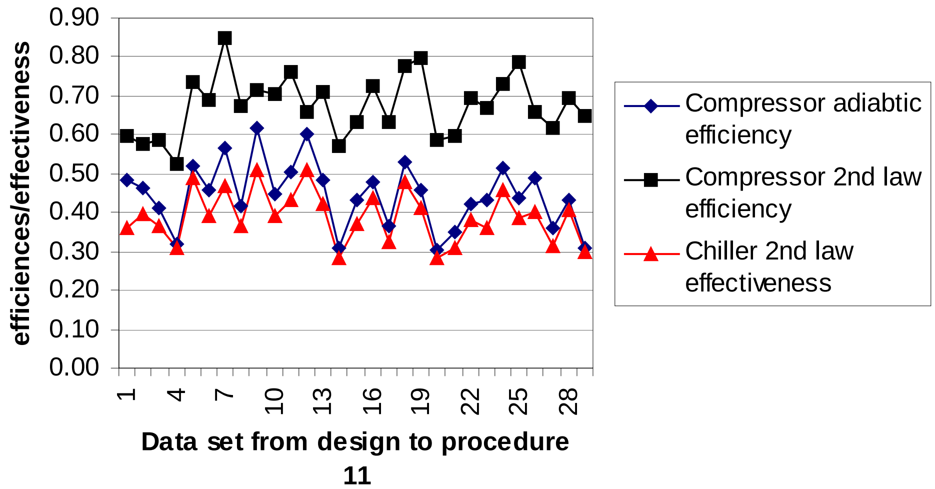

Figure 6.5.4 Comparison of compressor second law efficiencies and effectiveness

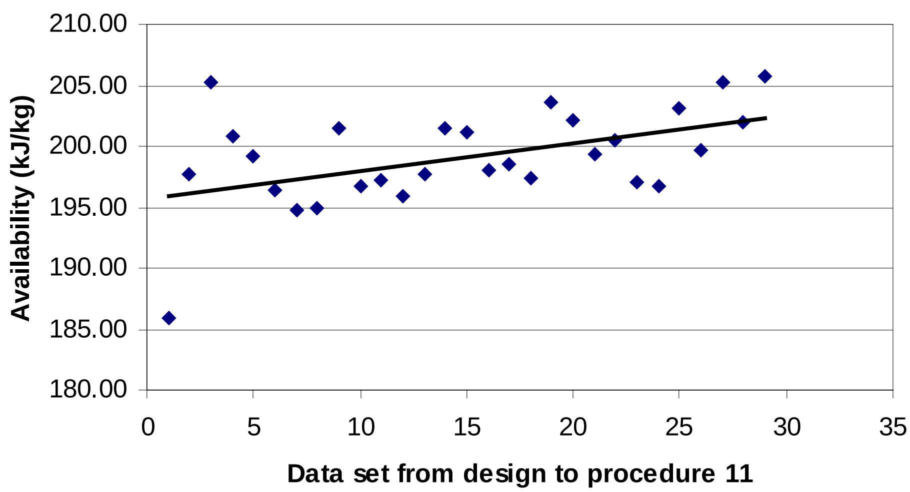

Figure 6.5.5 Heat engine availability for chillers

6.6 Discussion and Conclusions

A detailed discussion on the results found is conducted in chapter 7.0. However, some points worthy of note are around the detail required to calculate the properties used in the calculations in this chapter.

The properties of brine and ammonia used are tabulated in the Appendices C and D. Significant manipulation and calculation was required to find the values required to perform the analyses.

Bearing in mind the accuracy available from some of the field instrumentation, the accuracy of the results may vary as the range of measurements as shown in the tables in Appendix A are to varying significant figures.

The model however is robust and would yield results with increasing accuracy as the accuracy of the data entered improved.

It is concluded that the model yielded useful results based on the data entered and is a valid tool for analysis of the brine chiller system. The model could be applied to theoretical situations for the chillers although the analysis conducted was for real measurements from the system in operation.

7.0 Discussion

7.1 Chapter summary

The results of the test procedures compiled in chapter 6.0 were discussed and the best-fit heat transfer correlations identified based on the test conditions. The thermodynamic performances of the chillers were reviewed and further evaluated based on the loading and refrigerating effect. Both first and second law analyses were discussed. The performance of the compressors was discussed and the significance of compressor loading evaluated. The accuracy of the results based on measured and calculated inputs to the model affecting the outputs is considered. The number of chillers on line for a given heat load was considered with the lowest number on line with higher individual loadings shown to be the best operating condition. The future application of chiller models was discussed.

Keywords: heat transfer coefficient, COP, energy performance, second law analysis

7.2 Review of results

7.2.1 Overall heat transfer coefficients

The brine Reynolds number in all of the chillers in each test procedure was above 2300. Normally, this is the barrier below which flow is considered to be laminar. However, as stated in Chapter 4.0, laminar flow has been observed with Re up to 50,000. Laminar flow seems unlikely in a multi-pass heat exchanger, although there were concerns over low Reynolds numbers at the design stage due to re-using existing pumps.

In nine of the 25 chiller runs, brine flow was in the transition region where 2300 < Re < 4000. The remaining brine flow conditions were in the turbulent region with Re > 4000.

The results from the model for the convective coefficient of heat transfer due to internal flow of brine, show that the values for laminar flow were greater than those for transition flow by typically 10%. The turbulent flow coefficient was normally in excess of twice the value obtained from the laminar or transition flow conditions.
When calculating the ammonia side two-phase Reynolds number for use in the Chen correlation, the value was extremely low, being below 500 in each case. This agreed with the values found by Webb et al (1989).

This meant that the suppression factor S for use in the Forster Zuber correlation did not fall directly in the area of the graph with plotted values. However since the line was tending toward a value of 0.95, this was used in all calculations . Webb et al (1989) used a suppression factor of one in their calculations.
The results of filtering out the extremities seem to suggest that for lower heat loads on the chillers, the best combination of correlations is the transition brine flow condition with Mostinski. This is also the case for turbulent brine flow.

For turbulent brine flow conditions the best combination is with Mostinski. The combinations with Bromley, Cooper and Chen have relatively larger deviations.

Table 6.2.2 shows the deviation statistics with “extreme” values filtered out. The Laminar flow case is not now considered, since the values of Re in the tests were above 2000.

The results of filtering out the extremities seem to suggest that for lower heat loads on the chillers, the best combination of correlations is the transition brine flow condition with Mostinski. This is also the case for turbulent brine flow. As can be seen in table 6.2.2, the combinations of coefficient where the median and mean deviations are closest, track the shape of the log mean temperature difference calculated coefficient U_{lm} most closely. These may be best suited to further analysis in any attempt to improve the accuracy of the model.

The values for U_{lm} above 500 $Wm^{-2}K^{-1}$ were all found on chiller No.3. The only value below 200 $Wm^{-2}K^{-1}$ was for chiller No.4.

Reviewing the results for the test procedures shows that chiller No.3 almost always had higher internal brine pump power consumption and hence flow rate. The evaporator pressure in chiller No.3 was usually higher than the other chillers' and therefore had a higher saturation temperature. More often than not the dryness fraction in the evaporator of chiller No.3 was lower than the other chillers'. This wetter ammonia rendered No.3 chiller's evaporator more effective since a greater proportion of the ammonia was available to boil off and cool the brine.

It appears that the secondary refrigerant brine system geometry favours a higher flow rate through No.3 chiller. Coupled with wetter ammonia in the evaporator this accounts for the higher refrigerating effect and therefore higher overall heat transfer coefficient.

The reasons why the combination of correlations to calculate an overall heat transfer coefficient should yield such large deviations from the log mean temperature difference derived value are not obvious. There are a number of potential contributory factors. The previously mentioned measuring errors and the linear interpolation of properties all contribute. In addition, there was no clear mention of ammonia in the literature reviewed which detailed the correlations applied.

7.2.2 Thermodynamic performance of the chillers

In each case for every test procedure, the trend lines show an increase in COP with increasing refrigerating capacity. However, with two chillers on line, the COP appears higher than with three or four chillers on line for the same refrigerating capacity. These differences however, appear marginal.

There is a marked difference in the COSP as the number of chillers on line increases. With only two chillers on line, there is a significant improvement in COSP compared with three or four.

This appears to contradict the observations made prior to the evaluation that the higher number of chillers on line, the better the energy performance of the chillers.

It is also worth noting that the temperature of the cooling water in the condenser was significantly lower than design. The design inlet temperature is 22 ^{o}C, the actual temperature was only 15.5 ^{o}C. This impacts on the condensing temperature and therefore the pressure at the compressor discharge.

This low condenser pressure impacted on the first stage expansion and with three and four chillers on line the pressure was frequently below the 2.75 barg set point for the vapour feed to the compressor. This also lowered the enthalpy of flash vapour to the compressor.

These results are as expected. The impact of the oil cooler on the COP was proportionately higher at lower loads since the oil flow was determined by the discharge pressure of the compressor and not strictly the refrigerant mass flow rate.

7.2.3 Compressor Performance

As expected, the trend line shows an increasing refrigerating effect increases the load on the compressor. The capacity figure shown for the design condition appears above the trend line. This would infer that the chillers are frequently delivering a higher relative refrigerating load with lower load on the compressors than suggested by design. This may be explained by the measuring techniques and subsequent errors arising.

However, the general indication is that a higher chilling load is achieved with a relatively small increase in compressor load. This indicates that running fewer chillers with a higher heat load would absorb significantly less electrical power than the equivalent cumulative load across a greater number of chillers. This is not so surprising since the compressors are very inefficient at lower loads. In any case the margin of gain in refrigerating effect for relatively little increase in compressor load appears to be significant even allowing for errors in measurements. When the absorbed power from the internal pump is taken into account, the case is even stronger on energy efficiency grounds. The COP and COSP analysis in the previous section verified this result.

7.2.4 Second law analysis

Taking the measurements from the test procedures and applying a second law analysis yielded some interesting results. In figure 6.5.1, the adjusted irreversibility applied to the compressors on the chillers yielded a value for reversible work that was almost identical to the isentropic work at most data points.

The chiller systems are more complex than the usual examples quoted in texts for second law analysis. The Carnot principle deals with heat engines operating between two heat reservoirs. The effect of the heat transfer from the ammonia refrigerant to the lubricating oil is significant. In addition there are inevitable heat transfers to and from the environment at various points around the system. This complexity increases the difficulty in analysing the system

The results for reversible work in the system appear to show a clear relationship with isentropic work. This is interesting since the compression process is clearly polytropic rather than adiabatic. If this result is accepted then it is clear that the reversible work and isentropic work could almost be considered equal. This would allow a simpler calculation for irreversibilties in the compressors. The irreversibility could be calculated by replacing the reversible work with the isentropic work in equation 5.4.48. The resultant difference in calculated cycle irreversibilities between the two methods described above would be relatively small.

It is generally found that the isentropic work is lower than the reversible work. In most of the procedures this appears to be the case.

As described in Chapter 5.0, when considering the design conditions, the case was made for attributing the shortfall in component irreversibilities versus the Carnot COP method to the compressor. Figure 6.5.2 shows this shortfall. The trend for both methods appears to show a decrease in ireversibilities as the number of chillers on line increases.

As discussed above, this re-allocation of irreversibility to the compressor derived a reversible work figure almost identical to the isentropic work in most cases. This pattern is too obvious to be ignored and does suggest that the Carnot COP method is accurate and the complexity of the compressor system with the oil cooler and flash port is not readily handled by a straightforward application of equation 5.2.44. If the cooling water flows and temperatures in the oil cooler were readily available, the irreversibility in the compressor could be calculated conventionally. However this facility did not exist and could not be justified on cost.

Figure 6.5.3 shows the spread of Carnot COP versus refrigerating capacity for the various test procedure results. The trend for the Carnot COP appears to increase as the number of chillers on line increases. This is expected since the temperature difference between the high and low temperature reservoirs is closer together at lower loads.

When considering the spread of these results versus and the calculation of the cycle irreversibilities using the Carnot COP and actual COP, the results for the reversible work shown above in figure 6.5.1 seem even more credible.

In terms of the second law performance of the systems, figure 6.5.4 compared the compressor isentropic efficiency, compressor second law efficiency and the chiller second law effectiveness. As the number of chillers on line increases, the general trend is for a decrease in adiabatic efficiency and second law effectiveness of the chillers. Obviously there are peaks and troughs in the results. Conversely, the trend is up for the compressor second law efficiency.

His appears to contradict the analysis from a COP perspective where an increasing number of chillers on line appears to be less effective and more energy intensive than a decreasing number.

The availability of the chillers for each test procedure is shown in figure 6.5.5 below. The trend here appears to be for increasing availability as the number of on line chillers increases. This suggests that as the number of chillers on line increases, the chillers are available to more useful work or chilling.

7.3 Complexity of chiller modelling in relation to control and operating philosophies

A number of the papers reviewed in chapter 3.0 considered application of the models proposed in the control of the equipment modelled. As with most such schemes the main issue would be in the ability of the measuring devices in the systems to feed measurements to the control system. The conventional controllers used on most chiller units are probably sufficient for acceptable operation.

The factors that govern the performance and control of such systems are the condenser temperature (and saturation pressure) and the return temperature and flow of secondary refrigerant. As the mass flow and temperature of the secondary refrigerant increases, the compressor load increases and the throttle device produces a greater refrigerating effect from the evaporator. In a multiple chiller system, it is sufficient to control the number of chillers on line based on the external secondary refrigerant flow rate.

Based on the analysis of the real system following test procedure measurements and entering the data to the model, there is little justification for changing the control philosophy of the plant when a manned control room remains in place.

Based on the results of the analyses there is little justification for changing the philosophy of minimum chillers on line loaded to their maximum. The original observations from on plant that less electrical power would be consumed with more chillers on line with lower refrigerating loads is not supported by the analyses. This is further supported by the second law analyses as discussed above.

In terms of equipment geometry, the literature and the equipment analysed in this document modelled or analysed behaviour in shell and tube heat exchangers. Where operating pressures are relatively low (up to about 20 barg for most refrigeration plant) shell and tube exchangers are prohibitively expensive and large. The alternative of using plate heat exchangers reduces the size and capital cost of equipment. The increased overall heat transfer values for plate heat exchangers compared with shell and tube exchangers allows this. The models used would require adaptation to work with the alternative geometry of plate heat exchangers.

However as environmental pressures increase on refrigerant producers and consumers to minimise the impact on the environment of operating plant. Alternative refrigerants must be sought. In order to better understand their behaviours and applicability predictive models are a valuable means of progressing such assessment.

8.0 Conclusions

A detailed analysis of some key aspects of the thermal behaviour of an industrial brine chilling system consisting of four large chillers was conducted. The heat transfer processes in the evaporators and first and second law thermodynamic analysis of each chiller were modelled and analysed. A spreadsheet model was developed for this purpose. The model was used to analyse all running configurations of the four chillers. From this data, conclusions were reached on the most suitable heat transfer correlations to model the evaporators from a number selected for analysis. The control and operating philosophies for the brine chilling system were reviewed. The following conclusions were reached:

1. When extreme results were filtered out, the combination of correlations which most closely represents the overall heat transfer coefficient for the evaporators for low refrigerating loads was the heat transfer coefficient for transition brine flow with Mostinski's correlation for ammonia boiling.

2. For turbulent brine flow conditions, combining that heat transfer coefficient with Bromley's coefficient for ammonia best represented the overall heat transfer coefficient. In both brine flow conditions above, Chen's and Cooper's correlation for ammonia heat transfer coefficient yielded results which deviated further from the overall heat transfer coefficient than the two selected correlations.

3. Based on the system COP for the number of chillers on line in any given test procedure, for a given refrigerating load (or brine cooling demand) the results suggest that minimising the number of chillers on line and loading them more fully was the most energy efficient operating philosophy. This was verified from the performance of the compressors where most efficient performance was achieved with higher loadings on the compressors.

4. The second law analyses of the system suggested that with more chillers on line, the adiabatic efficiency and second law effectiveness of the chillers decreased. However, the second law efficiency of the compressors appeared to increase as the number on line increased. These results considered the heat load with respect to the number of chillers on line.

5. The availability of the system increased as the number of chillers on line increased. This was as expected as there was more available capacity for chilling.

6. The Carnot COP method for calculating system irreversibilties was more straightforward to use than calculating the individual component irreversibilties. This was due to the complexity of heat loss calculations from the compressors, where oil cooling and carry-over plus other losses contributed to the problem.

7. The operating and control philosophy in place at the time of the analyses is the most effective. The number of chillers on line was minimised and increased based on heat load from external users.

8. The accuracy of the model would increase as the accuracy of measured parameters increased.

9. Modelling such as that described in this document is valid. The energy performance of industrial chillers is a key concern for operators. Developing and modelling heat transfer correlations will be vital in aiding cost effective design of heat exchangers as new refrigerants are developed.

9.0 Recommendations

It is recommended that:

1. In similar test procedures where a number of measure parameters are required simultaneously, a data logger is employed to ensure best time based data.

2. Measuring instruments should have sufficient resolution to give greater accuracy in analyses.

3. Work in heat transfer correlations continues in order to improve design data for heat exchangers with alternative refrigerants.

4. The current control and operating philosophies employed for the brine chiller system remain in place.

10.0 References

Cleland, A.C. (1983) Simulation of industrial refrigeration plants under variable load conditions
International Journal of Refrigeration; Volume 6 Number 1

Hasse, H., Becker, M., Grossman, K., Maurer, G. (1996) Top-down model for dynamic simulation of cold-storage plants
International Journal of Refrigeration; Volume 19 Number1

Gordon, J.M., Ng, K.C., Chau, H.T. (1997) Optimizing Chiller operation based on finite-time thermodynamics: universal modelling and experimental confirmation
International Journal of Refrigeration; Volume 20 Number 3

Browne, M.W., Bansal, P.K. (1998) Steady-state model of centrifugal liquid chillers
International Journal of Refrigeration; Volume 21 Number 5

Willatzen, M., Pettit, N.B.O.L., Ploug-Sørensen, L. (1998) A general dynamic simulation model for evaporators and condensers in refrigeration . Part I: moving-boundary formulation of two-phase flows with heat exchange
International Journal of Refrigeration; Volume 21 Number 5

Lopez, A., Lacarra G. (1999) Mathematical modelling of thermal storage systems for the food industry
International Journal of Refrigeration; Volume 22

Richards, R.J. (1979) An introduction to dynamics and control
Longman Scientific and Technical

Lovatt, S.J., Loeffen, M.P.F.,Cleland, A.C. (1998) Improved dynamic simulation of multi-temperature industrial refrigeration systems for food chilling, freezing and cold storage
International Journal of Refrigeration; Volume 21 Number 3

Incropera, F.P., De Witt, D. P. (1985) Fundamentals of heat and mass transfer
John Wiley and Sons

Markovitz, R.E. (1971) Picking the best vessel jacket
Chemical Engineering Magazine

Dream, R.F. (1999) Heat transfer in agitated jacketed vessels
Chemical Engineering Magazine

Sinnott, R.K. (1999) Coulson and Richardson's chemical engineering: volume six
Butterworth Heinemann

Eastop, T.D., Croft, D.R. (1990) Energy efficiency for engineers and technologists
Longman

Winterbone, D.E. (1997) Advanced thermodynamics for engineers
Arnold

Chau, H.T., Gordon, J.M., Ng, K.C., Han, Q. (1997) Entropy production analysis and experimental confirmation of absorption systems
International Journal of Refrigeration; Volume 20 Number 3

Van Wylen, G. Sonntag, R., Borgnakke, C. (1994) Fundamentals of Classical Thermodynamics
John Wiley and Sons

Stephanopoulos, G. (1984) Chemical process control, an introduction to theory and practice
P T R Prentice Hall

Schwarzenbach, J., Gill. K. F. (1979) System modelling and control, second edition
Edward Arnold

Fikiin, K.A. (1996) Generalized modelling of unsteady heat transfer during cooling and freezing using an improved enthalpy method and quasi-one-dimensional formulation
International Journal of Refrigeration; Volume 19 Number 2

Fenton, D.L., A.S. Khan, R.D. Kelley, and K.S .Chapman. (1995). Combustion Characteristics Review of Ammonia-Air Mixtures. *ASHRAE Transactions* pp. 476-485.

Khan A.S., R.D. Kelley, K.S. Chapman, and D.L. Fenton (1995) Flammability limits of ammonia-air mixtures (682-RP), *ASHRAE Transactions 101(2):454-462*

Carey, Van P, (1992) Liquid-vapour phase-change phenomena; an introduction to the thermo physics of vaporization and condensation processes in heat transfer, *Hemisphere Publishing Corporation*

Welty, James R, (1974) Engineering heat transfer, *John Wiley and Sons*

Bergles, A.E., Collier, J.G., Delhaye, J.M., Hewitt, G.F., Mayinger, F., (1981) Two-phase flow and heat transfer in the power and process industries, *Hemisphere Publishing Corporation*

Kandlikar, S.G., Joshi, S., Tian, S., (2003) Effect of surface roughness on heat transfer and fluid flow characteristics at low Reynolds numbers in small diameter tubes, *Heat transfer engineering, Taylor and Francis*

Kandlikar, S.G., Balasubramanian, P., (2003) Extending the applicability of the flow boiling correlation to low Reynolds number flows in microchannels, *ASME ICMM2003-1075*

Webb, R.E., Choi, K-D., Apparao, T.R., (1989) A theoretical model for prediction of the heat load in flooded refrigerant evaporators, *ASHRAE transactions Volume 95, part 1*

Kandlikar, S.G., (2002) Proceedings of IMECE2002, *ASME IMCE2002-39573*

Kalinin, E.K., Dreitser, G.A., (1998) Heat transfer enhancement in heat exchangers, Advances in heat transfer, *Academic Press*

Kreith, F. (1984) Data books heat transfer and fluid flow *General Electric and Genium Publishing Corporation*

Grace, I.N., Tassou, S.A., (2001) simulation of the performance of alternative refrigerants in liquid chillers *Proceedings of the Institution of Mechanical Engineers journal of power and energy*

Domanski, P.A., (1995) Theoretical evaluation of the vapour compression cycle with a liquid-line/suction-line heat exchanger, economizer and ejector *US Department of Commerce*

Marshal, S.A., James, R.W., (1975) Dynamic analysis of an industrial refrigeration system to investigate capacity control *Proceedings of the Institution of Mechanical Engineers Volume 189 44/75*

Haar, L., Gallagher, J.S. (1978) Thermodynamic properties of ammonia *Journal of physical and chemical reference data Volume &, No.3 American Chemical Society*

Edison, T.A., Sengers, J.V. (1999) Thermodynamic properties of ammonia in the critical region I*nternational journal of Refrigeration 22 365-378*

Dossat, R.J., (1997) Principles of refrigeration *Prentice Hall*

Maclaine-Cross, I (1999) Replacement refrigerants for water chillers *Bandung Institute of Technology*

Whalley, P.B., (1996) Two-phase low and heat transfer *Oxford University Press*

Bolton, W., (1996) Newnes engineering materials pocket book *Newnes*

Institute of Refrigeration (2002), Safety code for compression refrigeration systems utilizing ammonia *The Institute of Refrigeration*

Appendices

Appendix A

Brine chiller absorbed power versus chiller refrigeration effect trials DESIGN FIGURES

Date		Time	

	CHILLER NO.1	CHILLER NO.2	CHILLER NO.3	CHILLER NO.4
Brine flow (m^3/hr); kW	465; 41.6	465; 41.6	465; 41.6	465; 41.6
Brine inlet temperature (^oC)	-21.0	-21.0	-21.0	-21.0
Brine outlet temperature (^oC)	-24.0	-24.0	-24.0	-24.0
Compressor suction pressure (bar abs)	1.26	1.26	1.26	1.26
Compressor suction temperature (^oC)	-28.7	-28.7	-28.7	-28.7
Enthalpy of Ammonia at this point (kJ/kg)	1407.5	1407.5	1407.5	1407.5
Compressor slide valve position (%)				
Compressor motor absorbed power (kW)				
Compressor discharge pressure (bar abs)	12.03	12.03	12.03	12.03
Compressor discharge temperature (^oC)	86.6	86.6	86.6	86.6
Enthalpy of Ammonia at this point (kJ/kg)	1625.7	1625.7	1625.7	1625.7
Condenser pressure (bar abs)	11.67	11.67	11.67	11.67
Condenser temperature (^oC)	30.0	30.0	30.0	30.0
Enthalpy of Ammonia at this point (kJ/kg)	323	323	323	323
First stage expansion pressure (bar abs)	3.0	3.0	3.0	3.0
First stage expansion temperature (^oC)	-9.2	-9.2	-9.2	-9.2
Enthalpy of Ammonia at this point (kJ/kg)	323	323	323	323
Quality x	0.1431	0.1431	0.1431	0.1431
Flash economiser vapour pressure (bar abs)	2.75	2.75	2.75	2.75
Flash economiser vapour temperature (^oC)	-9.2	-9.2	-9.2	-9.2
Enthalpy of Ammonia at this point (kJ/kg)	1433.5	1433.5	1433.5	1433.5
Second stage expansion pressure (bar abs)	1.28	1.28	1.28	1.28
Second stage expansion temperature (^oC)	-28.7	-28.7	-28.7	-28.7
Enthalpy of Ammonia at this point (kJ/kg)	138.6	138.6	138.6	138.6
Quality x	0.06493	0.06493	0.06493	0.06493
h_g (kJ/kg)	1406	1406	1406	1406
	PUMP NO.1	PUMP NO.2	PUMP NO.3	PUMP NO.4
External brine pump flow (m^3/hr)				
Total brine pump flow (m^3/hr)				
Discharge pressure (barg)				

Room Temperature (^oC)	
Ambient temperature (^oC)	

Brine chiller absorbed power versus chiller refrigeration effect trials

PROCEDURE 1

Date	14/03/2003	Time	10.53

	CHILLER NO.1	CHILLER NO.2	CHILLER NO.3	CHILLER NO.4
Brine flow (m^3/hr); kW	585; 51	526; 49		
Brine inlet temperature (°C)	-23.1	-23.1		
Brine outlet temperature (°C)	-24.4	-24.4		
Compressor suction pressure (bar abs)	1.28	1.30		
Compressor suction temperature (°C)	-21.1	-20.2		
Enthalpy of Ammonia at this point (kJ/kg)	1423	1425		
Compressor slide valve position (%)	100	70		
Compressor motor absorbed power (kW)	390	373		
Compressor discharge pressure (bar abs)	8.825(10.5)	8.439(10.5)		
Compressor discharge temperature (°C)	73	74		
Enthalpy of Ammonia at this point (kJ/kg)	1602	1605		
Condenser pressure (bar abs)	8.825(10.5)	8.439(10.5)		
Condenser temperature (°C)	20.9	19.7		
Enthalpy of Ammonia at this point (kJ/kg)	278.7	273		
First stage expansion pressure (bar abs)	3.1	2.0		
First stage expansion temperature (°C)	-9.2 (-8.4)	-9.7 (-18.7)		
Enthalpy of Ammonia at this point (kJ/kg)	278.7	273		
Quality x	0.1062	0.1349		
Flash economiser vapour pressure (bar abs)	2.75	2.0		
Flash economiser vapour temperature (°C)	-9.2 (-8.4)	-9.7 (-18.7)		
Enthalpy of Ammonia at this point (kJ/kg)	1433	1420		
Second stage expansion pressure (bar abs)	1.28	1.3		
Second stage expansion temperature (°C)	-28.58	-28.25		
Enthalpy of Ammonia at this point (kJ/kg)	141.6	94.19		
Quality x	0.06714	0.03112		
h_g (kJ/kg)	1406	1407		
	PUMP NO.1	PUMP NO.2	PUMP NO.3	PUMP NO.4
External brine pump flow (m^3/hr)			x	x
Total brine pump flow (m^3/hr)	488			
Discharge pressure (barg)	6.6			

Room Temperature (°C)	16
Ambient temperature (°C)	9.1

Brine chiller absorbed power versus chiller refrigeration effect trials

PROCEDURE 2

Date	14/03/2003	Time	11.26

	CHILLER NO.1	CHILLER NO.2	CHILLER NO.3	CHILLER NO.4
Brine flow (m^3/hr); kW	555; 50		600; 52	
Brine inlet temperature (°C)	-23.5		-23.2	
Brine outlet temperature (°C)	-24.4		-24.7	
Compressor suction pressure (bar abs)	1.32		1.37	
Compressor suction temperature (°C)	-23.5		-24.6	
Enthalpy of Ammonia at this point (kJ/kg)	1417		1414	
Compressor slide valve position (%)	80		65	
Compressor motor absorbed power (kW)	365		340	
Compressor discharge pressure (bar abs)	9.195(10.82)		8.713(9.64)	
Compressor discharge temperature (°C)	73		70	
Enthalpy of Ammonia at this point (kJ/kg)	1600		1595	
Condenser pressure (bar abs)	9.915(10.5)		8.713(9.64)	
Condenser temperature (°C)	22.2		20.5	
Enthalpy of Ammonia at this point (kJ/kg)	285.1		276.7	
First stage expansion pressure (bar abs)	3.0		3.0	
First stage expansion temperature (°C)	-9.9 (-9.2)		-10.4 (-9.2)	
Enthalpy of Ammonia at this point (kJ/kg)	285.1		276.7	
Quality x	0.1138		0.1073	
Flash economiser vapour pressure (bar abs)	2.75		2.75	
Flash economiser vapour temperature (°C)	-9.9 (-9.2)		-10.4 (-9.2)	
Enthalpy of Ammonia at this point (kJ/kg)	1432		1432	
Second stage expansion pressure (bar abs)	1.32		1.37	
Second stage expansion temperature (°C)	-27.93		-27.15	
Enthalpy of Ammonia at this point (kJ/kg)	137.9		137.9	
Quality x	0.06238		0.05564	
h_g (kJ/kg)	1407		1408	
	PUMP NO.1	PUMP NO.2	PUMP NO.3	PUMP NO.4
External brine pump flow (m^3/hr)			x	x
Total brine pump flow (m^3/hr)	495			
Discharge pressure (barg)	6.6			

Room Temperature (°C)	16
Ambient temperature (°C)	9.2

Brine chiller absorbed power versus chiller refrigeration effect trials

PROCEDURE 3

Date	14/03/2003	Time	12.37

	CHILLER NO.1	CHILLER NO.2	CHILLER NO.3	CHILLER NO.4
Brine flow (m^3/hr); kW	555; 50			585; 51
Brine inlet temperature (°C)	-22.9			-22.9
Brine outlet temperature (°C)	-24.4			-24.5
Compressor suction pressure (bar abs)	1.24			1.23
Compressor suction temperature (°C)	-25.1			-24.8
Enthalpy of Ammonia at this point (kJ/kg)	1415			1415
Compressor slide valve position (%)	100			75
Compressor motor absorbed power (kW)	433			395
Compressor discharge pressure (bar abs)	9.487(10.82)			8.685(10.48)
Compressor discharge temperature (°C)	75			71.2
Enthalpy of Ammonia at this point (kJ/kg)	1604			1598
Condenser pressure (bar abs)	9.487(10.5)			8.685(10.5)
Condenser temperature (°C)	23.2			20.4
Enthalpy of Ammonia at this point (kJ/kg)	289.6			276.3
First stage expansion pressure (bar abs)	3.1			3.4
First stage expansion temperature (°C)	-9.3 (-8.4)			-7 (-6.1)
Enthalpy of Ammonia at this point (kJ/kg)	289.6			276.3
Quality x	0.1146			0.09666
Flash economiser vapour pressure (bar abs)	2.75			2.75
Flash economiser vapour temperature (°C)	-9.3 (-8.4)			-7 (-6.1)
Enthalpy of Ammonia at this point (kJ/kg)	1433			1435
Second stage expansion pressure (bar abs)	1.24			1.23
Second stage expansion temperature (°C)	-29.24			-29.4
Enthalpy of Ammonia at this point (kJ/kg)	141.6			152.3
Quality x	0.09621			0.07761
h_g (kJ/kg)	1405			1405
	PUMP NO.1	PUMP NO.2	PUMP NO.3	PUMP NO.4
External brine pump flow (m^3/hr)			x	X
Total brine pump flow (m^3/hr)	502			
Discharge pressure (barg)	6.6			

Room Temperature (°C)	16
Ambient temperature (°C)	9.4

Brine chiller absorbed power versus chiller refrigeration effect trials

PROCEDURE 4

Date	14/03/2003	Time	13.19

	CHILLER NO.1	CHILLER NO.2	CHILLER NO.3	CHILLER NO.4
Brine flow (m^3/hr); kW		481.5; 48	600; 52	
Brine inlet temperature (°C)		-22.6	-22.5	
Brine outlet temperature (°C)		-24.0	-24.6	
Compressor suction pressure (bar abs)		1.32	1.28	
Compressor suction temperature (°C)		-19.9	-27.1	
Enthalpy of Ammonia at this point (kJ/kg)		1425	1409	
Compressor slide valve position (%)		65	95	
Compressor motor absorbed power (kW)		377	411	
Compressor discharge pressure (bar abs)		8.575(10.6)	8.835(10.64)	
Compressor discharge temperature (°C)		73.2	73.0	
Enthalpy of Ammonia at this point (kJ/kg)		1603	1601	
Condenser pressure (bar abs)		8.575(10.5)	10.5	
Condenser temperature (°C)		20.0	21.0	
Enthalpy of Ammonia at this point (kJ/kg)		274.4	279.1	
First stage expansion pressure (bar abs)		3.1	2.0	
First stage expansion temperature (°C)		-9.0 (-8.4)	-10.2 (-18.9)	
Enthalpy of Ammonia at this point (kJ/kg)		274.4	279.1	
Quality x		0.1028	0.1395	
Flash economiser vapour pressure (bar abs)		2.75	2.0	
Flash economiser vapour temperature (°C)		-9.0 (-8.4)	-10.2 (-18.9)	
Enthalpy of Ammonia at this point (kJ/kg)		1433	1420	
Second stage expansion pressure (bar abs)		1.32	1.28	
Second stage expansion temperature (°C)		-27.93	-28.58	
Enthalpy of Ammonia at this point (kJ/kg)		141.6	94.19	
Quality x		0.06512	0.03216	
h_g (kJ/kg)		1407	1406	
	PUMP NO.1	PUMP NO.2	PUMP NO.3	PUMP NO.4
External brine pump flow (m^3/hr)			X	x
Total brine pump flow (m^3/hr)	493			
Discharge pressure (barg)	6.6			

Room Temperature (°C)	16
Ambient temperature (°C)	9.5

Brine chiller absorbed power versus chiller refrigeration effect trials

PROCEDURE 5

Date	14/03/2003	Time	10.08

	CHILLER NO.1	CHILLER NO.2	CHILLER NO.3	CHILLER NO.4
Brine flow (m^3/hr); kW		526; 49		585; 51
Brine inlet temperature (^oC)		-23.0		-23.1
Brine outlet temperature (^oC)		-24.4		-24.5
Compressor suction pressure (bar abs)		1.30		1.26
Compressor suction temperature (^oC)		-20.5		-22.0
Enthalpy of Ammonia at this point (kJ/kg)		1424		1421
Compressor slide valve position (%)		75		70
Compressor motor absorbed power (kW)		386		370
Compressor discharge pressure (bar abs)		8.685(10.5)		8.251(10.5)
Compressor discharge temperature (^oC)		73		72
Enthalpy of Ammonia at this point (kJ/kg)		1602		1601
Condenser pressure (bar abs)		8.685(10.5)		8.251(10.5)
Condenser temperature (^oC)		20.4		18.8
Enthalpy of Ammonia at this point (kJ/kg)		276.3		268.7
First stage expansion pressure (bar abs)		3.2		3.2
First stage expansion temperature (^oC)		-8.5 (-7.6)		-8.7 (-7.6)
Enthalpy of Ammonia at this point (kJ/kg)		276.3		268.7
Quality x		0.1017		0.09582
Flash economiser vapour pressure (bar abs)		2.75		2.75
Flash economiser vapour temperature (^oC)		-8.5 (-7.6)		-8.7 (-7.6)
Enthalpy of Ammonia at this point (kJ/kg)		1434		1434
Second stage expansion pressure (bar abs)		1.30		1.26
Second stage expansion temperature (^oC)		-28.25		-28.91
Enthalpy of Ammonia at this point (kJ/kg)		145.3		145.3
Quality x		0.06885		0.0709
h_g (kJ/kg)		1407		1406
	PUMP NO.1	PUMP NO.2	PUMP NO.3	PUMP NO.4
External brine pump flow (m^3/hr)			x	x
Total brine pump flow (m^3/hr)	489			
Discharge pressure (barg)	6.7			

Room Temperature (^oC)	16
Ambient temperature (^oC)	9.1

Brine chiller absorbed power versus chiller refrigeration effect trials

PROCEDURE 6

Date	14/03/2003	Time	14.00

	CHILLER NO.1	CHILLER NO.2	CHILLER NO.3	CHILLER NO.4
Brine flow (m^3/hr); kW			585; 51	585; 51
Brine inlet temperature (^oC)			-22.6	-22.8
Brine outlet temperature (^oC)			-24.7	-24.1
Compressor suction pressure (bar abs)			1.29	1.26
Compressor suction temperature (^oC)			-27.1	-22.1
Enthalpy of Ammonia at this point (kJ/kg)			1409	1421
Compressor slide valve position (%)			95	50
Compressor motor absorbed power (kW)			404	50
Compressor discharge pressure (bar abs)			8.881(10.64)	8.251(10.13)
Compressor discharge temperature (^oC)			73	70.8
Enthalpy of Ammonia at this point (kJ/kg)			1601	1598
Condenser pressure (bar abs)			8.881(10.5)	8.251(10.2)
Condenser temperature (^oC)			21.1	18.8
Enthalpy of Ammonia at this point (kJ/kg)			279.6	268.7
First stage expansion pressure (bar abs)			2.9	2.8
First stage expansion temperature (^oC)			-10.1 (-10)	-12.3 (-10.9)
Enthalpy of Ammonia at this point (kJ/kg)			279.6	268.7
Quality x			0.1122	0.1066
Flash economiser vapour pressure (bar abs)			2.75	2.75
Flash economiser vapour temperature (^oC)			-10.1 (-10)	-12.3 (-10.9)
Enthalpy of Ammonia at this point (kJ/kg)			1431	1430
Second stage expansion pressure (bar abs)			1.29	1.26
Second stage expansion temperature (^oC)			-29.24	-28.91
Enthalpy of Ammonia at this point (kJ/kg)			134.1	130.2
Quality x			0.06110	0.05976
h_g (kJ/kg)			1406	1406
	PUMP NO.1	PUMP NO.2	PUMP NO.3	PUMP NO.4
External brine pump flow (m^3/hr)			x	x
Total brine pump flow (m^3/hr)	497			
Discharge pressure (barg)	6.7			

Room Temperature (^oC)	16
Ambient temperature (^oC)	9.8

Brine chiller absorbed power versus chiller refrigeration effect trials

PROCEDURE 7

Date	14/03/2003	Time	15.55

	CHILLER NO.1	CHILLER NO.2	CHILLER NO.3	CHILLER NO.4
Brine flow (m^3/hr); kW	448.5; 46	426; 45	471; 47	
Brine inlet temperature (°C)	-23.2	-22.9	-23	
Brine outlet temperature (°C)	-24.2	-24.4	-24.7	
Compressor suction pressure (bar abs)	1.32	1.3	1.35	
Compressor suction temperature (°C)	-18.3	-15.6	-25.7	
Enthalpy of Ammonia at this point (kJ/kg)	1429	1435	1412	
Compressor slide valve position (%)	55	45	55	
Compressor motor absorbed power (kW)	349	345	327	
Compressor discharge pressure (bar abs)	10.82	10.47	10.57	
Compressor discharge temperature (°C)	73.1	72.2	70.9	
Enthalpy of Ammonia at this point (kJ/kg)	1594	1593	1589	
Condenser pressure (bar abs)	10.5	10.5	10.5	
Condenser temperature (°C)	21.2	19.2	20.9	
Enthalpy of Ammonia at this point (kJ/kg)	280.1	270.6	278.7	
First stage expansion pressure (bar abs)	2.6	2.4	3.0	
First stage expansion temperature (°C)	-13.4 (-12.7)	-15.4 (-14.6)	-10.6 (-9.9)	
Enthalpy of Ammonia at this point (kJ/kg)	280.1	270.6	278.7	
Quality x	0.1211	0.1199	0.1088	
Flash economiser vapour pressure (bar abs)	2.6	2.4	3.0	
Flash economiser vapour temperature (°C)	-13.4 (-12.7)	-15.4 (-14.6)	-10.6 (-9.9)	
Enthalpy of Ammonia at this point (kJ/kg)	1427	1425	1432	
Second stage expansion pressure (bar abs)	1.32	1.30	1.35	
Second stage expansion temperature (°C)	-27.93	-28.25	-27.46	
Enthalpy of Ammonia at this point (kJ/kg)	122	113.3	137.9	
Quality x	0.05064	0.04523	0.06089	

	PUMP NO.1	PUMP NO.2	PUMP NO.3	PUMP NO.4
External brine pump flow (m^3/hr)			x	x
Total brine pump flow (m^3/hr)	512			
Discharge pressure (barg)	7.1			

Room Temperature (°C)	16
Ambient temperature (°C)	9.6

Brine chiller absorbed power versus chiller refrigeration effect trials

PROCEDURE 8

Date	14/03/2003	Time	14.40

	CHILLER NO.1	CHILLER NO.2	CHILLER NO.3	CHILLER NO.4
Brine flow (m^3/hr); kW	448.5; 46		471; 47	471; 47
Brine inlet temperature (^{o}C)	-23.1		-22.9	-23.1
Brine outlet temperature (^{o}C)	-24.4		-24.8	-24.3
Compressor suction pressure (bar abs)	1.30		1.35	1.26
Compressor suction temperature (^{o}C)	-20.8		-25.7	-20.6
Enthalpy of Ammonia at this point (kJ/kg)	1423		1412	1424
Compressor slide valve position (%)	80		60	20
Compressor motor absorbed power (kW)	355		334	284
Compressor discharge pressure (bar abs)	10.87		10.57	10.23
Compressor discharge temperature (^{o}C)	74.1		70	67.4
Enthalpy of Ammonia at this point (kJ/kg)	1596		1587	1581
Condenser pressure (bar abs)	10.6		10.5	9.4
Condenser temperature (^{o}C)	22.4		20.7	17.0
Enthalpy of Ammonia at this point (kJ/kg)	285.8		277.7	260.1
First stage expansion pressure (bar abs)	3.0		3.0	2.2
First stage expansion temperature (^{o}C)	-10.4 (-9.2)		-10.4 (-9.2)	-16.5
Enthalpy of Ammonia at this point (kJ/kg)	285.8		277.7	260.1
Quality x	0.1143		0.1081	0.1183
Flash economiser vapour pressure (bar abs)	3.0		3.0	2.2
Flash economiser vapour temperature (^{o}C)	-10.4 (-9.2)		-10.4 (-9.2)	-16.5
Enthalpy of Ammonia at this point (kJ/kg)	1432		1432	1422
Second stage expansion pressure (bar abs)	1.3		1.35	1.26
Second stage expansion temperature (^{o}C)	-28.25		-27.46	-28.91
Enthalpy of Ammonia at this point (kJ/kg)	137.9		137.9	104.1
Quality x	0.06339		0.06089	0.04052
	PUMP NO.1	PUMP NO.2	PUMP NO.3	PUMP NO.4
External brine pump flow (m^3/hr)			x	x
Total brine pump flow (m^3/hr)	512			
Discharge pressure (barg)	7.1			

Room Temperature (^{o}C)	16
Ambient temperature (^{o}C)	9.8

Brine chiller absorbed power versus chiller refrigeration effect trials

PROCEDURE 9

Date	14/03/2003	Time	16.30

	CHILLER NO.1	CHILLER NO.2	CHILLER NO.3	CHILLER NO.4
Brine flow (m^3/hr); kW	363; 42	348; 41		387; 43
Brine inlet temperature (^oC)	-22.8	-22.6		-22.7
Brine outlet temperature (^oC)	-24.0	-24.0		-24.1
Compressor suction pressure (bar abs)	1.35	1.32		1.26
Compressor suction temperature (^oC)	-19.8	-15.1		-19.1
Enthalpy of Ammonia at this point (kJ/kg)	1425	1436		1428
Compressor slide valve position (%)	55	40		35
Compressor motor absorbed power (kW)	350	336		310
Compressor discharge pressure (bar abs)	10.82	10.41		9.65
Compressor discharge temperature (^oC)	72.0	72.1		68.7
Enthalpy of Ammonia at this point (kJ/kg)	1591	1593		1587
Condenser pressure (bar abs)	10.5	10.5		9.8
Condenser temperature (^oC)	20.9	19.1		18.7
Enthalpy of Ammonia at this point (kJ/kg)	278.7	270.1		268.2
First stage expansion pressure (bar abs)	2.2	2.4		2.3
First stage expansion temperature (^oC)	-13.1 (-16.7)	-15.4 (-14.6)		-16.2 (-15.6)
Enthalpy of Ammonia at this point (kJ/kg)	278.7	270.1		268.2
Quality x	0.1324	0.1195		0.1212
Flash economiser vapour pressure (bar abs)	2.2	2.4		2.3
Flash economiser vapour temperature (^oC)	-13.1 (-16.7)	-15.4 (-14.6)		-16.2 (-15.6)
Enthalpy of Ammonia at this point (kJ/kg)	1422	1425		1424
Second stage expansion pressure (bar abs)	1.35	1.32		1.26
Second stage expansion temperature (^oC)	-27.46	-27.93		-28.91
Enthalpy of Ammonia at this point (kJ/kg)	104.1	113.3		108.8
Quality x	0.03589	0.04672		0.04399
	PUMP NO.1	PUMP NO.2	PUMP NO.3	PUMP NO.4
External brine pump flow (m^3/hr)			x	x
Total brine pump flow (m^3/hr)	512			
Discharge pressure (barg)	7.2			

Room Temperature (^oC)	16
Ambient temperature (^oC)	9.5

Brine chiller absorbed power versus chiller refrigeration effect trials

PROCEDURE 10

Date	14/03/2003	Time	15.20

	CHILLER NO.1	CHILLER NO.2	CHILLER NO.3	CHILLER NO.4
Brine flow (m^3/hr); kW		405; 44	448.5; 46	448.5; 46
Brine inlet temperature (°C)		-22.8	-22.7	-22.9
Brine outlet temperature (°C)		-24.4	-24.7	-24.1
Compressor suction pressure (bar abs)		1.28	1.33	1.26
Compressor suction temperature (°C)		-13.5	-26.2	-20.9
Enthalpy of Ammonia at this point (kJ/kg)		1440	1411	1424
Compressor slide valve position (%)		70	70	25
Compressor motor absorbed power (kW)		363	344	293
Compressor discharge pressure (bar abs)		10.41	10.64	10.37
Compressor discharge temperature (°C)		73.2	71.2	67.8
Enthalpy of Ammonia at this point (kJ/kg)		1596	1589	1582
Condenser pressure (bar abs)		10.5	10.5	9.5
Condenser temperature (°C)		19.9	20.8	17.3
Enthalpy of Ammonia at this point (kJ/kg)		273.9	278.2	261.5
First stage expansion pressure (bar abs)		2.9	2.9	2.1
First stage expansion temperature (°C)		-10.8 (-10.1)	-10.4 (-10.1)	-18.4 (-17.8)
Enthalpy of Ammonia at this point (kJ/kg)		273.9	278.2	261.5
Quality x		0.1078	0.1112	0.1228
Flash economiser vapour pressure (bar abs)		2.9	2.9	2.1
Flash economiser vapour temperature (°C)		-10.8 (-10.1)	-10.4 (-10.1)	-18.4 (-17.8)
Enthalpy of Ammonia at this point (kJ/kg)		1431	1431	1421
Second stage expansion pressure (bar abs)		1.28	1.33	1.26
Second stage expansion temperature (°C)		-28.58	-27.78	-28.91
Enthalpy of Ammonia at this point (kJ/kg)		134.1	134.1	99.23
Quality x		0.06161	0.05908	0.03693
	PUMP NO.1	PUMP NO.2	PUMP NO.3	PUMP NO.4
External brine pump flow (m^3/hr)			x	x
Total brine pump flow (m^3/hr)	512			
Discharge pressure (barg)	7.1			

Room Temperature (°C)	16
Ambient temperature (°C)	9.7

Brine chiller absorbed power versus chiller refrigeration effect trials

PROCEDURE 11

Date	14/03/2003	Time	17.00

	CHILLER NO.1	CHILLER NO.2	CHILLER NO.3	CHILLER NO.4
Brine flow (m^3/hr); kW	363; 42	363; 42	405; 44	363; 42
Brine inlet temperature (^oC)	-23.3	-23.1	-22.9	-23.1
Brine outlet temperature (^oC)	-24.4	-24.4	-24.6	-24.4
Compressor suction pressure (bar abs)	1.32	1.3	1.37	1.24
Compressor suction temperature (^oC)	-18.3	-12.1	-19.5	-19.5
Enthalpy of Ammonia at this point (kJ/kg)	1429	1443	1426	1427
Compressor slide valve position (%)	25	25	20	15
Compressor motor absorbed power (kW)	322	325	297	281
Compressor discharge pressure (bar abs)	10.8	10.41	9.57	9.1
Compressor discharge temperature (^oC)	72.1	71.5	71.2	68.7
Enthalpy of Ammonia at this point (kJ/kg)	1591	1591	1594	1590
Condenser pressure (bar abs)	10.5	10.5	10.5	10.5
Condenser temperature (^oC)	19.9	18.8	20.1	17.1
Enthalpy of Ammonia at this point (kJ/kg)	273.9	268.7	274.9	260.6
First stage expansion pressure (bar abs)	2.1	2.0	2.3	1.9
First stage expansion temperature (^oC)	-18.3 (-17.6)	-19.9 (-18.9)	-16.2 (-15.6)	-21.0 (-20)
Enthalpy of Ammonia at this point (kJ/kg)	273.9	268.7	274.9	260.6
Quality x	0.1321	0.1317	0.1263	0.1292
Flash economiser vapour pressure (bar abs)	2.1	2.0	2.3	1.9
Flash economiser vapour temperature (^oC)	-18.3 (-17.6)	-19.9 (-18.9)	-16.2 (-15.6)	-21.0 (-20)
Enthalpy of Ammonia at this point (kJ/kg)	1421	1420	1424	1418
Second stage expansion pressure (bar abs)	1.32	1.3	1.37	1.24
Second stage expansion temperature (^oC)	-27.93	-28.25	-27.15	-29.24
Enthalpy of Ammonia at this point (kJ/kg)	99.23	94.19	108.8	88.95
Quality x	0.03381	0.03112	0.03837	0.03042
	PUMP NO.1	PUMP NO.2	PUMP NO.3	PUMP NO.4
External brine pump flow (m^3/hr)			x	x
Total brine pump flow (m^3/hr)	525			
Discharge pressure (barg)	7.3			

Room Temperature (^oC)	16
Ambient temperature (^oC)	9.5

Procedure Number	0	1		2		3	
Chiller Number	Design	1	2	1	3	1	4
Brine Properties							
Brine Inlet Temperature T_{ei} (°C)	-21	-23.1	-23.1	-23.5	-23.2	-22.9	-22.9
Brine Outlet Temperature T_{eo} (°C)	-24	-24.4	-24.4	-24.4	-24.7	-24.4	-24.5
Brine Bulk (mean) Temperature T_b (°C)	-22.5	-23.8	-23.8	-24.0	-24.0	-23.7	-23.7
Volumetric Flow Rate of Brine (m^3hr^{-1})	465	585	526	555	600	555	585
Brine Mass Flow Rate $\dot{m}_b$ (kgs^{-1})	165.00	207.67	186.73	197.04	213.01	197.02	207.66
Specific Heat Capacity C_p ($kJkg^{-1}K^{-1}$) (mean temperature)	2.7341	2.73011	2.73011	2.7295	2.7295	2.730417	2.730417
Brine density ρ_b (kgm^{-3}) (mean temperature)	1277.43	1277.984	1277.984	1278.076	1278.076	1277.938	1277.938
Thermal Conductivity k_b ($Wm^{-1}K^{-1}$)(mean temperature)	0.4996	0.4976	0.4976	0.4973	0.4973	0.4978	0.4978
Brine dynamic viscocity at wall μ_w (Nsm^{-2})	0.0138708	0.0140979	0.014098	0.014098	0.014268	0.014098	0.014155
Brine dynamic viscocity (bulk) μ_b (Nsm^{-2})	0.0130193	0.0137573	0.013757	0.013871	0.013871	0.013701	0.013701
Ammonia Properties in Evaporator							
Pressure (bar a)	1.28	1.28	1.3	1.32	1.37	1.24	1.23
Temperature T_{evap} (°C)	-28.7	-28.58	-28.25	-27.93	-27.15	-29.24	-29.4
Liquid Thermal Conductivity k_l ($Wm^{-1}K^{-1}$)	0.6057285	0.6048362	0.60415	0.603463	0.601747	0.606243	0.606552
Vapour Thermal Conductivity k_v ($Wm^{-1}K^{-1}$)	0.0192056	0.0192165	0.019248	0.019279	0.019357	0.019153	0.019139
Liquid Density ρ (kgm^{-3})	675.6757	675.6757	657.2194	674.7638	673.8544	676.59	676.59
Vapour Density ρ (kgm^{-3})	1.1008	1.1068	1.1234	1.1396	1.1789	1.0739	1.0667
Liquid Dynamic Viscosity μ_l (Nsm^{-2})	0.000270337	0.00026876	0.000268	0.000266	0.000263	0.000271	0.000272
Vapour Dynamic Viscosity μ_v (Nsm-2)	9.3879E-06	9.39E-06	9.40E-06	9.41E-06	9.44E-06	9.37E-06	9.37E-06
Surface Tension σ mNm^{-1}	33	32.9	32.88	32.75	32.56	33.05	33.09
Latent Heat λ ($kJkg^{-1}$)	1356.7221	1356.88	1355.91	1354.94	1352.53	1358.85	1359.29
h_g ($kJkg^{-1}$)	1406	1406	1407	1407	1408	1405	1405
h_f ($kJkg^{-1}$)	50.05	50.58	52.06	53.48	56.97	47.6	46.93
Enthalpy Difference h_{fg} ($kJkg^{-1}$)	1355.95	1355.42	1354.94	1353.52	1351.03	1357.4	1358.07
Vapor Specific Heat Capacity ($kJkg^{-1}K^{-1}$)	2.2782	2.203	2.21	2.216	2.231	2.191	2.188
Liquid Specific Heat Capacity ($kJkg^{-1}K^{-1}$)	4.489	4.489	4.49	4.492	4.495	4.486	4.486
Pressure $P_{satwall}$ (bar a)	1.675	1.592	1.594	1.582	1.576	1.598	1.593

Test Number	0	1		2		3	
Chiller Number	Design	1	2	1	3	1	4
Evaporator Tube Properties							
Tube Length (m)	5.4864	5.4864	5.4864	5.4864	5.4864	5.4864	5.4864
K Thermal Conductivity ($Wm^{-1}K^{-1}$)	40	40	40	40	40	40	40
Internal Diameter (m)	0.027432	0.027432	0.027432	0.027432	0.027432	0.027432	0.027432
Thickness (m)	0.002159	0.002159	0.002159	0.002159	0.002159	0.002159	0.002159
External Diameter (m)	0.03175	0.03175	0.03175	0.03175	0.03175	0.03175	0.03175
Performance Calculations							
Chilling Heat Load (kW)	1353.390778	737.059045	662.7232	484.0305	872.1271	806.9015	907.2189
Evaporator Heat Transfer Area (m^2)	434.5118	434.5118	434.5118	434.5118	434.5118	434.5118	434.5118
Log Mean Temperature Difference	6.077083918	4.80069979	4.468528	3.962982	3.140522	5.556295	5.662374
U_{lm} Overall Heat Transfer Coefficient ($Wm^{-2}K^{-1}$)	512.5383947	353.342727	341.3235	281.0924	639.111	334.2209	368.733
Area for Flow per Pass (m^2)	0.078015	0.078015	0.078015	0.078015	0.078015	0.078015	0.078015
Brine Flowrate (m^3s^{-1})	465	585	526	555	600	555	585
Brine velocity (ms^{-1})	1.655664509	2.08293277	1.872859	1.976116	2.136341	1.976116	2.082933
Tube Calculations							
Heat flux (Wm^{-2})	3114.738836	1696.29236	1525.213	1113.964	2007.143	1857.03	2087.904
Tube Outer Wall Temperature (°C)	-22.8302	-23.9298	-23.9117	-24.0681	-24.1628	-23.8469	-23.9213
NH3 Pcrit (bar a)	112.9	112.9	112.9	112.9	112.9	112.9	112.9
P_R	0.011337467	0.01133747	0.011515	0.011692	0.012135	0.010983	0.010895
$f(P_R)$	0.859017965	0.85901796	0.861584	0.864123	0.870356	0.853802	0.852479
NH_3 Molecular Weight	17.0304	17.0304	17.0304	17.0304	17.0304	17.0304	17.0304
A a constant 30-55	55	55	55	55	55	55	55
Epsilon Surface Roughness (µm)	0.5	0.5	0.5	0.5	0.5	0.5	0.5

Test Number	0	1		2		3	
Chiller Number	Design	1	2	1	3	1	4
Brine Coefficient Calculations							
Brine Side Reynolds Number	4456.349952	5307.9269	4772.598	4994.879	5399.87	5056.421	5329.741
Brine Side Prandtl Number	71.24913557	75.4801895	75.48019	76.13181	76.13181	75.1468	75.1468
Laminar Brine Flow Regime							
Entry Length (m)	6.112329594	7.28035254	6.546095	6.850977	7.406461	6.935387	7.310273
Thermal Entry Length (m)	435.4981999	549.522389	494.1005	521.5772	563.8673	521.1721	549.3436
Nusselt Number	74.58950893	88.4515434	81.86008	85.16063	90.11613	85.11244	88.43069
Br1 Convective Coefficient of Heat Transfer ($Wm^{-2}K^{-1}$)	1358.44702	1604.45786	1484.893	1543.831	1633.667	1544.509	1604.724
Brine Transition Flow Regime							
Nusselt Number	69.46372493	84.154891	75.66747	79.41922	85.71441	80.05005	84.32959
Br2 Convective Coefficient of Heat Transfer ($Wm^{-2}K^{-1}$)	1265.09467	1526.51917	1372.563	1439.748	1553.871	1452.643	1530.303
Brine Turbulent Flow Regime							
Nusselt Number	164.3532092	186.042939	174.5465	179.8892	188.5038	180.4387	186.2291
Br3 Convective Coefficient of Heat Transfer ($Wm^{-2}K^{-1}$)	2993.251069	3374.70715	3166.168	3261.115	3417.284	3274.366	3379.441

Test Number	0	1		2		3	
Chiller Number	Design	1	2	1	3	1	4
Boiling Heat Transfer Coefficients							
Bromley's Correlation							
E1 Boiling Coefficient of Heat Transfer ($Wm^{-2}K^{-1}$)	49.35364009	52.3837725	53.17189	55.33343	59.58654	50.04425	49.74979
Mostinski's Correlation							
E2 Boiling Coefficient of Heat Transfer ($Wm^{-2}K^{-1}$)	662.3111679	432.83007	402.9894	324.3769	493.3629	458.3476	496.7592
Cooper's Correlation							
E3 Boiling Coefficient of Heat Transfer ($Wm^{-2}K^{-1}$)	298.9686869	199.378542	187.3102	153.1787	231.4582	208.1605	224.0873
Chen's Correlation							
Tube Pitch S_D=S_L (m)	0.0396875	0.0396875	0.039688	0.039688	0.039688	0.039688	0.039688
Effective Area Approach Bottom Tube Row (m^2)	3.603	3.603	3.603	3.603	3.603	3.603	3.603
Velocity Approaching Bottom Tube Row (ms^{-1})	0.000435415	0.00023945	0.000213	0.000157	0.000283	0.000262	0.000297
Liquid Phase Reynolds Number Re_l	80.77258372	44.5755824	40.27485	29.5813	54.2603	46.88107	54.14447
Liquid Phase Prandtl Number Pr_l	2.003443445	1.99465846	1.988326	1.982417	1.966673	2.007157	2.010185
Martinelli Parameter *X*	0.622985032	0.60447558	1.27566	0.65804	0.746067	0.418837	0.515975
1/*X*	1.605175001	1.65432656	0.783908	1.519664	1.340361	2.387563	1.938078
Two-phase Heat Transfer Coefficient Multiplier F -chart	3.7	3.75	2.3	3.3	3	4.8	1.8
Two-phase Reynolds Number Re_{TP}	414.4919785	232.61414	114.0759	131.5708	214.2317	333.0804	112.8872
Suppression Factor S -chart	0.95	0.95	0.95	0.95	0.95	0.95	0.95
Forster-Zuber Boiling Coefficient ($Wm^{-2}K^{-1}$)	460.9251388	366.046012	339.5295	307.2445	241.5355	420.3764	426.2791
Forced Convection Boiling Coefficient ($Wm^{-2}K^{-1}$)	7.194255435	4.51729225	2.548465	2.849972	4.184063	6.04927	2.54837
E4 Boiling Coefficient of Heat Transfer ($Wm^{-2}K^{-1}$)	468.1193943	370.563304	342.078	310.0945	245.7196	426.4257	428.8275

Test Number	0	1		2		3	
Chiller Number	Design	1	2	1	3	1	4
Overall Heat Transfer Coefficient Calculations							
Combinations							
Br1, E1, K U_{11} ($Wm^{-2}K^{-1}$)	54.64343997	58.2243762	58.89055	61.27381	65.91934	55.64771	55.40755
Br1, E2, K U_{12} ($Wm^{-2}K^{-1}$)	476.4914231	373.490521	347.7726	296.7955	412.9872	386.0254	413.1464
Br1, E3, K U_{13} ($Wm^{-2}K^{-1}$)	271.4377718	199.411934	187.121	157.574	227.1183	205.926	220.4189
Br1, E4, K U_{14} ($Wm^{-2}K^{-1}$)	378.811716	331.909982	307.0116	286.3686	238.8722	366.0837	370.9237
Br2, E1, K U_{21} ($Wm^{-2}K^{-1}$)	54.48172568	58.1166978	58.70003	61.09851	65.78303	55.5212	55.31467
Br2, E2, K U_{22} ($Wm^{-2}K^{-1}$)	464.4695575	369.103694	341.232	292.7272	407.6945	380.0188	408.0376
Br2, E3, K U_{23} (Wm^{-2}K-1)	267.4937129	198.154522	185.2109	156.4198	225.5083	204.2042	218.9563
Br2, E4, K U_{24} ($Wm^{-2}K^{-1}$)	371.1740522	328.441014	301.9032	282.5793	237.0919	360.6774	366.8005
Br3, E1, K U_{31} ($Wm^{-2}K^{-1}$)	448.4518357	373.408335	345.8167	318.1656	259.1372	419.8729	423.58
Br3, E2, K U_{32} ($Wm^{-2}K^{-1}$)	589.4058333	425.440917	397.1671	330.2261	475.7617	444.7506	477.7383
Br3, E3, K U_{33} ($Wm^{-2}K^{-1}$)	304.6889328	213.31952	200.5405	166.5243	244.8879	221.53	237.5543
Br3, E4, K U_{34} ($Wm^{-2}K^{-1}$)	457.6431361	379.759105	351.2568	322.7647	262.1799	427.9195	431.7707
U_{lm} ($Wm^{-2}K^{-1}$)	512.5383947	353.342727	341.3235	281.0924	639.111	334.2209	368.733

Test Number	0	1		2		3	
Chiller Number	Design	1	2	1	3	1	4
Deviations from Target Values of U (%)							
Combinations							
Br1, E1, K U_{11} (Wm^{-2}K^{-1})	-89.34	-83.52	-82.75	-78.20	-89.69	-83.35	-84.97
Br1, E2, K U_{12} (Wm^{-2}K^{-1})	-7.03	5.70	1.89	5.59	-35.38	15.50	12.04
Br1, E3, K U_{13} (Wm^{-2}K^{-1})	-47.04	-43.56	-45.18	-43.94	-64.46	-38.39	-40.22
Br1, E4, K U_{14} (Wm^{-2}K^{-1})	-26.09	-6.07	-10.05	1.88	-62.62	9.53	0.59
Br2, E1, K U_{21} (Wm^{-2}K^{-1})	-89.37	-83.55	-82.80	-78.26	-89.71	-83.39	-85.00
Br2, E2, K U_{22} (Wm^{-2}K^{-1})	-9.38	4.46	-0.03	4.14	-36.21	13.70	10.66
Br2, E3, K U_{23} (Wm^{-2}K-1)	-47.81	-43.92	-45.74	-44.35	-64.72	-38.90	-40.62
Br2, E4, K U_{24} (Wm^{-2}K^{-1})	-27.58	-7.05	-11.55	0.53	-62.90	7.92	-0.52
Br3, E1, K U_{31} (Wm^{-2}K^{-1})	-12.50	5.68	1.32	13.19	-59.45	25.63	14.87
Br3, E2, K U_{32} (Wm^{-2}K^{-1})	15.00	20.40	16.36	17.48	-25.56	33.07	29.56
Br3, E3, K U_{33} (Wm^{-2}K^{-1})	-40.55	-39.63	-41.25	-40.76	-61.68	-33.72	-35.58
Br3, E4, K U_{34} (Wm^{-2}K^{-1})	-10.71	7.48	2.91	14.83	-58.98	28.03	17.10
Overall Heat Transfer Coefficient	Max -ve Deviation (%)	Max +ve Deviation (%)		Median Deviation (%)		Mean Deviation (%)	
Br1, E1, K U_{11} (Wm-2K-1)	-89.77	-62.12		-75.95		81.67	
Br1, E2, K U_{12} (Wm^{-2}K^{-1})	-35.38	60.97		12.80		16.34	
Br1, E3, K U_{13} (Wm^{-2}K^{-1})	-64.46	-14.91		-39.69		43.59	
Br1, E4, K U_{14} (Wm^{-2}K^{-1})	-52.76	150.88		49.06		28.85	
Br2, E1, K U_{21} (Wm^{-2}K^{-1})	-89.71	-62.45		-76.08		81.77	
Br2, E2, K U_{22} (Wm^{-2}K^{-1})	-36.21	55.2		9.50		15.15	
Br2, E3, K U_{23} (Wm^{-2}K-1)	-64.72	-16.55		-40.64		44.42	
Br2, E4, K U_{24} (Wm^{-2}K^{-1})	-53.2	137.15		41.98		27.59	
Br3, E1, K U_{31} (Wm^{-2}K^{-1})	-47.57	206.4		79.42		36.70	
Br3, E2, K U_{32} (Wm^{-2}K^{-1})	-25.56	81.77		28.11		25.71	
Br3, E3, K U_{33} (Wm^{-2}K^{-1})	-61.68	-9.43		-35.56		39.13	
Br3, E4, K U_{34} (Wm^{-2}K^{-1})	-46.77	212.58		82.91		37.90	

Test Number	0	1		2		3	
Chiller Number	Design	1	2	1	3	1	4
Compressor Performance							
Quality x at flash economiser	0.1431	0.1269	0.1349	0.1138	0.1073	0.1146	0.09666
Quality x at evaporator	0.06493	0.06714	0.03112	0.06238	0.05564	0.09621	0.07761
Enthalpy at Evaporator inlet ($kJkg^{-1}$)	138.6	141.6	94.19	137.9	137.9	141.6	152.3
Enthalpy at Evaporator outlet ($kJkg^{-1}$)	1406	1406	1407	1407	1408	1405	1405
Total Mass Flow Rate From Compressor (kgs^{-1})	1.23	0.67	0.58	0.43	0.77	0.72	0.80
Mass flow rate through evaporator (kgs^{-1})	1.06	0.58	0.50	0.38	0.69	0.64	0.72
Mass flow rate from flash economiser (kgs^{-1})	0.17	0.08	0.08	0.05	0.08	0.08	0.08
Mass ratio evaporator	0.8618	0.8731	0.8651	0.8862	0.8927	0.8854	0.9033
Mass ratio flash economiser	0.138211382	0.1269	0.1349	0.1138	0.1073	0.1146	0.09666
Enthalpy at Compressor Suction ($kJkg^{-1}$)	1407.5	1407.5	1408.5	1408.5	1409.5	1406.5	1406.5
Enthalpy at Flash Economiser Outlet ($kJkg^{-1}$)	1433.5	1433	1420	1432	1432	1433	1435
Enthalpy at Compresor Discharge ($kJkg^{-1}$)	1625.7	1595	1597	1593	1591	1599	1590
Suction Pressure (bar a)	1.26	1.28	1.3	1.32	1.37	1.24	1.23
Flash vapour Pressure (bar a)	2.75	2.75	2	2.75	2.75	2.75	2.75
Discharge Pressure (bar a)	12.03	10.5	10.5	10.82	9.64	10.82	10.48
Condenser pressure (bar a)	11.67	8.825	8.493	9.195	8.713	9.487	8.685
Compressor Heat Input (kW)	-263.97	-123.03	-109.09	-78.25	-137.75	-136.67	-144.90
Pressure Ratio	9.55	8.20	8.08	8.20	7.04	8.73	8.52
Specific Heat at Constant Pressure at Mean Temperature Cp ($kJkg^{-1}K^{-1}$)	4.79	4.8041	4.7711	4.7816	4.7579	4.7354	4.7601
Specific Heat at Constant Volume at Mean Temperature Cv ($kJkg^{-1}K^{-1}$)	2.84	2.8315	2.8421	2.8388	2.8464	2.8537	2.8457
Ratio of Specific Heats	1.69	1.70	1.68	1.68	1.67	1.66	1.67
Volume Ratio	3.81	3.46	3.47	3.49	3.21	3.69	3.60
Compressor load capacity (%)	76.00	68.00	68.20	68.50	63.00	72.00	71.00
Temperature of oil entering cooler T_{oilin} (^oC)	86.60	73.00	74.00	73.00	70.00	75.00	71.20
Temperature of oil leaving cooler T_{oilout} (^oC)	48.90	48.90	48.90	48.90	48.90	48.90	48.90
Specific heat capacity of oil Cp_{oil} ($kJkg^{-1}K^{-1}$)	2.02	2.02	2.02	2.02	2.02	2.02	2.02
Mass flow rate of oil to cooler m_{oil} (kgs^{-1})	3.70	3.46	3.46	3.51	3.31	3.51	3.45
Heat transferred to oil (kW)	-281.35	-168.03	-175.00	-170.57	-140.96	-184.73	-155.33

Test Number	0	1		2		3	
Chiller Number	Design	1	2	1	3	1	4
Refrigerating capacity (kW)	1343.44	737.06	662.72	484.03	872.13	806.90	907.22
Internal Pump Power (kW)	46.10	51.00	49.00	50.00	52.00	50.00	51.00
COP	2.46	2.53	2.33	1.95	3.13	2.51	3.02
Compressor Power (kW)	450.00	390.00	373.00	365.00	340.00	433.00	395.00
COSP	2.27	2.15	1.99	1.62	2.64	2.17	2.58
Total Refrigerating Effect for Procedure (all on-line chillers)	1343.44	1399.78		1356.16		1714.12	
Total COSP for Procedure (all on-line chillers)	2.27	1.62199562		1.680493		1.845124	

Actual surface area for heat transfer (m^2)	431.318345	434.5118	434.5118	434.5118	434.5118	434.5118	434.5118
Surface area using U_{11} (m^2)	4045.63132	2636.89531	2518.385	1993.314	4212.744	2609.684	2891.642
Surface area using U_{12} (m^2)	463.9479358	411.072238	426.4542	411.5223	672.421	376.2005	387.8015
Surface area using U_{13} (m^2)	814.4305441	769.921746	792.5836	775.115	1222.716	705.2191	726.8834
Surface area using U_{14} (m^2)	583.5807152	462.569952	483.0731	426.5061	1162.552	396.6932	431.9455
Surface area using U_{21} (m^2)	4057.639684	2641.78094	2526.559	1999.034	4221.473	2615.63	2896.498
Surface area using U_{22} (m^2)	475.9563003	415.957865	434.6282	417.2416	681.1504	382.1467	392.657
Surface area using U_{23} (m^2)	826.4389086	774.807373	800.7577	780.8343	1231.446	711.1653	731.7389
Surface area using U_{24} (m^2)	595.5890797	467.455578	491.2472	432.2254	1171.281	402.6394	436.801
Surface area using U_{31} (m^2)	492.9564215	411.162714	428.8661	383.8817	1071.638	345.8735	378.2493
Surface area using U_{32} (m^2)	375.0679068	360.876395	373.4173	369.8616	583.6983	326.5267	335.3694
Surface area using U_{33} (m^2)	725.5505152	719.725903	739.5468	733.4542	1133.994	655.5453	674.4513
Surface area using U_{34} (m^2)	483.0558894	404.286776	422.2241	378.4117	1059.201	339.3697	371.0739

2nd Law Analysis

Test Number	0	1		2		3	
Chiller Number	Design	1	2	1	3	1	4
COP_{act} based on per kg flow	2.2023	3.1336	3.1378	3.1915	3.5427	2.9894	3.3671
COP_{Carnot}	5.8640	6.4780	6.4780	6.4013	6.4587	6.5169	6.5169
Condenser temperature T_H (K)	295.1500	288.65	288.65	288.65	288.65	288.65	288.65
Evaporator temperature T_L (K)	252.1500	250.0500	250.0500	249.6500	249.9500	250.2500	250.2500
Temperature of surroundings T_o (K)	289.1500	289.15	289.15	289.15	289.15	289.15	289.15
Temperature of brine T (K)	252.1500	249.4	249.4	249.2	249.2	249.5	249.5
Cooling tower water temperature T_{ct} (K)	295.1500	288.7	288.7	288.7	288.7	288.7	288.7
Entropy of ammonia into evaporator s_9 ($kJkg^{-1}K^{-1}$)	0.5713	0.5836	0.3895	0.5675	0.5664	0.5846	0.6288
Entropy of ammonia exit evaporator s_1 (kJkg-1K-1)	5.7670	5.754	5.74	5.743	5.73	5.765	5.768
Entropy of ammonia at compressor suction s'_1 ($kJkg^{-1}K^{-1}$)	5.7670	5.754	5.74	5.743	5.73	5.765	5.768
Entropy of ammonia exit compressor s_2 ($kJkg^{-1}K^{-1}$)	5.4430	5.518	5.425	5.494	5.445	5.415	5.406
Entropy of ammonia exit flash economiser s_6 ($kJkg^{-1}K^{-1}$)	5.5030	5.445	5.598	5.456	5.456	5.445	5.413
Entropy of ammonia entering condenser s_3 ($kJkg^{-1}K^{-1}$)	5.443	5.518	5.425	5.494	5.445	5.415	5.406
Entropy of ammonia leaving condenser s_4 ($kJkg^{-1}K^{-1}$)	1.2020	1.055	1.036	1.076	1.049	1.092	1.047
Entropy of ammonia after first throttle s_5 ($kJkg^{-1}K^{-1}$)	1.2550	1.085	1.089	1.111	1.08	1.127	1.072
Entropy leaving flash economiser s_6 ($kJkg^{-1}K^{-1}$)	5.4560	5.445	5.598	5.456	5.456	5.445	5.413
Entropy leaving flash economiser s_8 ($kJkg^{-1}K^{-1}$)	0.5546	0.568	0.3859	0.554	0.554	0.568	0.6079
Entropy of flash to compressor s_7 ($kJkg^{-1}K^{-1}$)	5.5410	5.502	5.598	5.498	5.498	5.502	5.509
Enthalpy of ammonia entering evaporator h_9 ($kJkg^{-1}$)	138.6000	141.6	94.19	137.9	137.9	141.6	152.3
Enthalpy of ammonia leaving evaporator h_1 ($kJkg^{-1}$)	1406.0000	1406	1407	1407	1408	1405	1405
Enthalpy of ammonia at compressor suction h'_1 (kJkg-1)	1407.5000	1407.5	1408.5	1408.5	1409.5	1406.5	1406.5
Enthalpy of ammonia leaving compressor h_2 ($kJkg^{-1}$)	1625.7000	1595	1597	1593	1591	1599	1590
Enthalpy of ammonia from flash economiser h_6 (kJkg-1)	1433.5000	1433	1420	1432	1432	1433	1435
Isentropic enthalpy leaving compressor h_{s2} ($kJkg^{-1}$)	1750.0000	1746	1746.5	1736	1703	1745	1741
Isentropic enthalpy leaving compressor h'_{s2} ($kJkg^{-1}$)	1647.0000	1624	1659	1628	1628	1629	1627
Enthalpy of ammonia entering condenser h_3 ($kJkg^{-1}$)	1625.7000	1595	1597	1593	1591	1604	1598
Enthalpy of ammonia leaving condenser h_4 ($kJkg^{-1}$)	323.0000	278.7	272.9	285.1	276.7	289.6	276.3

2nd Law Analysis

Test Number	0	1		2		3	
Chiller Number	Design	1	2	1	3	1	4
Refrigerating capacity Q_L (kW)	1343.44	737.06	662.72	484.03	872.13	806.90	907.22
Specific refrigerating capacity q_L ($kJkg^{-1}$)	1267.40	1264.40	1312.81	1269.10	1270.10	1263.40	1252.70
Condenser heat load Q_H (kW)	-1602.321	-878.838	-772.653	-562.885	-1010.953	-948.130	-1059.612
Condenser specific heat load q_H ($kJkg^{-1}$)	-1302.700	-1316.300	-1324.100	-1307.900	-1314.300	-1314.400	-1321.700
Cycle irreversibility I_{cycle} (kW)	**359.3642**	**208.3135**	**215.7344**	**199.3921**	**161.8635**	**228.7576**	**179.8157**
Heat engine (evaporator) W_{rev} (kJ)	-197.13	-115.25	-103.63	-76.58	-136.78	-125.43	-141.02
Availability (evaporator) ($kJkg^{-1}$)	-185.98	-197.71	-205.28	-200.80	-199.19	-196.39	-194.73
Evaporator irreversibility i_{evap} (kW)	48.961	29.098	25.048	23.943	19.341	33.736	33.932
Condenser irreversibility i_{cond} ($kJkg^{-1}$)	49.933	28.104	57.314	32.701	45.473	66.681	63.585
Compressor irreversibility i_{comp} ($kJkg^{-1}$)	125.319	72.030	48.845	72.466	38.943	55.007	30.994
Throttle 4-5 irreversibility i_{4-5} ($kJkg^{-1}$)	15.325	8.675	15.325	10.120	8.964	10.120	7.229
Throttle 6-7 irreversibility i_{6-7} ($kJkg^{-1}$)	21.433	14.216	0.000	10.466	10.466	14.221	23.947
Throttle 8-9 irreversibility i_{8-9} ($kJkg^{-1}$)	4.929	4.503	1.039	3.897	3.579	4.792	6.033
Total of irreversibilities i_{tot} ($kJkg^{-1}$)	**265.899**	**156.624**	**147.571**	**153.593**	**126.767**	**184.557**	**165.720**
Adjusted compressor irreversibility i_{comp} ($kJkg^{-1}$)	**218.784**	**123.719**	**117.008**	**118.265**	**74.040**	**99.207**	**45.090**
Compressor isentropic work W_{isen}	-399.345	-213.505	-189.440	-134.507	-217.712	-232.394	-257.127
Compressor adiabatic efficiency	0.483	0.465	0.413	0.321	0.519	0.459	0.564
Compressor second law efficiency	0.599	0.575	0.588	0.525	0.734	0.691	0.850
Compressor actual work rate Wact (kW)	-545.317	-291.055	-284.092	-248.824	-278.712	-321.394	-300.236
Compressor reversible work W_{rev} (kW)	-326.533	-167.336	-167.084	-130.559	-204.672	-222.187	-255.146
Chiller second law effectiveness	0.3615	0.3960	0.3648	0.3078	0.4907	0.3903	0.4697

Procedure Number	4		5		6	
Chiller Number	2	3	2	4	3	4
Brine Properties						
Brine Inlet Temperature T_{ei} (°C)	-22.6	-22.5	-23	-23.1	-22.6	-22.8
Brine Outlet Temperature T_{eo} (°C)	-24	-24.6	-24.4	-24.5	-24.7	-24.1
Brine Bulk (mean) Temperature T_b (°C)	-23.3	-23.6	-23.7	-23.8	-23.7	-23.5
Volumetric Flow Rate of Brine (m^3hr^{-1})	481.5	600	526	585	585	585
Brine Mass Flow Rate $\dot{m}_b$ (kgs^{-1})	170.90	212.98	186.72	207.67	207.66	207.65
Specific Heat Capacity C_p ($kJkg^{-1}K^{-1}$) **(mean temperature)**	2.731648	2.730725	2.730417	2.73011	2.730417	2.731033
Brine density ρ_b (kgm^{-3}) **(mean temperature)**	1277.753	1277.891	1277.938	1277.984	1277.938	1277.845
Thermal Conductivity k_b ($Wm^{-1}K^{-1}$)**(mean temperature)**	0.4984	0.4979	0.4978	0.4976	0.4978	0.4981
Brine dynamic viscocity at wall μ_w (Nsm^{-2})	0.013871	0.014211	0.014098	0.014155	0.014268	0.013928
Brine dynamic viscocity (bulk) μ_b (Nsm^{-2})	0.013473	0.013644	0.013701	0.013757	0.013701	0.013587
Ammonia Properties in Evaporator						
Pressure (bar a)	1.32	1.28	1.3	1.26	1.29	1.26
Temperature T_{evap} (°C)	-27.93	-28.58	-28.25	-28.91	-29.24	-28.91
Liquid Thermal Conductivity k_l ($Wm^{-1}K^{-1}$)	0.603463	0.604836	0.60415	0.605523	0.604493	0.605523
Vapour Thermal Conductivity k_v ($Wm^{-1}K^{-1}$)	0.019279	0.019217	0.019248	0.019185	0.019232	0.019185
Liquid Density ρ (kgm^{-3})	674.7638	675.6757	657.2194	676.1325	675.6757	676.1325
Vapour Density ρ (kgm^{-3})	1.1396	1.1068	1.1234	1.091	1.1151	1.091
Liquid Dynamic Viscosity μ_l (Nsm^{-2})	0.000266	0.000269	0.000268	0.00027	0.000266	0.00027
Vapour Dynamic Viscosity μ_v **(Nsm-2)**	9.41E-06	9.39E-06	9.40E-06	9.38E-06	9.40E-06	9.38E-06
Surface Tension σ mNm^{-1}	32.75	32.9	32.88	32.98	32.86	32.98
Latent Heat λ ($kJkg^{-1}$)	1354.94	1356.88	1355.91	1357.84	1356.39	1357.84
h_g ($kJkg^{-1}$)	1407	1406	1407	1406	1406	1406
h_f ($kJkg^{-1}$)	53.48	50.58	52.06	49.11	51.32	49.11
Enthalpy Difference h_{fg} ($kJkg^{-1}$)	1353.52	1355.42	1354.94	1356.89	1354.68	1356.89
Vapor Specific Heat Capacity ($kJkg^{-1}K^{-1}$)	2.216	2.203	2.21	2.197	2.206	2.197
Liquid Specific Heat Capacity ($kJkg^{-1}K^{-1}$)	4.492	4.489	4.49	4.488	4.49	4.488
Pressure $P_{satwall}$ **(bar a)**	1.627	1.598	1.597	1.588	1.592	1.615

Test Number	4		5		6	
Chiller Number	2	3	2	4	3	4
Evaporator Tube Properties						
Tube Length (m)	5.4864	5.4864	5.4864	5.4864	5.4864	5.4864
K Thermal Conductivity ($Wm^{-1}K^{-1}$)	40	40	40	40	40	40
Internal Diameter (m)	0.027432	0.027432	0.027432	0.027432	0.027432	0.027432
Thickness (m)	0.002159	0.002159	0.002159	0.002159	0.002159	0.002159
External Diameter (m)	0.03175	0.03175	0.03175	0.03175	0.03175	0.03175
Performance Calculations						
Chilling Heat Load (kW)	653.572	1221.349	713.7564	793.7559	1190.725	737.228
Evaporator Heat Transfer Area (m^2)	434.5118	434.5118	434.5118	434.5118	434.5118	434.5118
Log Mean Temperature Difference	4.594505	4.956069	4.513873	5.077875	5.523627	5.434108
U_{lm} Overall Heat Transfer Coefficient ($Wm^{-2}K^{-1}$)	327.3808	567.1538	363.9143	359.7521	496.1186	312.2281
Area for Flow per Pass (m^2)	0.078015	0.078015	0.078015	0.078015	0.078015	0.078015
Brine Flowrate (m^3s^{-1})	481.5	600	526	585	585	585
Brine velocity (ms^{-1})	1.714414	2.136341	1.872859	2.082933	2.082933	2.082933
Tube Calculations						
Heat flux (Wm^{-2})	1504.153	2810.854	1642.663	1826.776	2740.374	1696.681
Tube Outer Wall Temperature (°C)	-23.4595	-23.8480	-23.8741	-23.9937	-23.9405	-23.6299
NH3 Pcrit (bar a)	112.9	112.9	112.9	112.9	112.9	112.9
P_R	0.011692	0.011337	0.011515	0.01116	0.011426	0.01116
$f(P_R)$	0.864123	0.859018	0.861584	0.856424	0.860304	0.856424
NH_3 Molecular Weight	17.0304	17.0304	17.0304	17.0304	17.0304	17.0304
A a constant 30-55	55	55	55	55	55	55
Epsilon Surface Roughness (µm)	0.5	0.5	0.5	0.5	0.5	0.5

Test Number	4		5		6	
Chiller Number	2	3	2	4	3	4
Brine Coefficient Calculations						
Brine Side Reynolds Number	4460.082	5488.956	4792.211	5307.927	5329.741	5373.872
Brine Side Prandtl Number	73.84548	74.82867	75.1468	75.48019	75.1468	74.49618
Laminar Brine Flow Regime						
Entry Length (m)	6.117449	7.528652	6.572997	7.280353	7.310273	7.370803
Thermal Entry Length (m)	451.7459	563.359	493.9397	549.5224	549.3436	549.0966
Nusselt Number	76.63835	90.05743	81.84057	88.45154	88.43069	88.40189
Br1 Convective Coefficient of Heat Transfer ($Wm^{-2}K^{-1}$)	1392.409	1634.573	1485.136	1604.458	1604.724	1605.168
Brine Transition Flow Regime						
Nusselt Number	70.35825	86.67613	75.86725	84.10753	84.23535	84.97351
Br2 Convective Coefficient of Heat Transfer ($Wm^{-2}K^{-1}$)	1278.308	1573.201	1376.739	1525.66	1528.593	1542.917
Brine Turbulent Flow Regime						
Nusselt Number	166.3895	189.2821	174.7211	186.0429	186.2291	186.6165
Br3 Convective Coefficient of Heat Transfer ($Wm^{-2}K^{-1}$)	3023.058	3435.534	3170.61	3374.707	3379.441	3388.512

Test Number	4		5		6	
Chiller Number	2	3	2	4	3	4
Boiling Heat Transfer Coefficients						
Bromley's Correlation						
E1 Boiling Coefficient of Heat Transfer ($Wm^{-2}K^{-1}$)	53.35083	52.15649	53.05778	51.45137	50.8166	50.54425
Mostinski's Correlation						
E2 Boiling Coefficient of Heat Transfer ($Wm^{-2}K^{-1}$)	400.2621	616.3873	424.4692	454.4995	606.4342	431.5924
Cooper's Correlation						
E3 Boiling Coefficient of Heat Transfer ($Wm^{-2}K^{-1}$)	187.131	279.1923	196.8068	207.6907	275.67	197.7092
Chen's Correlation						
Tube Pitch S_D=S_L (m)	0.039688	0.039688	0.039688	0.039688	0.039688	0.039688
Effective Area Approach Bottom Tube Row (m^2)	3.603	3.603	3.603	3.603	3.603	3.603
Velocity Approaching Bottom Tube Row (ms^{-1})	0.000212	0.000382	0.000239	0.000258	0.000385	0.000237
Liquid Phase Reynolds Number Re_l	39.94247	73.86441	43.37578	47.73522	72.75726	44.33628
Liquid Phase Prandtl Number Pr_l	1.982417	1.994658	1.988326	2.000971	1.97686	2.000971
Martinelli Parameter *X*	0.631403	1.211898	0.602326	0.569479	0.663623	0.67135
1/*X*	1.583775	0.825152	1.66023	1.75599	1.506879	1.489537
Two-phase Heat Transfer Coefficient Multiplier F -chart	3.7	2.5	3.5	3.8	3.475	3.47
Two-phase Reynolds Number Re_{TP}	204.9685	232.1989	207.6502	253.261	345.1993	209.9767
Suppression Factor S -chart	0.95	0.95	0.95	0.95	0.95	0.95
Forster-Zuber Boiling Coefficient ($Wm^{-2}K^{-1}$)	358.3983	372.8709	342.833	385.0331	369.5063	415.6279
Forced Convection Boiling Coefficient ($Wm^{-2}K^{-1}$)	4.063148	4.510841	4.115187	4.846916	6.169098	4.172032
E4 Boiling Coefficient of Heat Transfer ($Wm^{-2}K^{-1}$)	362.4615	377.3818	346.9482	389.88	375.6754	419.7999

Test Number	4		5		6	
Chiller Number	2	3	2	4	3	4
Overall Heat Transfer Coefficient Calculations						
Combinations						
Br1, E1, K U_{11} ($Wm^{-2}K^{-1}$)	58.92445	58.02036	58.76998	57.22842	56.54991	56.25899
Br1, E2, K U_{12} ($Wm^{-2}K^{-1}$)	340.7408	482.739	361.4233	387.2559	474.8568	372.732
Br1, E3, K U_{13} ($Wm^{-2}K^{-1}$)	185.4158	265.6439	195.2573	206.5556	262.0986	197.9783
Br1, E4, K U_{14} ($Wm^{-2}K^{-1}$)	316.4659	337.9228	310.4008	345.1435	335.4541	365.0798
Br2, E1, K U_{21} ($Wm^{-2}K^{-1}$)	58.70271	57.94013	58.58744	57.12319	56.45083	56.17954
Br2, E2, K U_{22} ($Wm^{-2}K^{-1}$)	333.4572	477.2406	354.6284	382.4878	467.9601	369.2724
Br2, E3, K U_{23} (Wm^{-2}K-1)	183.2379	263.9704	193.2568	205.1912	259.9837	196.998
Br2, E4, K U_{24} ($Wm^{-2}K^{-1}$)	310.1735	335.2193	305.3756	341.3509	331.9976	361.7601
Br3, E1, K U_{31} ($Wm^{-2}K^{-1}$)	361.7136	380.1327	350.1636	390.2417	377.9446	416.0834
Br3, E2, K U_{32} ($Wm^{-2}K^{-1}$)	392.5582	571.1649	415.1279	443.394	562.2258	424.6249
Br3, E3, K U_{33} ($Wm^{-2}K^{-1}$)	199.7645	290.3826	209.9294	221.5148	286.6886	211.7215
Br3, E4, K U_{34} ($Wm^{-2}K^{-1}$)	367.6696	386.7163	355.7424	397.1833	384.4519	423.9841
U_{lm} ($Wm^{-2}K^{-1}$)	327.3808	567.1538	363.9143	359.7521	496.1186	312.2281

Test Number	4		5		6	
Chiller Number	2	3	2	4	3	4
Deviations from Target Values of U (%)						
Combinations						
Br1, E1, K U_{11} ($Wm^{-2}K^{-1}$)	-82.00	-89.77	-83.85	-84.09	-88.60	-81.98
Br1, E2, K U_{12} ($Wm^{-2}K^{-1}$)	4.08	-14.88	-0.68	7.65	-4.29	19.38
Br1, E3, K U_{13} ($Wm^{-2}K^{-1}$)	-43.36	-53.16	-46.35	-42.58	-47.17	-36.59
Br1, E4, K U_{14} ($Wm^{-2}K^{-1}$)	-3.33	-40.42	-14.70	-4.06	-32.38	16.93
Br2, E1, K U_{21} ($Wm^{-2}K^{-1}$)	-82.07	-89.78	-83.90	-84.12	-88.62	-82.01
Br2, E2, K U_{22} ($Wm^{-2}K^{-1}$)	1.86	-15.85	-2.55	6.32	-5.68	18.27
Br2, E3, K U_{23} (Wm^{-2}K-1)	-44.03	-53.46	-46.89	-42.96	-47.60	-36.91
Br2, E4, K U_{24} ($Wm^{-2}K^{-1}$)	-5.26	-40.89	-16.09	-5.11	-33.08	15.86
Br3, E1, K U_{31} ($Wm^{-2}K^{-1}$)	10.49	-32.98	-3.78	8.48	-23.82	33.26
Br3, E2, K U_{32} ($Wm^{-2}K^{-1}$)	19.91	0.71	14.07	23.25	13.32	36.00
Br3, E3, K U_{33} ($Wm^{-2}K^{-1}$)	-38.98	-48.80	-42.31	-38.43	-42.21	-32.19
Br3, E4, K U_{34} ($Wm^{-2}K^{-1}$)	12.31	-31.81	-2.25	10.40	-22.51	35.79

Test Number	4		5		6	
Chiller Number	2	3	2	4	3	4
Compressor Performance						
Quality x at flash economiser	0.1028	0.1395	0.1017	0.09582	0.1122	0.1066
Quality x at evaporator	0.06512	0.03216	0.06885	0.0709	0.0611	0.05976
Enthalpy at Evaporator inlet ($kJkg^{-1}$)	141.6	94.19	145.3	145.3	134.1	130.2
Enthalpy at Evaporator outlet ($kJkg^{-1}$)	1407	1406	1407	1406	1406	1406
Total Mass Flow Rate From Compressor (kgs^{-1})	0.58	1.08	0.63	0.70	1.05	0.65
Mass flow rate through evaporator (kgs^{-1})	0.52	0.93	0.57	0.63	0.94	0.58
Mass flow rate from flash economiser (kgs^{-1})	0.06	0.15	0.06	0.07	0.12	0.07
Mass ratio evaporator	0.8972	0.8605	0.8983	0.9042	0.8878	0.8934
Mass ratio flash economiser	0.1028	0.1395	0.1017	0.09582	0.1122	0.1066
Enthalpy at Compressor Suction ($kJkg^{-1}$)	1408.5	1407.5	1408.5	1407.5	1407.5	1407.5
Enthalpy at Flash Economiser Outlet ($kJkg^{-1}$)	1433	1420	1434	1434	1431	1430
Enthalpy at Compresor Discharge ($kJkg^{-1}$)	1595	1594	1595	1592	1594	1591
Suction Pressure (bar a)	1.32	1.28	1.3	1.26	1.29	1.26
Flash vapour Pressure (bar a)	2.75	2	2.75	2.75	2.75	2.75
Discharge Pressure (bar a)	10.6	10.64	10.5	10.5	10.5	10.5
Condenser pressure (bar a)	8.575	8.853	8.685	8.251	8.881	8.251
Compressor Heat Input (kW)	-105.91	-199.90	-115.82	-126.71	-193.88	-117.14
Pressure Ratio	8.03	8.31	8.08	8.33	8.14	8.33
Specific Heat at Constant Pressure at Mean Temperature Cp ($kJkg^{-1}K^{-1}$)	4.7618	4.7788	4.7381	4.7744	4.7497	4.7381
Specific Heat at Constant Volume at Mean Temperature Cv ($kJkg^{-1}K^{-1}$)	2.8452	2.8397	2.8528	2.8411	2.8491	2.8528
Ratio of Specific Heats	1.67	1.68	1.66	1.68	1.67	1.66
Volume Ratio	3.47	3.52	3.52	3.53	3.52	3.58
Compressor load capacity (%)	68.20	69.50	69.50	69.75	70.50	69.50
Temperature of oil entering cooler T_{oilin} (^oC)	73.20	73.00	73.00	72.00	73.00	70.80
Temperature of oil leaving cooler T_{oilout} (^oC)	48.90	48.90	48.90	48.90	48.90	48.90
Specific heat capacity of oil Cp_{oil} ($kJkg^{-1}K^{-1}$)	2.02	2.02	2.02	2.02	2.02	2.02
Mass flow rate of oil to cooler m_{oil} (kgs^{-1})	3.47	3.48	3.46	3.46	3.46	3.46
Heat transferred to oil (kW)	-170.23	-169.15	-168.03	-161.06	-168.03	-152.69

Test Number	4		5		6	
Chiller Number	2	3	2	4	3	4
Refrigerating capacity (kW)	653.57	1221.35	713.76	793.76	1190.72	737.23
Internal Pump Power (kW)	48.00	52.00	49.00	51.00	51.00	51.00
COP	2.37	3.31	2.51	2.76	3.29	2.73
Compressor Power (kW)	377.00	411.00	386.00	370.00	404.00	250.00
COSP	2.02	2.90	2.14	2.34	2.88	2.30
Total Refrigerating Effect for Procedure (all on-line chillers)	1874.92		1507.51		1927.95	
Total COSP for Procedure (all on-line chillers)	2.111398		1.761113		2.550202	

Actual surface area for heat transfer (m^2)	434.5118	434.5118	434.5118	434.5118	434.5118	434.5118
Surface area using U_{11} (m^2)	2414.122	4247.389	2690.575	2731.45	3812.02	2411.469
Surface area using U_{12} (m^2)	417.4751	510.4934	437.5065	403.6518	453.9671	363.9794
Surface area using U_{13} (m^2)	767.1989	927.6894	809.8293	756.7772	822.4745	685.2608
Surface area using U_{14} (m^2)	449.498	729.2643	509.4222	452.9031	642.6196	371.6086
Surface area using U_{21} (m^2)	2423.241	4253.27	2698.958	2736.481	3818.71	2414.879
Surface area using U_{22} (m^2)	426.5939	516.3748	445.8895	408.6838	460.6576	367.3895
Surface area using U_{23} (m^2)	776.3178	933.5708	818.2123	761.8091	829.165	688.6709
Surface area using U_{24} (m^2)	458.6168	735.1457	517.8051	457.935	649.3101	375.0186
Surface area using U_{31} (m^2)	393.2692	648.2869	451.5748	400.5634	570.373	326.0567
Surface area using U_{32} (m^2)	362.3687	431.4604	380.9069	352.5455	383.4213	319.498
Surface area using U_{33} (m^2)	712.0925	848.6564	753.2296	705.6709	751.9287	640.7794
Surface area using U_{34} (m^2)	386.8985	637.2502	444.4932	393.5627	560.7187	319.9808

2nd Law Analysis

Test Number	4		5		6	
Chiller Number	2	3	2	4	3	4
COP_{act}	3.2052	3.1896	3.2204	3.3231	3.2089	3.4147
COP_{Carnot}	6.5761	6.5961	6.4974	6.4780	6.5761	6.5366
Condenser temperature T_H (K)	288.65	288.65	288.65	288.65	288.65	288.65
Evaporator temperature T_L (K)	250.5500	250.6500	250.1500	250.0500	250.5500	250.3500
Temperature of surroundings T_o (K)	289.15	289.15	289.15	289.15	289.15	289.15
Temperature of brine T (K)	249.9	249.6	249.5	249.4	249.5	249.7
Cooling tower water temperature T_{ct} (K)	288.7	288.7	288.7	288.7	288.7	288.7
Entropy of ammonia into evaporator s_9 ($kJkg^{-1}K^{-1}$)	0.5826	0.3898	0.5982	0.5993	0.5527	0.5399
Entropy of ammonia exit evaporator s_1 (kJkg-1K-1)	5.743	5.754	5.748	5.759	5.751	5.759
Entropy of ammonia at compressor suction s'_1 ($kJkg^{-1}K^{-1}$)	5.743	5.754	5.748	5.759	5.751	5.759
Entropy of ammonia exit compressor s_2 ($kJkg^{-1}K^{-1}$)	5.414	5.41	5.418	5.411	5.514	5.422
Entropy of ammonia exit flash economiser s_6 ($kJkg^{-1}K^{-1}$)	5.445	5.598	5.434	5.434	5.468	5.481
Entropy of ammonia entering condenser s_3 ($kJkg^{-1}K^{-1}$)	5.414	5.41	5.418	5.411	5.514	5.422
Entropy of ammonia leaving condenser s_4 ($kJkg^{-1}K^{-1}$)	1.041	1.057	1.047	1.021	1.059	1.021
Entropy of ammonia after first throttle s_5 ($kJkg^{-1}K^{-1}$)	1.069	1.113	1.075	1.046	1.092	1.053
Entropy leaving flash economiser s_6 ($kJkg^{-1}K^{-1}$)	5.445	5.598	5.434	5.434	5.468	5.481
Entropy leaving flash economiser s_8 ($kJkg^{-1}K^{-1}$)	0.568	0.3859	0.5816	0.5816	0.5395	0.5247
Entropy of flash to compressor s_7 ($kJkg^{-1}K^{-1}$)	5.502	5.598	5.505	5.505	5.505	5.49
Enthalpy of ammonia entering evaporator h_9 ($kJkg^{-1}$)	141.6	94.19	145.3	145.3	134.1	130.2
Enthalpy of ammonia leaving evaporator h_1 ($kJkg^{-1}$)	1407	1406	1407	1406	1406	1406
Enthalpy of ammonia at compressor suction h'_1 (kJkg-1)	1408.5	1407.5	1408.5	1407.5	1407.5	1407.5
Enthalpy of ammonia leaving compressor h_2 ($kJkg^{-1}$)	1595	1594	1595	1592	1594	1591
Enthalpy of ammonia from flash economiser h_6 (kJkg-1)	1433	1420	1434	1434	1431	1430
Isentropic enthalpy leaving compressor h_{s2} ($kJkg^{-1}$)	1745	1726	1745	1746	1725	1739
Isentropic enthalpy leaving compressor h'_{s2} ($kJkg^{-1}$)	1626	1661	1625	1625	1624	1614
Enthalpy of ammonia entering condenser h_3 ($kJkg^{-1}$)	1595	1594	1595	1592	1594	1591
Enthalpy of ammonia leaving condenser h_4 ($kJkg^{-1}$)	274.4	279.1	276.3	268.7	279.6	268.7

2nd Law Analysis

Test Number	4		5		6	
Chiller Number	2	3	2	4	3	4
Refrigerating capacity Q_L (kW)	653.57	1221.35	713.76	793.76	1190.72	737.23
Specific refrigerating capacity q_L ($kJkg^{-1}$)	1265.40	1311.81	1261.70	1260.70	1271.90	1275.80
Condenser heat load Q_H (kW)	-760.235	-1422.691	-830.460	-921.465	-1386.024	-855.270
Condenser specific heat load q_H ($kJkg^{-1}$)	-1320.600	-1314.900	-1318.700	-1323.300	-1314.400	-1322.300
Cycle irreversibility I_{cycle} (kW)	**202.3719**	**212.3975**	**197.5953**	**184.7565**	**202.9533**	**178.4412**
Heat engine (evaporator) W_{rev} (kJ)	-100.69	-187.60	-111.28	-124.12	-183.44	-114.26
Availability (evaporator) ($kJkg^{-1}$)	-194.95	-201.49	-196.71	-197.13	-195.95	-197.73
Evaporator irreversibility i_{evap} (kW)	27.689	31.388	26.565	30.001	29.061	31.740
Condenser irreversibility i_{cond} ($kJkg^{-1}$)	58.435	58.508	57.110	56.224	28.514	52.041
Compressor irreversibility i_{comp} ($kJkg^{-1}$)	51.102	35.585	49.293	39.794	74.240	34.670
Throttle 4-5 irreversibility $i_{4\text{-}5}$ ($kJkg^{-1}$)	8.096	16.192	8.096	7.229	9.542	9.253
Throttle 6-7 irreversibility $i_{6\text{-}7}$ ($kJkg^{-1}$)	14.241	0.000	17.711	17.704	9.231	2.247
Throttle 8-9 irreversibility $i_{8\text{-}9}$ ($kJkg^{-1}$)	4.214	1.126	4.792	5.109	3.810	4.387
Total of irreversibilities i_{tot} ($kJkg^{-1}$)	**163.778**	**142.799**	**163.566**	**156.060**	**154.398**	**134.338**
	89.696	**105.184**	**83.322**	**68.490**	**122.795**	**78.773**
Compressor isentropic work W_{isen}	-185.222	-332.912	-202.594	-225.869	-320.071	-204.246
Compressor adiabatic efficiency	0.415	0.619	0.448	0.503	0.604	0.483
Compressor second law efficiency	0.675	0.715	0.706	0.762	0.661	0.708
Compressor actual work rate Wact (kW)	-276.142	-369.048	-283.846	-287.764	-361.912	-269.828
Compressor reversible work W_{rev} (kW)	-186.446	-263.864	-200.524	-219.274	-239.117	-191.056
Chiller second law effectiveness	0.3646	0.5083	0.3920	0.4313	0.5069	0.4234

Procedure Number		7			8	
Chiller Number	1	2	3	1	3	4
Brine Properties						
Brine Inlet Temperature T_{ei} (°C)	-23.2	-22.9	-23	-23.1	-22.9	-23.1
Brine Outlet Temperature T_{eo} (°C)	-24.2	-24.4	-24.7	-24.4	-24.8	-24.3
Brine Bulk (mean) Temperature T_b (°C)	-23.7	-23.7	-23.9	-23.8	-23.9	-23.7
Volumetric Flow Rate of Brine (m^3hr^{-1})	448.5	426	471	448.5	471	471
Brine Mass Flow Rate $\dot{m}_b$ (kgs^{-1})	159.21	151.22	167.21	159.22	167.21	167.20
Specific Heat Capacity C_p ($kJkg^{-1}K^{-1}$) (mean temperature)	2.730417	2.730417	2.729802	2.73011	2.729802	2.730417
Brine density ρ_b (kgm^{-3}) (mean temperature)	1277.938	1277.938	1278.076	1277.984	1278.076	1277.938
Thermal Conductivity k_b ($Wm^{-1}K^{-1}$)(mean temperature)	0.4978	0.4978	0.4975	0.4976	0.4975	0.4978
Brine dynamic viscocity at wall μ_w (Nsm^{-2})	0.0139843	0.0140979	0.014682	0.0140979	0.014325	0.0140411
Brine dynamic viscocity (bulk) μ_b (Nsm^{-2})	0.0137005	0.0137005	0.013814	0.0137573	0.013814	0.0137005
Ammonia Properties in Evaporator						
Pressure (bar a)	1.32	1.3	1.35	1.3	1.35	1.26
Temperature T_{evap} (°C)	-27.93	-28.25	-27.46	-28.25	-27.46	-28.91
Liquid Thermal Conductivity k_l ($Wm^{-1}K^{-1}$)	0.6034633	0.6041498	0.6024337	0.6041498	0.6024337	0.6055226
Vapour Thermal Conductivity k_v ($Wm^{-1}K^{-1}$)	0.0192789	0.0192477	0.0193257	0.0192477	0.0193257	0.0191853
Liquid Density ρ (kgm^{-3})	674.7638	657.2194	674.3688	657.2194	674.3688	676.1325
Vapour Density ρ (kgm^{-3})	1.1396	1.1234	1.1367	1.1234	1.1367	1.091
Liquid Dynamic Viscosity μ_l (Nsm^{-2})	0.000266321	0.000267538	0.000264496	0.000267538	0.000264496	0.000269972
Vapour Dynamic Viscosity μ_v (Nsm-2)	9.41E-06	9.40E-06	9.43E-06	9.40E-06	9.43E-06	9.38E-06
Surface Tension σ mNm^{-1}	32.75	32.88	32.64	32.88	32.64	32.98
Latent Heat λ ($kJkg^{-1}$)	1354.94	1355.91	1353.5	1355.91	1353.5	1357.84
h_g ($kJkg^{-1}$)	1407	1407	1408	1407	1408	1406
h_f ($kJkg^{-1}$)	53.48	52.06	55.58	52.06	55.58	49.11
Enthalpy Difference h_{fg} ($kJkg^{-1}$)	1353.52	1354.94	1352.42	1354.94	1352.42	1356.89
Vapor Specific Heat Capacity ($kJkg^{-1}K^{-1}$)	2.216	2.21	2.225	2.21	2.225	2.197
Liquid Specific Heat Capacity ($kJkg^{-1}K^{-1}$)	4.492	4.49	4.494	4.49	4.494	4.488
Pressure $P_{satwall}$ (bar a)	1.601	1.602	1.584	1.595	1.583	1.6

Test Number	7			8		
Chiller Number	1	2	3	1	3	4
Evaporator Tube Properties						
Tube Length (m)	5.4864	5.4864	5.4864	5.4864	5.4864	5.4864
K Thermal Conductivity ($Wm^{-1}K^{-1}$)	40	40	40	40	40	40
Internal Diameter (m)	0.027432	0.027432	0.027432	0.027432	0.027432	0.027432
Thickness (m)	0.002159	0.002159	0.002159	0.002159	0.002159	0.002159
External Diameter (m)	0.03175	0.03175	0.03175	0.03175	0.03175	0.03175
Performance Calculations						
Chilling Heat Load (kW)	434.7090785	619.3513961	775.9882675	565.078601	867.2810048	547.8206715
Evaporator Heat Transfer Area (m^2)	434.5118	434.5118	434.5118	434.5118	434.5118	434.5118
Log Mean Temperature Difference	4.210225505	4.558946089	3.542271168	4.468527649	3.525069267	5.186885341
U_{lm} Overall Heat Transfer Coefficient ($Wm^{-2}K^{-1}$)	237.6248071	312.6591115	504.1639353	291.0334025	566.2270389	243.0693464
Area for Flow per Pass (m^2)	0.078015	0.078015	0.078015	0.078015	0.078015	0.078015
Brine Flowrate (m^3s^{-1})	448.5	426	471	448.5	471	471
Brine velocity (ms^{-1})	1.596915123	1.516802324	1.677027922	1.596915123	1.677027922	1.677027922
Tube Calculations						
Heat flux (Wm^{-2})	1000.454023	1425.396033	1785.885372	1300.490806	1995.989533	1260.772829
Tube Outer Wall Temperature (^oC)	-23.8061	-23.8011	-24.0393	-23.8879	-24.0616	-23.8337
NH3 Pcrit (bar a)	112.9	112.9	112.9	112.9	112.9	112.9
P_R	0.011691763	0.011514615	0.011957484	0.011514615	0.011957484	0.011160319
$f(P_R)$	0.864122712	0.861583876	0.867881859	0.861583876	0.867881859	0.856424181
NH_3 Molecular Weight	17.0304	17.0304	17.0304	17.0304	17.0304	17.0304
A a constant 30-55	55	55	55	55	55	55
Epsilon Surface Roughness (μm)	0.5	0.5	0.5	0.5	0.5	0.5

Test Number	7			8		
Chiller Number	1	2	3	1	3	4
Brine Coefficient Calculations						
Brine Side Reynolds Number	4086.134644	3881.144611	4256.327074	4069.410625	4256.327074	4291.124676
Brine Side Prandtl Number	75.14680215	75.14680215	75.79795945	75.48018952	75.79795945	75.14680215
Laminar Brine Flow Regime						
Entry Length (m)	5.604542277	5.323377949	5.837978215	5.581603613	5.837978215	5.885706605
Thermal Entry Length (m)	421.1634296	400.0348295	442.506836	421.3004985	442.506836	442.2920298
Nusselt Number	72.759748	70.02348775	75.47651972	72.77734463	75.47651972	75.44940699
Br1 Convective Coefficient of Heat Transfer ($Wm^{-2}K^{-1}$)	1320.348591	1270.694525	1368.823584	1320.13731	1368.823584	1369.156999
Brine Transition Flow Regime						
Nusselt Number	64.76240564	61.44381985	67.19486591	64.51874978	67.42683494	67.97277121
Br2 Convective Coefficient of Heat Transfer ($Wm^{-2}K^{-1}$)	1175.223299	1115.001951	1218.629549	1170.331361	1222.836482	1233.480807
Brine Turbulent Flow Regime						
Nusselt Number	158.785711	153.9570955	163.1854088	158.6270109	163.1854088	163.5183492
Br3 Convective Coefficient of Heat Transfer ($Wm^{-2}K^{-1}$)	2881.435074	2793.811685	2959.490409	2877.398682	2959.490409	2967.316791

Test Number	7			8		
Chiller Number	1	2	3	1	3	4
Boiling Heat Transfer Coefficients						
Bromley's Correlation						
E1 Boiling Coefficient of Heat Transfer ($Wm^{-2}K^{-1}$)	54.43503692	52.8393048	57.05678041	53.09934802	57.1498349	51.04237333
Mostinski's Correlation						
E2 Boiling Coefficient of Heat Transfer ($Wm^{-2}K^{-1}$)	300.8694554	384.3413668	453.3387072	360.4436248	490.0451299	350.5898956
Cooper's Correlation						
E3 Boiling Coefficient of Heat Transfer ($Wm^{-2}K^{-1}$)	142.5878284	179.0460488	212.4086693	168.4273317	228.7575085	162.2001733
Chen's Correlation						
Tube Pitch S_D=S_L (m)	0.0396875	0.0396875	0.0396875	0.0396875	0.0396875	0.0396875
Effective Area Approach Bottom Tube Row (m^2)	3.603	3.603	3.603	3.603	3.603	3.603
Velocity Approaching Bottom Tube Row (ms^{-1})	0.000139149	0.000202176	0.000251452	0.000188035	0.000281035	0.000172729
Liquid Phase Reynolds Number Re_l	26.56684138	37.63881853	47.78965634	34.34041054	53.41196886	32.94564013
Liquid Phase Prandtl Number Pr_l	1.982416708	1.988325607	1.973072677	1.988325607	1.973072677	2.000970715
Martinelli Parameter *X*	0.802809615	0.89919237	0.672239337	0.652246697	0.672239337	0.969913983
1/*X*						
Two-phase Heat Transfer Coefficient Multiplier F -chart	2.2	2.3	2	1.9	2	2.7
Two-phase Reynolds Number Re_{TP}	71.18168656	106.6094684	113.6635987	76.60330089	127.0357868	114.025676
Suppression Factor S -chart	0.95	0.95	0.95	0.95	0.95	0.95
Forster-Zuber Boiling Coefficient ($Wm^{-2}K^{-1}$)	328.9504427	348.5344612	275.9254785	340.8429671	274.609728	398.6025845
Forced Convection Boiling Coefficient ($Wm^{-2}K^{-1}$)	1.743442259	2.41412841	2.5260836	1.853197612	2.761159299	2.559840352
E4 Boiling Coefficient of Heat Transfer ($Wm^{-2}K^{-1}$)	330.693885	350.9485896	278.4515621	342.6961647	277.3708873	401.1624249

Test Number	7			8		
Chiller Number	1	2	3	1	3	4
Overall Heat Transfer Coefficient Calculations						
Combinations						
Br1, E1, K U_{11} ($Wm^{-2}K^{-1}$)	59.92501373	58.15153178	62.76919834	58.52436877	62.86649427	56.44772694
Br1, E2, K U_{12} ($Wm^{-2}K^{-1}$)	271.2181205	323.3118548	371.135972	311.2783021	391.8996786	307.4264574
Br1, E3, K U_{13} ($Wm^{-2}K^{-1}$)	145.4584562	176.3493754	205.9222793	168.1994714	219.034265	163.5284464
Br1, E4, K U_{14} ($Wm^{-2}K^{-1}$)	291.70847	302.3992563	256.9740104	299.6975851	256.1781635	339.8893794
Br2, E1, K U_{21} ($Wm^{-2}K^{-1}$)	59.59103166	57.78229322	62.41643855	58.19413834	62.52367725	56.19289967
Br2, E2, K U_{22} ($Wm^{-2}K^{-1}$)	264.508583	312.2192777	359.1347899	302.158513	378.9472188	300.0166887
Br2, E3, K U_{23} ($Wm^{-2}K$-1)	143.5061692	172.9969169	202.1737442	165.5003363	214.9284017	161.4079563
Br2, E4, K U_{24} ($Wm^{-2}K^{-1}$)	283.9613136	292.6736767	251.1626507	291.234529	250.579476	330.8551019
Br3, E1, K U_{31} ($Wm^{-2}K^{-1}$)	332.240987	348.4370375	286.4594413	342.6011681	285.4708356	393.5656926
Br3, E2, K U_{32} ($Wm^{-2}K^{-1}$)	305.1811063	375.3821819	434.4479036	356.8117289	463.1741544	349.7189676
Br3, E3, K U_{33} ($Wm^{-2}K^{-1}$)	154.6912749	190.7841943	224.0372837	180.6566886	239.6450914	174.7710208
Br3, E4, K U_{34} ($Wm^{-2}K^{-1}$)	337.2592249	353.9605246	290.182228	347.9397646	289.1678052	400.6271081
U_{lm} ($Wm^{-2}K^{-1}$)	237.6248071	312.6591115	504.1639353	291.0334025	566.2270389	243.0693464

Test Number	7			8		
Chiller Number	1	2	3	1	3	4
Deviations from Target Values of U (%)						
Combinations						
Br1, E1, K U_{11} ($Wm^{-2}K^{-1}$)	-74.78	-81.40	-87.55	-79.89	-88.90	-76.78
Br1, E2, K U_{12} ($Wm^{-2}K^{-1}$)	14.14	3.41	-26.39	6.96	-30.79	26.48
Br1, E3, K U_{13} ($Wm^{-2}K^{-1}$)	-38.79	-43.60	-59.16	-42.21	-61.32	-32.72
Br1, E4, K U_{14} ($Wm^{-2}K^{-1}$)	22.76	-3.28	-49.03	2.98	-54.76	39.83
Br2, E1, K U_{21} ($Wm^{-2}K^{-1}$)	-74.92	-81.52	-87.62	-80.00	-88.96	-76.88
Br2, E2, K U_{22} ($Wm^{-2}K^{-1}$)	11.31	-0.14	-28.77	3.82	-33.08	23.43
Br2, E3, K U_{23} ($Wm^{-2}K$-1)	-39.61	-44.67	-59.90	-43.13	-62.04	-33.60
Br2, E4, K U_{24} ($Wm^{-2}K^{-1}$)	19.50	-6.39	-50.18	0.07	-55.75	36.12
Br3, E1, K U_{31} ($Wm^{-2}K^{-1}$)	39.82	11.44	-43.18	17.72	-49.58	61.91
Br3, E2, K U_{32} ($Wm^{-2}K^{-1}$)	28.43	20.06	-13.83	22.60	-18.20	43.88
Br3, E3, K U_{33} ($Wm^{-2}K^{-1}$)	-34.90	-38.98	-55.56	-37.93	-57.68	-28.10
Br3, E4, K U_{34} ($Wm^{-2}K^{-1}$)	41.93	13.21	-42.44	19.55	-48.93	64.82

Test Number	7			8		
Chiller Number	1	2	3	1	3	4
Compressor Performance						
Quality x at flash economiser	0.1211	0.1199	0.1088	0.1143	0.1081	0.1183
Quality x at evaporator	0.05064	0.04523	0.06089	0.06339	0.06089	0.04052
Enthalpy at Evaporator inlet ($kJkg^{-1}$)	122	113.3	137.9	137.9	137.9	104.1
Enthalpy at Evaporator outlet ($kJkg^{-1}$)	1407	1407	1408	1407	1408	1406
Total Mass Flow Rate From Compressor (kgs^{-1})	0.38	0.54	0.69	0.50	0.77	0.48
Mass flow rate through evaporator (kgs^{-1})	0.34	0.48	0.61	0.45	0.68	0.42
Mass flow rate from flash economiser (kgs^{-1})	0.05	0.07	0.07	0.06	0.08	0.06
Mass ratio evaporator	0.8789	0.8801	0.8912	0.8857	0.8919	0.8817
Mass ratio flash economiser	0.1211	0.1199	0.1088	0.1143	0.1081	0.1183
Enthalpy at Compressor Suction ($kJkg^{-1}$)	1408.5	1408.5	1409.5	1408.5	1409.5	1407.5
Enthalpy at Flash Economiser Outlet ($kJkg^{-1}$)	1427	1425	1425	1432	1432	1422
Enthalpy at Compresor Discharge ($kJkg^{-1}$)	1594	1593	1589	1596	1587	1581
Suction Pressure (bar a)	1.32	1.3	1.35	1.3	1.35	1.26
Flash vapour Pressure (bar a)	2.6	2.4	2.75	2.75	2.75	2.2
Discharge Pressure (bar a)	10.82	10.5	10.57	10.87	10.57	10.23
Condenser pressure (bar a)	8.909	8.358	8.825	9.253	8.767	8.767
Compressor Heat Input (kW)	-70.54	-99.29	-121.90	-92.91	-134.03	-81.98
Pressure Ratio	8.20	8.08	7.83	8.36	7.83	8.12
Specific Heat at Constant Pressure at Mean Temperature Cp ($kJkg^{-1}K^{-1}$)	4.7535	4.7871	4.7970	4.7343	4.7788	4.7293
Specific Heat at Constant Volume at Mean Temperature Cv ($kJkg^{-1}K^{-1}$)	2.8478	2.8370	2.8338	2.8540	2.8397	2.8556
Ratio of Specific Heats	1.67	1.69	1.69	1.66	1.68	1.66
Volume Ratio	3.53	3.45	3.37	3.60	3.40	3.54
Compressor load capacity (%)	69.75	68.00	67.00	72.00	67.50	67.00
Temperature of oil entering cooler T_{oilin} (^oC)	73.10	72.20	70.90	74.10	70.00	67.40
Temperature of oil leaving cooler T_{oilout} (^oC)	48.90	48.90	48.90	48.90	48.90	48.90
Specific heat capacity of oil Cp_{oil} ($kJkg^{-1}K^{-1}$)	2.02	2.02	2.02	2.02	2.02	2.02
Mass flow rate of oil to cooler m_{oil} (kgs^{-1})	3.51	3.46	3.47	3.52	3.47	3.41
Heat transferred to oil (kW)	-171.28	-162.45	-153.90	-178.77	-147.60	-127.32

Test Number	7			8		
Chiller Number	1	2	3	1	3	4
Refrigerating capacity (kW)	434.71	619.35	775.99	565.08	867.28	547.82
Internal Pump Power (kW)	46.00	45.00	47.00	46.00	47.00	47.00
COP	1.80	2.37	2.81	2.08	3.08	2.62
Compressor Power (kW)	349.00	345.00	327.00	355.00	340.00	284.00
COSP	1.51	2.02	2.40	1.78	2.64	2.14
Total Refrigerating Effect for Procedure (all on-line chillers)	1830.05			1980.18		
Total COSP for Procedure (all on-line chillers)	1.578989424			1.769598103		

Actual surface area for heat transfer (m^2)	434.5118	434.5118	434.5118	434.5118	434.5118	434.5118
Surface area using U_{11} (m^2)	1722.999733	2336.207992	3490.010783	2160.765682	3913.568471	1871.049641
Surface area using U_{12} (m^2)	380.6927888	420.19515	590.255851	406.2520475	627.7941609	343.5504547
Surface area using U_{13} (m^2)	709.8300462	770.3688942	1063.824564	751.830232	1123.259549	645.8601029
Surface area using U_{14} (m^2)	353.951953	449.2539928	852.4799012	421.9501721	960.3954003	310.7378624
Surface area using U_{21} (m^2)	1732.656405	2351.136754	3509.735321	2173.027236	3935.026548	1879.5346
Surface area using U_{22} (m^2)	390.3494604	435.1239114	609.9803895	418.5136018	649.2522379	352.0354141
Surface area using U_{23} (m^2)	719.4867178	785.2976556	1083.549102	764.0917862	1144.717626	654.3450622
Surface area using U_{24} (m^2)	363.6086246	464.1827542	872.2044398	434.2117263	981.8534773	319.2228217
Surface area using U_{31} (m^2)	310.7707559	389.8956158	764.7336671	369.109797	861.8475137	268.3579926
Surface area using U_{32} (m^2)	338.3262611	361.9086889	504.2380852	354.4094472	531.1875189	302.0039203
Surface area using U_{33} (m^2)	667.4635186	712.0824331	977.806798	699.9876316	1026.652907	604.3135684
Surface area using U_{34} (m^2)	306.1466523	383.8113684	754.9227964	363.4463791	850.8289147	263.62794

2nd Law Analysis

Test Number	7			8		
Chiller Number	1	2	3	1	3	4
COP_{act}	3.1855	3.3005	3.4123	3.0916	3.5107	3.8378
COP_{Carnot}	6.4587	6.5169	6.4974	6.4780	6.5169	6.4780
Condenser temperature T_H (K)	288.65	288.65	288.65	288.65	288.65	288.65
Evaporator temperature T_L (K)	249.9500	250.2500	250.1500	250.0500	250.2500	250.0500
Temperature of surroundings T_o (K)	289.15	289.15	289.15	289.15	289.15	289.15
Temperature of brine T (K)	249.5	249.5	249.3	249.4	249.3	249.5
Cooling tower water temperature T_{ct} (K)	288.7	288.7	288.7	288.7	288.7	288.7
Entropy of ammonia into evaporator s_9 ($kJkg^{-1}K^{-1}$)	0.5027	0.4675	0.5669	0.568	0.5669	0.4306
Entropy of ammonia exit evaporator s_1 (kJkg-1K-1)	5.743	5.748	5.735	5.748	5.735	5.759
Entropy of ammonia at compressor suction s'_1 ($kJkg^{-1}K^{-1}$)	5.743	5.748	5.735	5.748	5.735	5.759
Entropy of ammonia exit compressor s_2 ($kJkg^{-1}K^{-1}$)	5.401	5.414	5.398	5.406	5.392	5.391
Entropy of ammonia exit flash economiser s_6 ($kJkg^{-1}K^{-1}$)	5.506	5.534	5.456	5.456	1432	5.565
Entropy of ammonia entering condenser s_3 ($kJkg^{-1}K^{-1}$)	5.401	5.414	5.398	5.406	5.392	5.391
Entropy of ammonia leaving condenser s_4 ($kJkg^{-1}K^{-1}$)	1.06	1.028	1.055	1.079	1.052	0.9923
Entropy of ammonia after first throttle s_5 ($kJkg^{-1}K^{-1}$)	1.1	1.068	1.087	1.108	1.083	1.032
Entropy leaving flash economiser s_6 ($kJkg^{-1}K^{-1}$)	5.506	5.534	5.456	5.456	5.456	5.565
Entropy leaving flash economiser s_8 ($kJkg^{-1}K^{-1}$)	0.4935	0.4602	0.554	0.544	0.544	0.4245
Entropy of flash to compressor s_7 ($kJkg^{-1}K^{-1}$)	5.506	5.534	5.498	5.498	5.498	5.565
Enthalpy of ammonia entering evaporator h_9 ($kJkg^{-1}$)	122	113.3	137.9	137.9	137.9	104.1
Enthalpy of ammonia leaving evaporator h_1 ($kJkg^{-1}$)	1407	1407	1408	1407	1408	1406
Enthalpy of ammonia at compressor suction h'_1 (kJkg-1)	1408.5	1408.5	1409.5	1408.5	1409.5	1407.5
Enthalpy of ammonia leaving compressor h_2 ($kJkg^{-1}$)	1594	1593	1589	1596	1587	1581
Enthalpy of ammonia from flash economiser h_6 (kJkg-1)	1427	1425	1425	1432	1432	1422
Isentropic enthalpy leaving compressor h_{s2} ($kJkg^{-1}$)	1756	1762	1720	1750	1720	1746
Isentropic enthalpy leaving compressor h'_{s2} ($kJkg^{-1}$)	1631	1635	1624	1646	1624	1643
Enthalpy of ammonia entering condenser h_3 ($kJkg^{-1}$)	1594	1593	1589	1596	1587	1581
Enthalpy of ammonia leaving condenser h_4 ($kJkg^{-1}$)	280	270.5	278.6	284.2	277.6	260

2nd Law Analysis

Test Number	7			8		
Chiller Number	1	2	3	1	3	4
Refrigerating capacity Q_L (kW)	434.71	619.35	775.99	565.08	867.28	547.82
Specific refrigerating capacity q_L ($kJkg^{-1}$)	1285.00	1293.70	1270.10	1269.10	1270.10	1301.90
Condenser heat load Q_H (kW)	-505.768	-719.395	-898.351	-659.468	-1002.485	-630.439
Condenser specific heat load q_H ($kJkg^{-1}$)	-1314.000	-1322.500	-1310.400	-1311.800	-1309.400	-1321.000
Cycle irreversibility I_{cycle} (kW)	**204.4311**	**193.4573**	**176.7305**	**214.5927**	**166.8864**	**138.2591**
Heat engine (evaporator) W_{rev} (kJ)	-68.18	-96.27	-120.98	-88.36	-134.81	-85.66
Availability (evaporator) ($kJkg^{-1}$)	-201.53	-201.10	-198.02	-198.45	-197.43	-203.58
Evaporator irreversibility i_{evap} (kW)	25.725	27.565	21.234	26.425	21.234	31.609
Condenser irreversibility i_{cond} ($kJkg^{-1}$)	61.076	56.579	56.891	62.920	56.757	51.404
Compressor irreversibility i_{comp} ($kJkg^{-1}$)	44.462	39.232	34.281	52.193	27.577	1.160
Throttle 4-5 irreversibility i_{4-5} ($kJkg^{-1}$)	11.566	11.566	9.253	8.385	8.964	11.479
Throttle 6-7 irreversibility i_{6-7} ($kJkg^{-1}$)	0.000	0.000	10.471	10.475	10.471	0.000
Throttle 8-9 irreversibility i_{8-9} ($kJkg^{-1}$)	2.656	2.107	3.724	6.928	6.610	1.761
Total of irreversibilities i_{tot} ($kJkg^{-1}$)	**145.484**	**137.049**	**135.853**	**167.326**	**131.612**	**97.414**
	103.409	**95.641**	**75.158**	**99.460**	**62.851**	**42.006**
Compressor isentropic work W_{isen}	-127.066	-182.933	-204.548	-164.353	-227.914	-154.913
Compressor adiabatic efficiency	0.308	0.431	0.476	0.365	0.531	0.460
Compressor second law efficiency	0.572	0.635	0.727	0.634	0.777	0.799
Compressor actual work rate Wact (kW)	-241.817	-261.738	-275.800	-271.678	-281.636	-209.299
Compressor reversible work W_{rev} (kW)	-138.408	-166.097	-200.641	-172.218	-218.785	-167.294
Chiller second law effectiveness	0.2819	0.3678	0.4387	0.3252	0.4787	0.4093

Procedure Number	9			10		
Chiller Number	1	2	4	2	3	4
Brine Properties						
Brine Inlet Temperature T_{ei} (°C)	-22.8	-22.6	-22.7	-22.8	-22.7	-22.9
Brine Outlet Temperature T_{eo} (°C)	-24	-24	-24.1	-24.4	-24.7	-24.1
Brine Bulk (mean) Temperature T_b (°C)	-23.4	-23.3	-23.4	-23.6	-23.7	-23.5
Volumetric Flow Rate of Brine (m^3hr^{-1})	363	348	387	405	448.5	448.5
Brine Mass Flow Rate $\dot{m}_b$ (kgs^{-1})	128.84	123.52	137.36	143.76	159.21	159.20
Specific Heat Capacity C_p ($kJkg^{-1}K^{-1}$) **(mean temperature)**	2.73134	2.731648	2.73134	2.730725	2.730417	2.731033
Brine density ρ_b (kgm^{-3}) **(mean temperature)**	1277.799	1277.753	1277.799	1277.891	1277.938	1277.845
Thermal Conductivity k_b ($Wm^{-1}K^{-1}$)**(mean temperature)**	0.4982	0.4984	0.4982	0.4979	0.4978	0.4981
Brine dynamic viscocity at wall μ_w (Nsm^{-2})	0.0138708	0.0138708	0.0139276	0.0140979	0.0142682	0.0139276
Brine dynamic viscocity (bulk) μ_b (Nsm^{-2})	0.0135302	0.0134734	0.0135302	0.0136437	0.0137005	0.013587
Ammonia Properties in Evaporator						
Pressure (bar a)	1.35	1.32	1.26	1.28	1.33	1.26
Temperature T_{evap} (°C)	-27.46	-27.93	-28.91	-28.58	-27.78	-28.91
Liquid Thermal Conductivity k_l ($Wm^{-1}K^{-1}$)	0.6024337	0.6034633	0.6055226	0.6048362	0.6031201	0.6055226
Vapour Thermal Conductivity k_v ($Wm^{-1}K^{-1}$)	0.0193257	0.0192789	0.0191853	0.0192165	0.0192945	0.0191853
Liquid Density ρ (kgm^{-3})	674.3688	674.7638	676.1325	675.6757	674.7638	676.1325
Vapour Density ρ (kgm^{-3})	1.1367	1.1396	1.091	1.1068	1.1472	1.091
Liquid Dynamic Viscosity μ_l (Nsm^{-2})	0.000264496	0.000266321	0.000269972	0.000268755	0.000265713	0.000269972
Vapour Dynamic Viscosity μ_v **(Nsm-2)**	9.43E-06	9.41E-06	9.38E-06	9.39E-06	9.42E-06	9.38E-06
Surface Tension σ mNm^{-1}	32.64	32.75	32.98	32.9	32.71	32.98
Latent Heat λ ($kJkg^{-1}$)	1353.5	1354.94	1357.84	1356.88	1354.46	1357.84
h_g ($kJkg^{-1}$)	1408	1407	1406	1406	107	1406
h_f ($kJkg^{-1}$)	55.58	53.48	49.11	50.58	42.15	49.11
Enthalpy Difference h_{fg} ($kJkg^{-1}$)	1352.42	1353.52	1356.89	1355.42	1352.85	1356.89
Vapor Specific Heat Capacity ($kJkg^{-1}K^{-1}$)	2.225	2.216	2.197	2.203	2.219	2.197
Liquid Specific Heat Capacity ($kJkg^{-1}K^{-1}$)	4.494	4.492	4.488	4.489	4.492	4.488
Pressure $P_{satwall}$ **(bar a)**	1.624	1.63	1.622	1.606	1.594	1.615

Test Number	9			10		
Chiller Number	1	2	4	2	3	4
Evaporator Tube Properties						
Tube Length (m)	5.4864	5.4864	5.4864	5.4864	5.4864	5.4864
K Thermal Conductivity ($Wm^{-1}K^{-1}$)	40	40	40	40	40	40
Internal Diameter (m)	0.027432	0.027432	0.027432	0.027432	0.027432	0.027432
Thickness (m)	0.002159	0.002159	0.002159	0.002159	0.002159	0.002159
External Diameter (m)	0.03175	0.03175	0.03175	0.03175	0.03175	0.03175
Performance Calculations						
Chilling Heat Load (kW)	422.302526	472.3635998	525.2605799	628.1224022	869.418157	521.7306112
Evaporator Heat Transfer Area (m^2)	434.5118	434.5118	434.5118	434.5118	434.5118	434.5118
Log Mean Temperature Difference	4.030269215	4.59450518	5.480228256	4.936863134	3.996949012	5.387745627
U_{lm} Overall Heat Transfer Coefficient ($Wm^{-2}K^{-1}$)	241.1504335	236.6116385	220.5842937	292.8138538	500.6088496	222.8628399
Area for Flow per Pass (m^2)	0.078015	0.078015	0.078015	0.078015	0.078015	0.078015
Brine Flowrate (m^3s^{-1})	363	348	387	405	448.5	448.5
Brine velocity (ms^{-1})	1.292486488	1.239077955	1.37794014	1.442030379	1.596915123	1.596915123
Tube Calculations						
Heat flux (Wm^{-2})	971.9011682	1087.113399	1208.852279	1445.58192	2000.908047	1200.728291
Tube Outer Wall Temperature (^oC)	-23.5030	-23.4153	-23.5282	-23.7533	-23.9121	-23.6273
NH3 Pcrit (bar a)	112.9	112.9	112.9	112.9	112.9	112.9
P_R	0.011957484	0.011691763	0.011160319	0.011337467	0.011780337	0.011160319
$f(P_R)$	0.867881859	0.864122712	0.856424181	0.859017965	0.865382217	0.856424181
NH_3 Molecular Weight	17.0304	17.0304	17.0304	17.0304	17.0304	17.0304
A a constant 30-55	55	55	55	55	55	55
Epsilon Surface Roughness (μm)	0.5	0.5	0.5	0.5	0.5	0.5

Test Number	9			10		
Chiller Number	1	2	4	2	3	4
Brine Coefficient Calculations						
Brine Side Reynolds Number	3348.434525	3223.486149	3569.818626	3705.04538	4086.134644	4119.968622
Brine Side Prandtl Number	74.17819444	73.84547786	74.17819444	74.82866576	75.14680215	74.49617621
Laminar Brine Flow Regime						
Entry Length (m)	4.592712794	4.421333602	4.896363227	5.081840244	5.604542277	5.650948962
Thermal Entry Length (m)	340.6791427	326.4954926	363.2033835	380.267325	421.1634296	420.9740897
Nusselt Number	62.06707003	60.10229957	65.13534663	67.41930013	72.759748	72.73543769
Br1 Convective Coefficient of Heat Transfer ($Wm^{-2}K^{-1}$)	1127.216911	1091.972372	1182.940715	1223.682908	1320.348591	1320.702884
Brine Transition Flow Regime						
Nusselt Number	52.90055695	50.85082335	56.36585717	58.57210304	64.58043837	65.14635598
Br2 Convective Coefficient of Heat Transfer ($Wm^{-2}K^{-1}$)	960.7413776	923.8863502	1023.675636	1063.103314	1171.921195	1182.903176
Brine Turbulent Flow Regime						
Nusselt Number	140.3038537	136.9353959	145.7982139	149.5174589	158.785711	159.1160199
Br3 Convective Coefficient of Heat Transfer ($Wm^{-2}K^{-1}$)	2548.09638	2487.919266	2647.880949	2713.792024	2881.435074	2889.169201

Test Number	9			10		
Chiller Number	1	2	4	2	3	4
Boiling Heat Transfer Coefficients						
Bromley's Correlation						
E1 Boiling Coefficient of Heat Transfer ($Wm^{-2}K^{-1}$)	55.02153903	53.22011574	50.3045375	51.89944592	55.42297561	50.53809813
Mostinski's Correlation						
E2 Boiling Coefficient of Heat Transfer ($Wm^{-2}K^{-1}$)	296.1152462	318.8838313	340.4198453	386.987402	489.4762713	338.8167926
Cooper's Correlation						
E3 Boiling Coefficient of Heat Transfer ($Wm^{-2}K^{-1}$)	141.5852203	150.7072911	157.7159353	179.2144748	227.2765822	157.0085305
Chen's Correlation						
Tube Pitch $S_D=S_L$ (m)	0.0396875	0.0396875	0.0396875	0.0396875	0.0396875	0.0396875
Effective Area Approach Bottom Tube Row (m^2)	3.603	3.603	3.603	3.603	3.603	3.603
Velocity Approaching Bottom Tube Row (ms^{-1})	0.000133296	0.000150185	0.000166216	0.000202856	0.000280943	0.000163889
Liquid Phase Reynolds Number Re_l	26.00795379	28.79232514	31.58868439	37.98721445	53.28364867	31.37662682
Liquid Phase Prandtl Number Pr_l	1.973072677	1.982416708	2.000970715	1.994658461	1.979012715	2.000970715
Martinelli Parameter X	1.107664652	0.866393008	0.89784425	0.656577633	0.695327823	1.057923032
$1/X$						
Two-phase Heat Transfer Coefficient Multiplier F -chart	2.95	3.9	3.95	1.95	1.975	2.8
Two-phase Reynolds Number Re_{TP}	100.5503773	157.8001809	175.9048882	87.53479373	124.7535265	113.645905
Suppression Factor S -chart	0.95	0.95	0.95	0.95	0.95	0.95
Forster-Zuber Boiling Coefficient ($Wm^{-2}K^{-1}$)	321.6422389	361.8755206	423.6953088	381.6959496	309.2411284	415.676582
Forced Convection Boiling Coefficient ($Wm^{-2}K^{-1}$)	2.290116424	3.296089129	3.621038005	2.066873372	2.727781674	2.553017488
E4 Boiling Coefficient of Heat Transfer ($Wm^{-2}K^{-1}$)	323.9323553	365.1716097	427.3163468	383.762823	311.9689101	418.2295995

Test Number	9			10		
Chiller Number	1	2	4	2	3	4
Overall Heat Transfer Coefficient Calculations						
Combinations						
Br1, E1, K U_{11} ($Wm^{-2}K^{-1}$)	60.06692094	58.1116505	55.31354012	57.06851179	60.95853166	55.83098189
Br1, E2, K U_{12} ($Wm^{-2}K^{-1}$)	258.8702018	271.5000255	290.5786147	321.765626	387.5152069	297.1556741
Br1, E3, K U_{13} ($Wm^{-2}K^{-1}$)	141.8945155	149.1033427	156.7012345	175.5537688	216.5942633	158.2760704
Br1, E4, K U_{14} ($Wm^{-2}K^{-1}$)	276.8257729	299.4190243	341.8466445	319.8350242	278.9479121	347.0969215
Br2, E1, K U_{21} ($Wm^{-2}K^{-1}$)	59.51736051	57.55440932	54.91404625	56.66931184	60.60415594	55.55738508
Br2, E2, K U_{22} ($Wm^{-2}K^{-1}$)	248.9629499	259.7503101	279.882297	309.4739873	373.6267571	289.5659585
Br2, E3, K U_{23} ($Wm^{-2}K$-1)	138.8655348	145.4890844	153.5369142	171.8302313	212.1857693	156.096839
Br2, E4, K U_{24} ($Wm^{-2}K^{-1}$)	265.5264921	285.1918735	327.1384901	307.687659	271.6783997	336.7859704
Br3, E1, K U_{31} ($Wm^{-2}K^{-1}$)	321.5641554	354.8516357	408.2119655	374.5311863	315.7879429	406.1578143
Br3, E2, K U_{32} ($Wm^{-2}K^{-1}$)	296.8901725	315.5162242	336.2792444	376.0621295	460.7833222	338.5025897
Br3, E3, K U_{33} ($Wm^{-2}K^{-1}$)	152.6065689	161.4745605	169.0937184	190.5653601	237.7216192	169.2900369
Br3, E4, K U_{34} ($Wm^{-2}K^{-1}$)	326.2627648	360.5820379	415.8138075	380.9205347	320.3180785	413.6826376
U_{lm} ($Wm^{-2}K^{-1}$)	241.1504335	236.6116385	220.5842937	292.8138538	500.6088496	222.8628399

Test Number	9			10		
Chiller Number	1	2	4	2	3	4
Deviations from Target Values of U (%)						
Combinations						
Br1, E1, K U_{11} ($Wm^{-2}K^{-1}$)	-75.09	-75.44	-74.92	-80.51	-87.82	-74.95
Br1, E2, K U_{12} ($Wm^{-2}K^{-1}$)	7.35	14.75	31.73	9.89	-22.59	33.34
Br1, E3, K U_{13} ($Wm^{-2}K^{-1}$)	-41.16	-36.98	-28.96	-40.05	-56.73	-28.98
Br1, E4, K U_{14} ($Wm^{-2}K^{-1}$)	14.79	26.54	54.97	9.23	-44.28	55.74
Br2, E1, K U_{21} ($Wm^{-2}K^{-1}$)	-75.32	-75.68	-75.11	-80.65	-87.89	-75.07
Br2, E2, K U_{22} ($Wm^{-2}K^{-1}$)	3.24	9.78	26.88	5.69	-25.37	29.93
Br2, E3, K U_{23} ($Wm^{-2}K$-1)	-42.42	-38.51	-30.40	-41.32	-57.61	-29.96
Br2, E4, K U_{24} ($Wm^{-2}K^{-1}$)	10.11	20.53	48.31	5.08	-45.73	51.12
Br3, E1, K U_{31} ($Wm^{-2}K^{-1}$)	33.35	49.97	85.06	27.91	-36.92	82.25
Br3, E2, K U_{32} ($Wm^{-2}K^{-1}$)	23.11	33.35	52.45	28.43	-7.96	51.89
Br3, E3, K U_{33} ($Wm^{-2}K^{-1}$)	-36.72	-31.76	-23.34	-34.92	-52.51	-24.04
Br3, E4, K U_{34} ($Wm^{-2}K^{-1}$)	35.29	52.39	88.51	30.09	-36.01	85.62

Test Number	9			10		
Chiller Number	1	2	4	2	3	4
Compressor Performance						
Quality x at flash economiser	0.1324	0.1195	0.1212	0.1078	0.1112	0.1228
Quality x at evaporator	0.03589	0.04672	0.04399	0.06161	0.05908	0.03693
Enthalpy at Evaporator inlet ($kJkg^{-1}$)	104.1	113.3	108.8	134.1	134.1	99.23
Enthalpy at Evaporator outlet ($kJkg^{-1}$)	1408	1407	1406	1406	1407	1406
Total Mass Flow Rate From Compressor (kgs^{-1})	0.37	0.41	0.46	0.55	0.77	0.46
Mass flow rate through evaporator (kgs^{-1})	0.32	0.37	0.40	0.49	0.68	0.40
Mass flow rate from flash economiser (kgs^{-1})	0.05	0.05	0.06	0.06	0.09	0.06
Mass ratio evaporator	0.8676	0.8805	0.8788	0.8922	0.8888	0.8772
Mass ratio flash economiser	0.1324	0.1195	0.1212	0.1078	0.1112	0.1228
Enthalpy at Compressor Suction ($kJkg^{-1}$)	1409.5	1408.5	1407.5	1407.5	1408.5	1407.5
Enthalpy at Flash Economiser Outlet ($kJkg^{-1}$)	1422	1425	1424	1431	1431	1421
Enthalpy at Compresor Discharge ($kJkg^{-1}$)	1591	1593	1587	1596	1589	1582
Suction Pressure (bar a)	1.35	1.32	1.26	1.28	1.33	1.26
Flash vapour Pressure (bar a)	2.2	2.4	2.3	2.75	2.75	2.1
Discharge Pressure (bar a)	10.82	10.41	9.65	10.41	10.64	10.37
Condenser pressure (bar a)	8.825	8.331	8.224	8.548	8.797	7.859
Compressor Heat Input (kW)	-67.14	-75.69	-81.79	-102.94	-136.79	-78.67
Pressure Ratio	8.01	7.89	7.66	8.13	8.00	8.23
Specific Heat at Constant Pressure at Mean Temperature Cp ($kJkg^{-1}K^{-1}$)	4.7431	4.7728	4.7992	4.7585	4.8140	4.7332
Specific Heat at Constant Volume at Mean Temperature Cv ($kJkg^{-1}K^{-1}$)	2.8512	2.8416	2.8331	2.8462	2.8283	2.8544
Ratio of Specific Heats	1.66	1.68	1.69	1.67	1.70	1.66
Volume Ratio	3.49	3.42	3.33	3.50	3.39	3.56
Compressor load capacity (%)	69.00	68.50	67.00	69.50	67.25	70.75
Temperature of oil entering cooler T_{oilin} (^oC)	72.00	72.10	68.70	73.20	71.20	67.80
Temperature of oil leaving cooler T_{oilout} (^oC)	48.90	48.90	48.90	48.90	48.90	48.90
Specific heat capacity of oil Cp_{oil} ($kJkg^{-1}K^{-1}$)	2.02	2.02	2.02	2.02	2.02	2.02
Mass flow rate of oil to cooler $m^{\cdot}_{oil}$ (kgs^{-1})	3.51	3.44	3.31	3.44	3.48	3.44
Heat transferred to oil (kW)	-163.49	-161.06	-132.34	-168.70	-156.51	-130.96

Test Number	9			10		
Chiller Number	1	2	4	2	3	4
Refrigerating capacity (kW)	422.30	472.36	525.26	628.12	869.42	521.73
Internal Pump Power (kW)	42.00	41.00	43.00	44.00	46.00	46.00
COP	1.83	2.00	2.45	2.31	2.96	2.49
Compressor Power (kW)	350.00	336.00	310.00	363.00	344.00	293.00
COSP	1.55	1.70	2.04	1.99	2.56	2.04
Total Refrigerating Effect for Procedure (all on-line chillers)	1419.93			2019.27		
Total COSP for Procedure (all on-line chillers)	1.265531823			1.777527439		

Actual surface area for heat transfer (m^2)	434.5118	434.5118	434.5118	434.5118	434.5118	434.5118
Surface area using U_{11} (m^2)	1744.432831	1769.189966	1732.785107	2229.444412	3568.33484	1734.458726
Surface area using U_{12} (m^2)	404.7692943	378.6760196	329.84698	395.415372	561.3210744	325.8781244
Surface area using U_{13} (m^2)	738.454961	689.5254466	611.651075	724.7413462	1004.276147	611.820432
Surface area using U_{14} (m^2)	378.5150054	343.3667891	280.3785852	397.8021951	779.7887809	278.9898951
Surface area using U_{21} (m^2)	1760.540253	1786.319244	1745.390935	2245.149457	3589.200261	1743.000208
Surface area using U_{22} (m^2)	420.8767166	395.8052983	342.452808	411.120417	582.1864954	334.419606
Surface area using U_{23} (m^2)	754.5623833	706.6547253	624.256903	740.4463912	1025.141568	620.3619136
Surface area using U_{24} (m^2)	394.6224277	360.4960678	292.9844131	413.5072401	800.6542019	287.5313767
Surface area using U_{31} (m^2)	325.8531996	289.7282656	234.7958576	339.707558	688.8181046	238.4209544
Surface area using U_{32} (m^2)	352.9342452	325.848692	285.0205004	338.3246137	472.0666783	286.0732434
Surface area using U_{33} (m^2)	686.6199119	636.698119	566.8245954	667.6505879	915.0217512	572.015551
Surface area using U_{34} (m^2)	321.1604885	285.123878	230.503357	334.0094931	679.0764148	234.0841141

2nd Law Analysis

Test Number	9			10		
Chiller Number	1	2	4	2	3	4
COP_{act}	3.2949	3.3153	3.6792	3.1996	3.3821	3.7732
COP_{Carnot}	6.5366	6.5761	6.5563	6.5366	6.5563	6.5169
Condenser temperature T_H (K)	288.65	288.65	288.65	288.65	288.65	288.65
Evaporator temperature T_L (K)	250.3500	250.5500	250.4500	250.3500	250.4500	250.2500
Temperature of surroundings T_o (K)	289.15	289.15	289.15	289.15	289.15	289.15
Temperature of brine T (K)	249.8	249.9	249.8	249.6	249.5	249.7
Cooling tower water temperature T_{ct} (K)	288.7	288.7	288.7	288.7	288.7	288.7
Entropy of ammonia into evaporator s_9 ($kJkg^{-1}K^{-1}$)	0.4293	0.4672	0.4498	0.5529	0.5518	0.4106
Entropy of ammonia exit evaporator s_1 (kJkg-1K-1)	5.735	5.743	5.759	5.754	5.74	5.759
Entropy of ammonia at compressor suction s'_1 ($kJkg^{-1}K^{-1}$)	5.735	5.743	5.759	5.754	5.74	5.759
Entropy of ammonia exit compressor s_2 ($kJkg^{-1}K^{-1}$)	5.393	5.416	5.435	5.401	5.39	5.386
Entropy of ammonia exit flash economiser s_6 ($kJkg^{-1}K^{-1}$)	5.565	5.534	5.549	5.468	5.468	5.581
Entropy of ammonia entering condenser s_3 ($kJkg^{-1}K^{-1}$)	5.393	5.416	5.435	5.401	5.39	5.386
Entropy of ammonia leaving condenser s_4 ($kJkg^{-1}K^{-1}$)	1.055	1.026	1.02	1.039	1.054	0.997
Entropy of ammonia after first throttle s_5 ($kJkg^{-1}K^{-1}$)	1.099	1.066	1.061	1.065	1.087	1.041
Entropy leaving flash economiser s_6 ($kJkg^{-1}K^{-1}$)	5.565	5.534	5.549	5.468	5.468	5.581
Entropy leaving flash economiser s_8 ($kJkg^{-1}K^{-1}$)	0.4245	0.4602	0.4498	0.539	0.5395	0.4056
Entropy of flash to compressor s_7 ($kJkg^{-1}K^{-1}$)	5.565	5.534	5.549	5.494	5.494	5.581
Enthalpy of ammonia entering evaporator h_9 ($kJkg^{-1}$)	104.1	113.3	108.8	134.1	134.1	99.23
Enthalpy of ammonia leaving evaporator h_1 ($kJkg^{-1}$)	1408	1407	1406	1406	1407	1406
Enthalpy of ammonia at compressor suction h'_1 (kJkg-1)	1409.5	1408.5	1407.5	1407.5	1408.5	1407.5
Enthalpy of ammonia leaving compressor h_2 ($kJkg^{-1}$)	1591	1593	1587	1596	1589	1582
Enthalpy of ammonia from flash economiser h_6 (kJkg-1)	1422	1425	1424	1431	1431	1421
Isentropic enthalpy leaving compressor h_{s2} ($kJkg^{-1}$)	1745	1760	1741	1772	1722	1749
Isentropic enthalpy leaving compressor h'_{s2} ($kJkg^{-1}$)	1652	1634	1627	1620	1624	1651
Enthalpy of ammonia entering condenser h_3 ($kJkg^{-1}$)	1591	1593	1587	1596	1589	1582
Enthalpy of ammonia leaving condenser h_4 ($kJkg^{-1}$)	277.1	270	268.1	272.4	278.1	261.4

2nd Law Analysis

Test Number	9			10		
Chiller Number	1	2	4	2	3	4
Refrigerating capacity Q_L (kW)	422.30	472.36	525.26	628.12	869.42	521.73
Specific refrigerating capacity q_L ($kJkg^{-1}$)	1303.90	1293.70	1297.20	1271.90	1272.90	1306.77
Condenser heat load Q_H (kW)	-490.481	-548.622	-607.701	-732.632	-1007.395	-601.063
Condenser specific heat load q_H ($kJkg^{-1}$)	-1313.900	-1323.000	-1318.900	-1323.600	-1310.900	-1320.600
Cycle irreversibility I_{cycle} (kW)	**196.2554**	**193.4926**	**154.7202**	**202.9329**	**182.2129**	**145.8080**
Heat engine (evaporator) W_{rev} (kJ)	-65.45	-72.77	-81.16	-97.35	-134.34	-81.10
Availability (evaporator) ($kJkg^{-1}$)	-202.08	-199.31	-200.45	-197.12	-196.69	-203.13
Evaporator irreversibility i_{evap} (kW)	24.543	28.306	33.312	30.166	24.686	32.961
Condenser irreversibility i_{cond} ($kJkg^{-1}$)	61.843	55.923	44.587	64.620	59.416	53.808
Compressor irreversibility i_{comp} ($kJkg^{-1}$)	33.769	40.057	18.007	42.517	32.500	1.388
Throttle 4-5 irreversibility $i_{4\text{-}5}$ ($kJkg^{-1}$)	12.723	11.566	11.855	7.518	9.542	12.723
Throttle 6-7 irreversibility $i_{6\text{-}7}$ ($kJkg^{-1}$)	0.000	0.000	0.000	6.488	6.486	0.000
Throttle 8-9 irreversibility $i_{8\text{-}9}$ ($kJkg^{-1}$)	1.386	2.021	0.000	4.012	3.550	1.443
Total of irreversibilities i_{tot} ($kJkg^{-1}$)	**134.264**	**137.872**	**107.761**	**155.321**	**136.180**	**102.323**
	95.761	**95.677**	**64.966**	**90.128**	**78.533**	**44.873**
Compressor isentropic work W_{isen}	-120.028	-138.699	-146.377	-191.284	-230.620	-149.200
Compressor adiabatic efficiency	0.305	0.349	0.422	0.434	0.513	0.438
Compressor second law efficiency	0.585	0.596	0.697	0.668	0.732	0.786
Compressor actual work rate Wact (kW)	-230.630	-236.751	-214.129	-271.632	-293.300	-209.624
Compressor reversible work W_{rev} (kW)	-134.869	-141.074	-149.163	-181.504	-214.768	-164.751
Chiller second law effectiveness	0.2838	0.3074	0.3790	0.3584	0.4580	0.3869

Procedure Number	11			
Chiller Number	1	2	3	4
Brine Properties				
Brine Inlet Temperature T_{ei} (°C)	-22.3	-23.1	-22.9	-23.1
Brine Outlet Temperature T_{eo} (°C)	-24.4	-24.4	-24.6	-24.1
Brine Bulk (mean) Temperature T_b (°C)	-23.4	-23.8	-23.8	-23.6
Volumetric Flow Rate of Brine (m^3hr^{-1})	363	363	405	363
Brine Mass Flow Rate $\dot{m}_b$ (kgs^{-1})	128.84	128.86	143.77	128.85
Specific Heat Capacity C_p ($kJkg^{-1}K^{-1}$) **(mean temperature)**	2.73134	2.73011	2.73011	2.730725
Brine density ρ_b (kgm^{-3}) **(mean temperature)**	1277.799	1277.984	1277.984	1277.891
Thermal Conductivity k_b ($Wm^{-1}K^{-1}$)**(mean temperature)**	0.4982	0.4976	0.4976	0.4979
Brine dynamic viscocity at wall μ_w (Nsm^{-2})	0.0140979	0.0140979	0.0142114	0.0139276
Brine dynamic viscocity (bulk) μ_b (Nsm^{-2})	0.0135302	0.0137573	0.0137573	0.0136437
Ammonia Properties in Evaporator				
Pressure (bar a)	1.32	1.3	1.37	1.24
Temperature T_{evap} (°C)	-27.93	-28.25	-27.15	-29.24
Liquid Thermal Conductivity k_l ($Wm^{-1}K^{-1}$)	0.6034633	0.6041498	0.6017473	0.6062434
Vapour Thermal Conductivity k_v ($Wm^{-1}K^{-1}$)	0.0192789	0.0192477	0.0193569	0.0191526
Liquid Density ρ (kgm^{-3})	674.7638	657.2194	673.8544	676.59
Vapour Density ρ (kgm^{-3})	1.1396	1.1234	1.1789	1.0739
Liquid Dynamic Viscosity μ_l (Nsm^{-2})	0.000266321	0.000267538	0.000263279	0.00027125
Vapour Dynamic Viscosity μ_v **(Nsm-2)**	9.41E-06	9.40E-06	9.44E-06	9.37E-06
Surface Tension σ mNm^{-1}	32.75	32.88	32.56	33.05
Latent Heat λ ($kJkg^{-1}$)	1354.94	1355.91	1352.53	1358.85
h_g ($kJkg^{-1}$)	1407	1407	1408	1405
h_f ($kJkg^{-1}$)	53.48	52.06	56.97	47.6
Enthalpy Difference h_{fg} ($kJkg^{-1}$)	1353.52	1354.94	1351.03	1357.4
Vapor Specific Heat Capacity ($kJkg^{-1}K^{-1}$)	2.216	2.21	2.231	2.191
Liquid Specific Heat Capacity ($kJkg^{-1}K^{-1}$)	4.492	4.49	4.495	4.486
Pressure $P_{satwall}$ **(bar a)**	1.622	1.598	1.594	1.61

Test Number	11			
Chiller Number	1	2	3	4
Evaporator Tube Properties				
Tube Length (m)	5.4864	5.4864	5.4864	5.4864
K Thermal Conductivity ($Wm^{-1}K^{-1}$)	40	40	40	40
Internal Diameter (m)	0.027432	0.027432	0.027432	0.027432
Thickness (m)	0.002159	0.002159	0.002159	0.002159
External Diameter (m)	0.03175	0.03175	0.03175	0.03175
Performance Calculations				
Chilling Heat Load (kW)	739.0294205	457.3545867	667.2783068	351.8648642
Evaporator Heat Transfer Area (m^2)	434.5118	434.5118	434.5118	434.5118
Log Mean Temperature Difference	4.49860314	4.468527649	3.327945821	5.625193492
U_{lm} Overall Heat Transfer Coefficient ($Wm^{-2}K^{-1}$)	378.0789261	235.5521184	461.4548169	143.9583504
Area for Flow per Pass (m^2)	0.078015	0.078015	0.078015	0.078015
Brine Flowrate (m^3s^{-1})	363	363	405	363
Brine velocity (ms^{-1})	1.292486488	1.292486488	1.442030379	1.292486488
Tube Calculations				
Heat flux (Wm^{-2})	1700.827044	1052.571154	1535.69663	809.7935756
Tube Outer Wall Temperature (^oC)	-23.5303	-23.8616	-23.9128	-23.6859
NH3 Pcrit (bar a)	112.9	112.9	112.9	112.9
P_R	0.011691763	0.011514615	0.012134632	0.010983171
$f(P_R)$	0.864122712	0.861583876	0.870356273	0.853801693
NH_3 Molecular Weight	17.0304	17.0304	17.0304	17.0304
A a constant 30-55	55	55	55	55
Epsilon Surface Roughness (μm)	0.5	0.5	0.5	0.5

Test Number	11			
Chiller Number	1	2	3	4
Brine Coefficient Calculations				
Brine Side Reynolds Number	3348.434525	3293.636693	3674.718624	3320.818452
Brine Side Prandtl Number	74.17819444	75.48018952	75.48018952	74.82866576
Laminar Brine Flow Regime				
Entry Length (m)	4.592712794	4.517552088	5.040244065	4.554834589
Thermal Entry Length (m)	340.6791427	340.9856877	380.4385772	340.832195
Nusselt Number	62.06707003	62.10924987	67.44205031	62.08813114
Br1 Convective Coefficient of Heat Transfer ($Wm^{-2}K^{-1}$)	1127.216911	1126.62448	1223.358276	1126.920403
Brine Transition Flow Regime				
Nusselt Number	52.78041932	52.21918879	58.1957109	52.58735883
Br2 Convective Coefficient of Heat Transfer ($Wm^{-2}K^{-1}$)	958.5595255	947.2247135	1055.635234	954.4781993
Brine Turbulent Flow Regime				
Nusselt Number	140.3038537	139.7216312	149.2081983	140.0112293
Br3 Convective Coefficient of Heat Transfer ($Wm^{-2}K^{-1}$)	2548.09638	2534.466452	2706.547079	2541.250767

Test Number	11			
Chiller Number	1	2	3	4
Boiling Heat Transfer Coefficients				
Bromley's Correlation				
E1 Boiling Coefficient of Heat Transfer ($Wm^{-2}K^{-1}$)	53.56370851	53.01988929	58.40370902	49.6788094
Mostinski's Correlation				
E2 Boiling Coefficient of Heat Transfer ($Wm^{-2}K^{-1}$)	436.216624	310.8409824	409.0492029	256.3797535
Cooper's Correlation				
E3 Boiling Coefficient of Heat Transfer ($Wm^{-2}K^{-1}$)	203.1068013	146.2767672	193.6232101	119.7021524
Chen's Correlation				
Tube Pitch S_D=S_L (m)	0.0396875	0.0396875	0.0396875	0.0396875
Effective Area Approach Bottom Tube Row (m^2)	3.603	3.603	3.603	3.603
Velocity Approaching Bottom Tube Row (ms^{-1})	0.000232442	0.000147118	0.000211544	0.000109677
Liquid Phase Reynolds Number Re_l	45.16544636	27.79360653	41.32774978	21.05414118
Liquid Phase Prandtl Number Pr_l	1.982416708	1.988325607	1.966673475	2.007157036
Martinelli Parameter *X*	1.173234126	1.275660231	1.059539778	1.257663752
1/*X*				
Two-phase Heat Transfer Coefficient Multiplier F -chart	2.95	2.975	2.8	2.97
Two-phase Reynolds Number Re_{TP}	174.615916	108.5934467	149.6887972	82.08864603
Suppression Factor S -chart	0.95	0.95	0.95	0.95
Forster-Zuber Boiling Coefficient ($Wm^{-2}K^{-1}$)	352.6568151	343.9348332	262.2063199	433.9541071
Forced Convection Boiling Coefficient ($Wm^{-2}K^{-1}$)	3.574209549	2.450003128	3.14081676	1.972832187
E4 Boiling Coefficient of Heat Transfer ($Wm^{-2}K^{-1}$)	356.2310247	346.3848363	265.3471367	435.9269392

Test Number	11			
Chiller Number	1	2	3	4
Overall Heat Transfer Coefficient Calculations				
Combinations				
Br1, E1, K U_{11} ($Wm^{-2}K^{-1}$)	58.56350267	57.99994766	63.82020386	54.53421618
Br1, E2, K U_{12} ($Wm^{-2}K^{-1}$)	341.7840373	268.4434294	334.7108306	231.7287015
Br1, E3, K U_{13} ($Wm^{-2}K^{-1}$)	192.3418526	145.9377929	187.3461481	122.4993949
Br1, E4, K U_{14} ($Wm^{-2}K^{-1}$)	296.6875521	290.7011475	242.0398992	341.6031118
Br2, E1, K U_{21} ($Wm^{-2}K^{-1}$)	58.03300815	57.43989239	63.29556955	54.06156365
Br2, E2, K U_{22} ($Wm^{-2}K^{-1}$)	324.4735287	256.8522961	320.7669219	223.4282407
Br2, E3, K U_{23} (Wm^{-2}K-1)	186.7355118	142.4431797	182.896003	120.1399721
Br2, E4, K U_{24} ($Wm^{-2}K^{-1}$)	283.5559744	277.1566851	234.6632813	323.8664422
Br3, E1, K U_{31} ($Wm^{-2}K^{-1}$)	348.6789058	340.2492554	272.0561016	412.2663258
Br3, E2, K U_{32} ($Wm^{-2}K^{-1}$)	411.330796	309.3932269	393.7463669	261.6757017
Br3, E3, K U_{33} ($Wm^{-2}K^{-1}$)	212.5676091	157.2527862	204.5087811	130.3876414
Br3, E4, K U_{34} ($Wm^{-2}K^{-1}$)	354.2101247	345.5142428	275.4117398	420.021355
U_{lm} ($Wm^{-2}K^{-1}$)	378.0789261	235.5521184	461.4548169	143.9583504

Test Number	11			
Chiller Number	1	2	3	4
Deviations from Target Values of U (%)				
Combinations				
Br1, E1, K U_{11} ($Wm^{-2}K^{-1}$)	-84.51	-75.38	-86.17	-62.12
Br1, E2, K U_{12} ($Wm^{-2}K^{-1}$)	-9.60	13.96	-27.47	60.97
Br1, E3, K U_{13} ($Wm^{-2}K^{-1}$)	-49.13	-38.04	-59.40	-14.91
Br1, E4, K U_{14} ($Wm^{-2}K^{-1}$)	-21.53	23.41	-47.55	137.29
Br2, E1, K U_{21} ($Wm^{-2}K^{-1}$)	-84.65	-75.61	-86.28	-62.45
Br2, E2, K U_{22} ($Wm^{-2}K^{-1}$)	-14.18	9.04	-30.49	55.20
Br2, E3, K U_{23} ($Wm^{-2}K$-1)	-50.61	-39.53	-60.37	-16.55
Br2, E4, K U_{24} ($Wm^{-2}K^{-1}$)	-25.00	17.66	-49.15	124.97
Br3, E1, K U_{31} ($Wm^{-2}K^{-1}$)	-7.78	44.45	-41.04	186.38
Br3, E2, K U_{32} ($Wm^{-2}K^{-1}$)	8.79	31.35	-14.67	81.77
Br3, E3, K U_{33} ($Wm^{-2}K^{-1}$)	-43.78	-33.24	-55.68	-9.43
Br3, E4, K U_{34} ($Wm^{-2}K^{-1}$)	-6.31	46.68	-40.32	191.77

Test Number	11			
Chiller Number	1	2	3	4
Compressor Performance				
Quality x at flash economiser	0.1321	0.1317	0.1263	0.1292
Quality x at evaporator	0.03381	0.03112	0.03837	0.03042
Enthalpy at Evaporator inlet ($kJkg^{-1}$)	99.23	94.16	108.8	88.95
Enthalpy at Evaporator outlet ($kJkg^{-1}$)	1407	1407	1408	1405
Total Mass Flow Rate From Compressor (kgs^{-1})	0.65	0.40	0.59	0.31
Mass flow rate through evaporator (kgs^{-1})	0.57	0.35	0.51	0.27
Mass flow rate from flash economiser (kgs^{-1})	0.09	0.05	0.07	0.04
Mass ratio evaporator	0.8679	0.8683	0.8737	0.8708
Mass ratio flash economiser	0.1321	0.1317	0.1263	0.1292
Enthalpy at Compressor Suction ($kJkg^{-1}$)	1408.5	1408.5	1409.5	1406.5
Enthalpy at Flash Economiser Outlet ($kJkg^{-1}$)	1421	1420	1424	1418
Enthalpy at Compresor Discharge ($kJkg^{-1}$)	1591	1591	1594	1590
Suction Pressure (bar a)	1.32	1.3	1.37	1.24
Flash vapour Pressure (bar a)	2.1	2	2.3	1.9
Discharge Pressure (bar a)	10.8	10.41	9.57	9.1
Condenser pressure (bar a)	8.534	8.251	8.603	7.808
Compressor Heat Input (kW)	-117.75	-72.61	-107.38	-55.88
Pressure Ratio	8.18	8.01	6.99	7.34
Specific Heat at Constant Pressure at Mean Temperature Cp ($kJkg^{-1}K^{-1}$)	4.7436	4.7816	4.8124	4.7700
Specific Heat at Constant Volume at Mean Temperature Cv ($kJkg^{-1}K^{-1}$)	2.8510	2.8388	2.8288	2.8425
Ratio of Specific Heats	1.66	1.68	1.70	1.68
Volume Ratio	3.54	3.44	3.14	3.28
Compressor load capacity (%)	70.65	68.75	66.00	70.85
Temperature of oil entering cooler T_{oilin} (^oC)	72.10	71.50	71.20	68.70
Temperature of oil leaving cooler T_{oilout} (^oC)	48.90	48.90	48.90	48.90
Specific heat capacity of oil Cp_{oil} ($kJkg^{-1}K^{-1}$)	2.02	2.02	2.02	2.02
Mass flow rate of oil to cooler $\dot{m}_{oil}$ (kgs^{-1})	3.51	3.44	3.30	3.22
Heat transferred to oil (kW)	-164.05	-156.89	-148.43	-128.52

Test Number	11			
Chiller Number	1	2	3	4
Refrigerating capacity (kW)	739.03	457.35	667.28	351.86
Internal Pump Power (kW)	42.00	42.00	44.00	42.00
COP	2.62	1.99	2.61	1.91
Compressor Power (kW)	322.00	325.00	297.00	281.00
COSP	2.28	1.68	2.23	1.55
Total Refrigerating Effect for Procedure (all on-line chillers)	2215.53			
Total COSP for Procedure (all on-line chillers)	1.588191526			

Actual surface area for heat transfer (m^2)	434.5118	434.5118	434.5118	434.5118
Surface area using U_{11} (m^2)	2805.155895	1764.659782	3141.756858	1147.015696
Surface area using U_{12} (m^2)	480.6536784	381.2727888	599.047132	269.9346328
Surface area using U_{13} (m^2)	854.1030074	701.3274147	1070.251858	510.6278442
Surface area using U_{14} (m^2)	553.7130006	352.0803954	828.4070674	183.1119208
Surface area using U_{21} (m^2)	2830.79854	1781.865716	3167.797755	1157.043891
Surface area using U_{22} (m^2)	506.2963237	398.4787231	625.0880294	279.9628272
Surface area using U_{23} (m^2)	879.7456528	718.533349	1096.292756	520.6560386
Surface area using U_{24} (m^2)	579.355646	369.2863297	854.4479649	193.1401152
Surface area using U_{31} (m^2)	471.149106	300.8094018	737.0081461	151.7261974
Surface area using U_{32} (m^2)	399.385984	330.8093587	509.2302557	239.0424542
Surface area using U_{33} (m^2)	772.8353131	650.8639846	980.4349818	479.7356656
Surface area using U_{34} (m^2)	463.7918097	296.2256321	728.0283814	148.9248135

2nd Law Analysis

Test Number	11			
Chiller Number	1	2	3	4
COP_{act}	3.2909	3.3738	3.4283	3.6905
COP_{Carnot}	6.636243386	6.4780	6.5169	6.4780
Condenser temperature T_H (K)	288.65	288.65	288.65	288.65
Evaporator temperature T_L (K)	250.8500	250.0500	250.2500	250.0500
Temperature of surroundings T_o (K)	289.15	289.15	289.15	289.15
Temperature of brine T (K)	249.8	249.4	249.4	249.6
Cooling tower water temperature T_{ct} (K)	288.65	288.7	288.7	288.7
Entropy of ammonia into evaporator s_9 ($kJkg^{-1}K^{-1}$)	0.4098	0.3859	0.4881	0.3688
Entropy of ammonia exit evaporator s_1 (kJkg-1K-1)	5.743	5.748	5.73	5.765
Entropy of ammonia at compressor suction s'_1 ($kJkg^{-1}K^{-1}$)	5.743	5.748	5.73	5.765
Entropy of ammonia exit compressor s_2 ($kJkg^{-1}K^{-1}$)	5.395	5.412	5.458	5.469
Entropy of ammonia exit flash economiser s_6 ($kJkg^{-1}K^{-1}$)	5.581	5.598	5.549	5.616
Entropy of ammonia entering condenser s_3 ($kJkg^{-1}K^{-1}$)	5.395	5.412	5.458	5.469
Entropy of ammonia leaving condenser s_4 ($kJkg^{-1}K^{-1}$)	1.039	1.021	1.042	0.9939
Entropy of ammonia after first throttle s_5 ($kJkg^{-1}K^{-1}$)	1.089	1.072	1.087	1.043
Entropy leaving flash economiser s_6 ($kJkg^{-1}K^{-1}$)	5.581	5.598	5.459	5.616
Entropy leaving flash economiser s_8 ($kJkg^{-1}K^{-1}$)	0.4056	0.3859	0.4481	0.3653
Entropy of flash to compressor s_7 ($kJkg^{-1}K^{-1}$)	5.581	5.598	5.549	5.616
Enthalpy of ammonia entering evaporator h_9 ($kJkg^{-1}$)	99.23	94.16	108.8	88.95
Enthalpy of ammonia leaving evaporator h_1 ($kJkg^{-1}$)	1407	1407	1408	1405
Enthalpy of ammonia at compressor suction h'_1 (kJkg-1)	1408.5	1408.5	1409.5	1406.5
Enthalpy of ammonia leaving compressor h_2 ($kJkg^{-1}$)	1591	1591	1594	1590
Enthalpy of ammonia from flash economiser h_6 (kJkg-1)	1421	1420	1424	1418
Isentropic enthalpy leaving compressor h_{s2} ($kJkg^{-1}$)	1756	1774	1721	1732
Isentropic enthalpy leaving compressor h'_{s2} ($kJkg^{-1}$)	1658	1658	1626	1641
Enthalpy of ammonia entering condenser h_3 ($kJkg^{-1}$)	1591	1591	1594	1590
Enthalpy of ammonia leaving condenser h_4 ($kJkg^{-1}$)	273.8	268.6	274.8	260.5

2nd Law Analysis

Test Number	11			
Chiller Number	1	2	3	4
Refrigerating capacity Q_L (kW)	739.0294	457.35	667.28	351.86
Specific refrigerating capacity q_L ($kJkg^{-1}$)	1307.7700	1312.84	1299.20	1316.05
Condenser heat load Q_H (kW)	-857.655	-530.560	-775.496	-408.200
Condenser specific heat load q_H ($kJkg^{-1}$)	-1317.2000	-1322.400	-1319.200	-1329.500
Cycle irreversibility I_{cycle} (kW)	**200.3291**	**186.4665**	**179.6092**	**153.4471**
Heat engine (evaporator) W_{rev} (kJ)	-112.8357	-71.52	-103.72	-55.02
Availability (evaporator) ($kJkg^{-1}$)	-199.67	-205.29	-201.95	-205.79
Evaporator irreversibility i_{evap} (kW)	28.317	28.367	9.426	35.423
Condenser irreversibility i_{cond} ($kJkg^{-1}$)	59.944	55.033	44.599	37.828
Compressor irreversibility i_{comp} ($kJkg^{-1}$)	32.216	29.779	43.837	19.749
Throttle 4-5 irreversibility i_{4-5} ($kJkg^{-1}$)	14.458	14.747	13.012	14.197
Throttle 6-7 irreversibility i_{6-7} ($kJkg^{-1}$)	0.000	0.000	22.446	0.000
Throttle 8-9 irreversibility i_{8-9} ($kJkg^{-1}$)	1.212	0.000	11.546	1.010
Total of irreversibilities i_{tot} ($kJkg^{-1}$)	**136.1468**	**127.926**	**144.865**	**108.208**
	96.398	**88.319**	**78.581**	**64.989**
Compressor isentropic work W_{isen}	-216.760	-139.905	-174.986	-95.873
Compressor adiabatic efficiency	0.486	0.362	0.433	0.306
Compressor second law efficiency	0.658	0.615	0.693	0.648
Compressor actual work rate Wact (kW)	-281.804	-229.508	-255.817	-184.401
Compressor reversible work W_{rev} (kW)	-185.406	-141.189	-177.236	-119.413
Chiller second law effectiveness	0.4004	0.3116	0.4055	0.2984

Appendix C

Development of Specific Properties for 27.5 % $CaCl_2$ in Water Brine Solution

Using linear interpolation relies on assuming that ρ, μ, k, $C_p = f(T)$

(i) From graph on figure C1, a linear relationship is found between density and temperature which is of the form-

$$\rho = -0.4615 \times T + 1267 \qquad \text{kgm}^{-3}$$

The table of properties below uses this relationship to calculate the density at the relevant temperature.

(ii) From graph on figure C2, a linear relationship is found between viscosity and temperature but a separate relationship exists between certain temperatures as shown below-

For the range –30 ^{o}C to –26 ^{o}C

$$\mu = -0.5(26 + T) + 15 \qquad \text{cP}$$

For the range –26 ^{o}C to –20 ^{o}C

$$\mu = -0.5677(20 + T) + 11.6 \qquad \text{cP}$$

For the range –20 °C to –17 °C

$$\mu = -0.5333(17+T)+10 \qquad \text{cP}$$

For the range –17 °C to –15 °C

$$\mu = -0.5(15+T)+9 \qquad \text{cP}$$

The table of properties below uses this relationship to calculate the viscosity in centipoise at the relevant temperature. A conversion factor of 1000 is required to give values in the units $mNsm^{-2}$.

(iii) From graph on figure C3, a linear relationship is assumed between thermal conductivity and temperature in the range of interest, which is of the form-

$$k = (1.3077 \times 10^{-3}) \times T + 0.459 \qquad \text{Kcal m}^{-1}\text{h}^{-1}{}^{o}\text{C}^{-1}$$

The table of properties below uses this relationship to calculate the thermal conductivity at the relevant temperature converting from Kcal $m^{-1}h^{-1}{}^{o}C^{-1}$ to $Wm^{-1}K^{-1}$ using a conversion factor of 1.163.

(iv) From the graph on figure C4, by assuming a straight line relationships at appropriate points corresponding to temperatures in the range between –37.222°C and –15 °C, linear interpolation is used to find the specific heat capacity in Kcal/kg^{o}C, a conversion factor of 4.1868 is then applied to convert to the units kJ/kgK.

$$C_p = (4.0816 \times 10^{-4})T + 0.6565 \qquad \text{Kcal/kg}^{o}\text{C}$$

The results are tabulated in the temperature range of interest at the end of this appendix in section C-5.

.

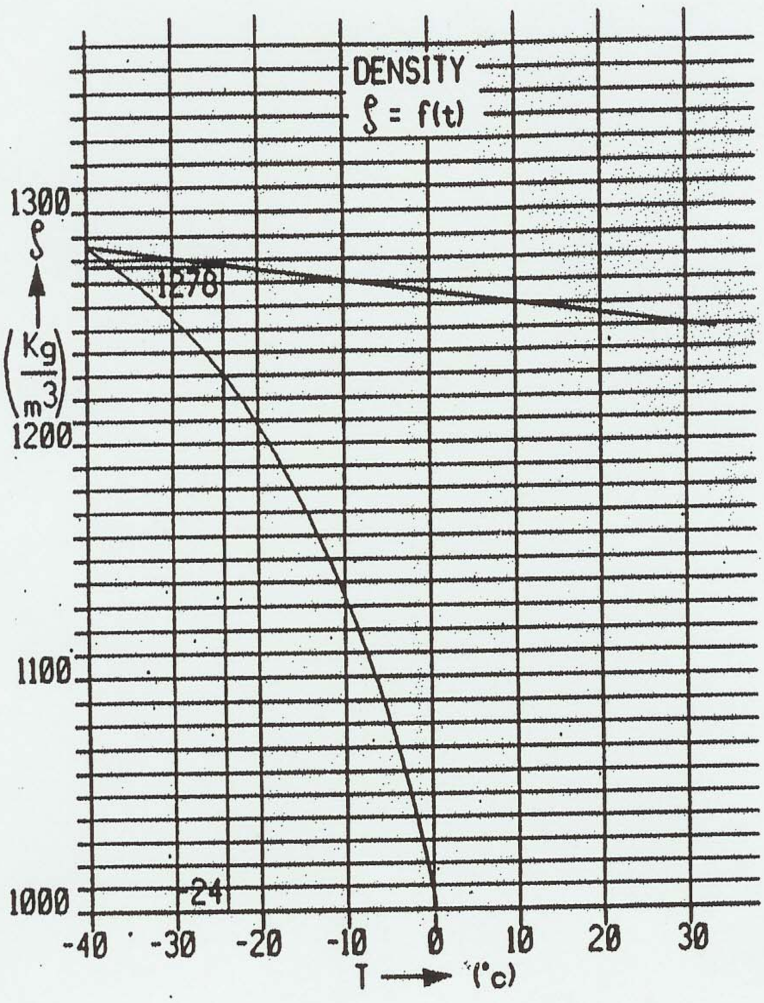

Figure C1 density versus temperature relationship for 27% CaCl brine

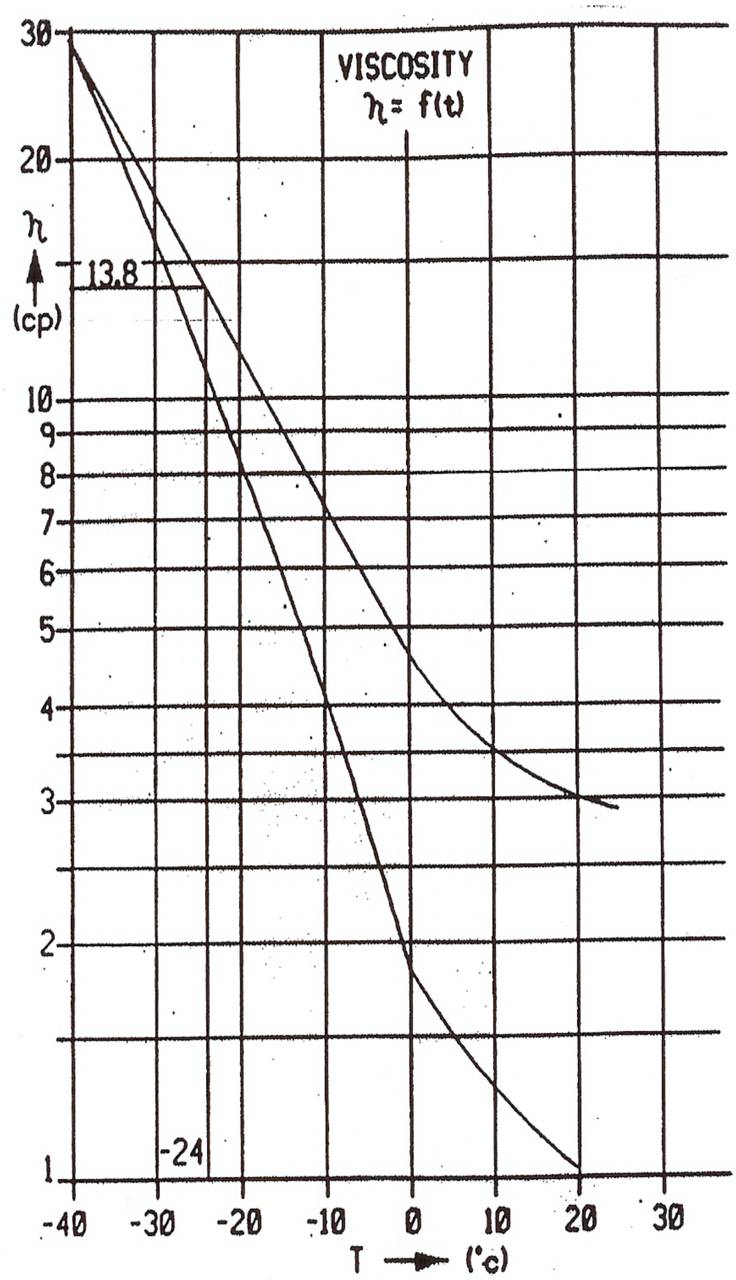

Figure C2 viscosity versus temperature relationship for 27% CaCl brine

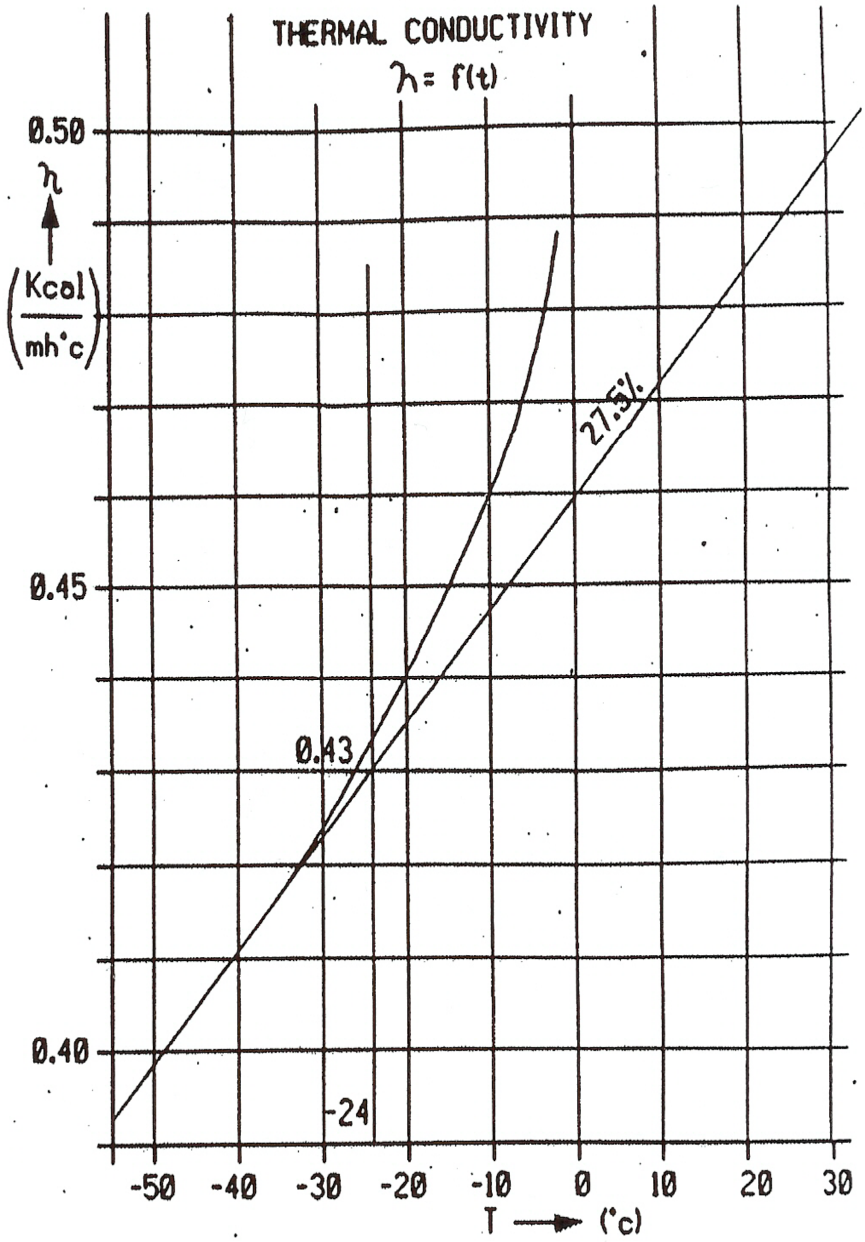

Figure C3 thermal conductivity versus temperature relationship for 27% CaCl brine

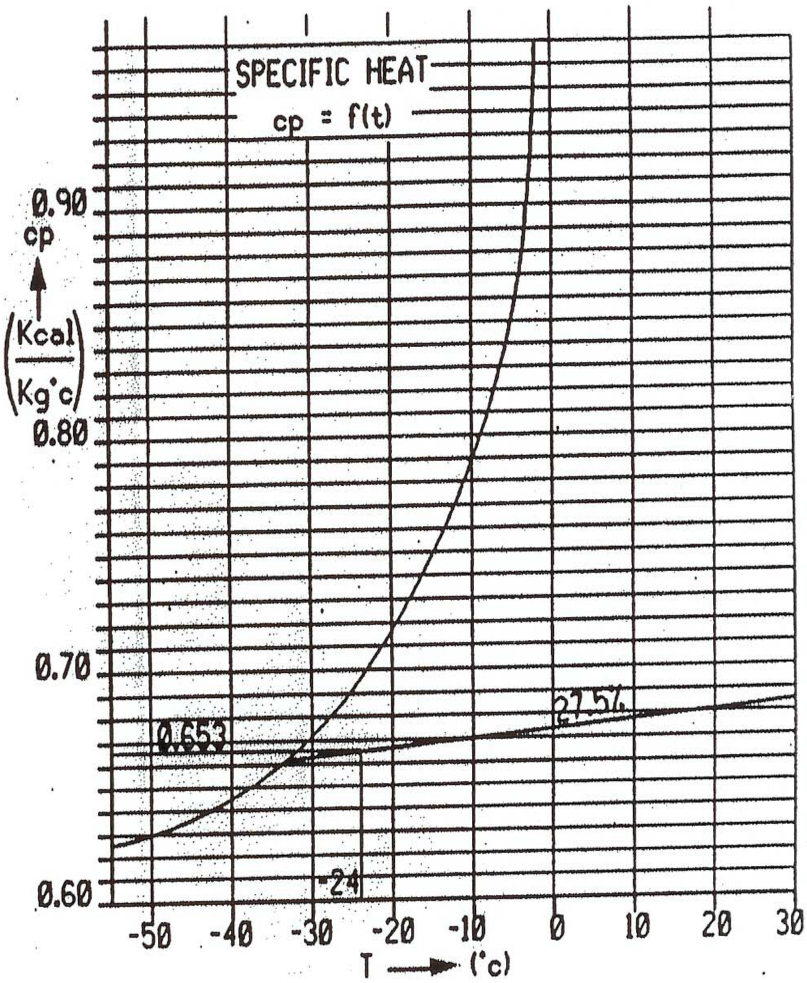

Figure C4 specific heat capacity versus temperature relationship for 27% CaCl brine

Appendix C Specific Properties of 27.5 % $CaCl_2$ calcium chloride in water brine solution.

Temperature T (^oC)	Thermal Conductivity k_l (mW/mK)	Density ρ_l (kgm^{-3})	Dynamic Viscosity μ_l (μNsm^{-2})	Enthalpy h_l (kJ/kg)	Specifc Heat Capacity C_{pv} (kJ/kgK)
-28.0	0.4912	1280.000	16.0000	-5.9025	2.717191
-27.9	0.4914	1279.8759	15.9500	-5.8461	2.717498
-27.8	0.4915	1279.8297	15.9000	-5.7897	2.717806
-27.7	0.4917	1279.7836	15.8500	-5.7332	2.718114
-27.6	0.4918	1279.7374	15.8000	-5.6768	2.718421
-27.5	0.4920	1279.6913	15.7500	-5.6203	2.718729
-27.4	0.4921	1279.6451	15.7000	-5.5637	2.719036
-27.3	0.4923	1279.599	15.6500	-5.5072	2.719344
-27.2	0.4924	1279.5528	15.6000	-5.4506	2.719652
-27.1	0.4926	1279.5067	15.5500	-5.3939	2.719959
-27.0	0.4928	1279.4605	15.5000	-5.3373	2.720267
-26.9	0.4929	1279.4144	15.4500	-5.2806	2.720574
-26.8	0.4931	1279.3682	15.4000	-5.2239	2.720882
-26.7	0.4932	1279.3221	15.3500	-5.1672	2.72119
-26.6	0.4934	1279.2759	15.3000	-5.1105	2.721497
-26.5	0.4935	1279.2298	15.2500	-5.0537	2.721805
-26.4	0.4937	1279.1836	15.2000	-4.9969	2.722112
-26.3	0.4938	1279.1375	15.1500	-4.9401	2.72242
-26.2	0.4940	1279.0913	15.1000	-4.8832	2.722728
-26.1	0.4941	1279.0452	15.0500	-4.8263	2.723035
-26.0	0.4943	1278.999	15.0000	-4.7694	2.723343
-25.9	0.4944	1278.9529	14.9494	-4.7125	2.72365
-25.8	0.4946	1278.9067	14.8927	-4.6555	2.723958
-25.7	0.4947	1278.8606	14.8359	-4.5986	2.724266
-23.2	0.4985	1277.7068	13.4166	-3.1653	2.731955
-23.1	0.4987	1277.6607	13.3599	-3.1077	2.732263
-23.0	0.4988	1277.6145	13.3031	-3.0500	2.732571
-22.9	0.4990	1277.5684	13.2463	-2.9922	2.732878
-22.8	0.4991	1277.5222	13.1896	-2.9345	2.733186
-22.7	0.4993	1277.4761	13.1328	-2.8767	2.733493
-22.6	0.4994	1277.4299	13.0760	-2.8189	2.733801
-22.5	0.4996	1277.3838	13.0193	-2.7611	2.734109
-22.4	0.4997	1277.3376	12.9625	-2.7032	2.734416
-22.3	0.4999	1277.2915	12.9057	-2.6453	2.734724
-22.2	0.5001	1277.2453	12.8489	-2.5874	2.735031
-22.1	0.5002	1277.1992	12.7922	-2.5295	2.735339
-22.0	0.5004	1277.153	12.7354	-2.4715	2.735647
-21.9	0.5005	1277.1069	12.6786	-2.4135	2.735954
-21.8	0.5007	1277.0607	12.6219	-2.3555	2.736262
-21.7	0.5008	1277.0146	12.5651	-2.2975	2.736569
-21.6	0.5010	1276.9684	12.5083	-2.2394	2.736877
-21.5	0.5011	1276.9223	12.4516	-2.1813	2.737185
-21.4	0.5013	1276.8761	12.3948	-2.1232	2.737492
-21.3	0.5014	1276.83	12.3380	-2.0650	2.7378
-21.2	0.5016	1276.7838	12.2812	-2.0068	2.738107

Temperature T (°C)	Thermal Conductivity k_l (mW/mK)	Density ρ_l (kgm^{-3})	Dynamic Viscosity μ_l (μNsm^{-2})	Enthalpy h_l (kJ/kg)	Specifc Heat Capacity C_{pv} (kJ/kgK)
-21.1	0.5017	1276.7377	12.2245	-1.9486	2.738415
-21.0	0.5019	1276.6915	12.1677	-1.8904	2.738723
-20.9	0.5020	1276.6454	12.1109	-1.8322	2.73903
-20.8	0.5022	1276.5992	12.0542	-1.7739	2.739338
-20.7	0.5023	1276.5531	11.9974	-1.7156	2.739645
-20.6	0.5025	1276.5069	11.9406	-1.6572	2.739953
-20.5	0.5026	1276.4608	11.8839	-1.5989	2.740261
-17.6	0.5070	1275.1224	10.3200	0.1051	2.710199
-17.5	0.5072	1275.0763	10.2667	0.1643	2.709906
-17.4	0.5074	1275.0301	10.2133	0.2234	2.709613
-17.3	0.5075	1274.984	10.1600	0.2826	2.70932
-17.2	0.5077	1274.9378	10.1067	0.3419	2.709027
-17.1	0.5078	1274.8917	10.0533	0.4011	2.708734
-17.0	0.5080	1274.8455	10.0000	0.4604	2.708441
-16.9	0.5081	1274.7994	9.9500	0.5197	2.708148
-16.8	0.5083	1274.7532	9.9000	0.5791	2.707855
-16.7	0.5084	1274.7071	9.8500	0.6384	2.707562
-16.6	0.5086	1274.6609	9.8000	0.6978	2.707269
-16.5	0.5087	1274.6148	9.7500	0.7572	2.706976
-16.4	0.5089	1274.5686	9.7000	0.8167	2.706682
-16.3	0.5090	1274.5225	9.6500	0.8762	2.706389
-16.2	0.5092	1274.4763	9.6000	0.9357	2.706096
-16.1	0.5093	1274.4302	9.5500	0.9952	2.705803
-16.0	0.5095	1274.384	9.5000	1.0547	2.70551
-15.9	0.5096	1274.3379	9.4500	1.1143	2.705217
-15.8	0.5098	1274.2917	9.4000	1.1739	2.704924
-15.7	0.5099	1274.2456	9.3500	1.2336	2.704631
-15.6	0.5101	1274.1994	9.3000	1.2932	2.704338
-15.5	0.5102	1274.1533	9.2500	1.3529	2.704045
-15.4	0.5104	1274.1071	9.2000	1.4126	2.703752
-15.3	0.5105	1274.061	9.1500	1.4723	2.703459
-15.2	0.5107	1274.0148	9.1000	1.5321	2.703166
-15.1	0.5109	1273.9687	9.0500	1.5919	2.702872
-15.0	0.5110	1273.9225	9.0000	1.6517	2.702579

Temperature T (°C)	Thermal Conductivity k_l (mW/mK)	Density ρ_l (kgm^{-3})	Dynamic Viscosity μ_l (μNsm^{-2})	Enthalpy h_l (kJ/kg)	Specifc Heat Capacity C_{pv} (kJ/kgK)
-25.6	0.4949	1278.814	14.7791	-4.5415	2.724573
-25.5	0.4950	1278.768	14.7224	-4.4845	2.724881
-25.4	0.4952	1278.722	14.6656	-4.4274	2.725188
-25.3	0.4953	1278.676	14.6088	-4.3704	2.725496
-25.2	0.4955	1278.63	14.5520	-4.3132	2.725804
-25.1	0.4956	1278.584	14.4953	-4.2561	2.726111
-25.0	0.4958	1278.538	14.4385	-4.1989	2.726419
-24.9	0.4959	1278.491	14.3817	-4.1417	2.726726
-24.8	0.4961	1278.445	14.3250	-4.0845	2.727034
-24.7	0.4963	1278.399	14.2682	-4.0273	2.727342
-24.6	0.4964	1278.353	14.2114	-3.9700	2.727649
-24.5	0.4966	1278.307	14.1547	-3.9127	2.727957
-24.4	0.4967	1278.261	14.0979	-3.8553	2.728264
-24.3	0.4969	1278.214	14.0411	-3.7980	2.728572
-24.2	0.4970	1278.168	13.9843	-3.7406	2.728879
-24.1	0.4972	1278.122	13.9276	-3.6832	2.729187
-24.0	0.4973	1278.076	13.8708	-3.6258	2.729495
-23.9	0.4975	1278.03	13.8140	-3.5683	2.729802
-23.8	0.4976	1277.984	13.7573	-3.5108	2.73011
-23.7	0.4978	1277.938	13.7005	-3.4533	2.730417
-23.6	0.4979	1277.891	13.6437	-3.3958	2.730725
-23.5	0.4981	1277.845	13.5870	-3.3382	2.731033
-23.4	0.4982	1277.799	13.5302	-3.2806	2.73134
-23.3	0.4984	1277.753	13.4734	-3.2230	2.731648
-20.4	0.5028	1276.415	11.8271	-1.5405	2.740568
-20.3	0.5029	1276.368	11.7703	-1.4821	2.740876
-20.2	0.5031	1276.322	11.7135	-1.4236	2.741183
-20.1	0.5032	1276.276	11.6568	-1.3652	2.741491
-20.0	0.5034	1276.23	11.6000	-1.3067	2.741799
-19.9	0.5036	1276.184	11.5466	-1.2481	2.742106
-19.8	0.5037	1276.138	11.4932	-1.1896	2.742414
-19.7	0.5039	1276.092	11.4399	-1.1310	2.742721
-19.6	0.5040	1276.045	11.3866	-1.0724	2.743029
-19.5	0.5042	1275.999	11.3333	-1.0138	2.743337
-19.4	0.5043	1275.953	11.2799	-0.9552	2.743644
-19.3	0.5045	1275.907	11.2266	-0.8965	2.743952
-19.2	0.5046	1275.861	11.1733	-0.8378	2.744259
-19.1	0.5048	1275.815	11.1199	-0.7790	2.744567
-19.0	0.5049	1275.769	11.0666	-0.7203	2.744875
-18.9	0.5051	1275.722	11.0133	-0.6615	2.745182
-18.8	0.5052	1275.676	10.9599	-0.6027	2.74549
-18.7	0.5054	1275.63	10.9066	-0.5439	2.745797
-18.6	0.5055	1275.584	10.8533	-0.4850	2.746105
-18.5	0.5057	1275.538	10.8000	-0.4261	2.746413
-18.4	0.5058	1275.492	10.7466	-0.3672	2.74672

Temperature T (^oC)	Thermal Conductivity k_l (mW/mK)	Density ρ_l (kgm^{-3})	Dynamic Viscosity μ_l (μNsm^{-2})	Enthalpy h_l (kJ/kg)	Specifc Heat Capacity C_{pv} (kJ/kgK)
-18.3	0.5060	1275.445	10.6933	-0.3082	2.747028
-18.2	0.5061	1275.399	10.6400	-0.2493	2.747335
-18.1	0.5063	1275.353	10.5866	-0.1903	2.747643
-18.0	0.5064	1275.307	10.5333	-0.1313	2.747951
-17.9	0.5066	1275.261	10.4800	-0.0722	2.748258
-17.8	0.5067	1275.215	10.4266	-0.0131	2.748566
-17.7	0.5069	1275.169	10.3733	0.0460	2.748873

Specific Properties of Ammonia R717

Temperature T (°C)	Saturation Pressure P_s (bar abs)	Liquid Thermal Conductivity k_l (mW/mK)	Vapour Thermal Conductivity k_v (mW/mK)	Liquid Density ρ_l (kgm^{-3})	Vapour Density ρ_v (kgm^{-3})	Liquid Dynamic Viscosity μ_l (μNsm^{-2})	Vapour Dynamic Viscosity μ_v (μNsm^{-2})	Surface Tension σ (mN/m)	Latent Heat λ (kJ/kg)	Vapour Enthalpy h_v (kJ/kg)	Liquid Enthalpy h_l (kJ/kg)	Enthalpy Difference h_{fg} (kJ/kg)	Vapor Specifc Heat Capacity C_{pv} (kJ/kgK)	Liquid Specifc Heat Capacity C_{pl} (kJ/kgK)
-33.40	**1.013**	**614.0000**	**18.8000**	**682.0000**	**0.8600**	**285.0000**	**9.2500**	**33.90**	**1369.7670**				2.120	4.472
-33.00	1.031	613.3822	18.8281	681.1989	0.9042	283.9048	9.2595	33.83	1368.90	1400	30.92	1369.08	2.126	4.473
-32.00	1.083	611.5975	18.9092	681.9891	0.9470	280.7410	9.2871	33.64	1366.39	1401	35.36	1365.64	2.142	4.476
-31.00	1.138	609.7098	18.9950	678.8866	0.9921	277.3947	9.3163	33.43	1363.73	1403	39.81	1363.19	2.159	4.480
-30.00	1.195	607.7535	19.0839	677.5068	1.0380	273.9267	9.3465	33.22	1360.98	1404	44.26	1359.74	2.177	4.484
-29.00	1.254	605.7285	19.1760	676.1325	1.0861	270.3370	9.3778	33.00	1358.13	1405	48.71	1356.29	2.195	4.487
-28.70	1.273	605.0764	19.2056	675.6757	1.1008	269.1810	9.3879	32.93	1357.21	1406.00	50.05	1355.95	2.201	4.489
-28.00	1.316	603.6006	19.2727	674.7638	1.1360	266.5647	9.4107	32.77	1355.14	1407	53.17	1353.83	2.215	4.491
-27.00	1.380	601.4041	19.3725	673.8544	1.1876	262.6708	9.4447	32.53	1352.05	1408	57.64	1350.36	2.235	4.495
-26.69	1.400	600.7176	19.4037			261.4540	9.4553	32.45	1351.08				2.241	4.497
-26.00	1.446	599.1388	19.4755	672.4950	1.2413	258.6552	9.4797	32.28	1348.86	1410	62.11	1347.89	2.255	4.500
-25.00	1.516	596.7363	19.5847	671.1409	1.2967	254.3963	9.5168	32.02	1345.48	1411	66.58	1344.42	2.277	4.504
-24.00	1.587	594.2995	19.6955	669.7923	1.3541	250.0764	9.5545	31.75	1342.05	1413	71.07	1341.93	2.299	4.509
-23.15	**1.654**	**592.0000**	**19.8000**	**669.0000**	**1.4100**	**246.0000**	**9.5900**	**31.50**	**1338.8174**				2.320	4.513
-23.00	1.662													
-22.00	1.739													
-21.00	1.819													
-20.00	1.902													
-19.00	1.988													
-18.00	2.077													
-17.00	2.169													
-16.00	2.264													
-15.00	2.363													
-14.00	2.465													
-13.00	2.571													
-12.00	2.680													
-11.00	2.792													

Temperature T (°C)	Saturation Pressure P_s (bar abs)	Liquid Thermal Conductivity k_l (mW/mK)	Vapour Thermal Conductivity k_v (mW/mK)	Liquid Density ρ_l (kgm^{-3})	Vapour Density ρ_v (kgm^{-3})	Liquid Dynamic Viscosity μ_l (μNsm^{-2})	Vapour Dynamic Viscosity μ_v (μNsm^{-2})	Surface Tension σ (mN/m)	Latent Heat λ (kJ/kg)	Vapour Enthalpy h_v (kJ/kg)	Liquid Enthalpy h_l (kJ/kg)	Enthalpy Difference h_{fg} (kJ/kg)	Vapor Specifc Heat Capacity C_{pv} (kJ/kgK)	Vapor Specifc Heat Capacity C_{pv} (kJ/kgK)
-7.00	3.281													
-6.00	3.413													
-5.00	3.549													
-4.00	3.690													
-3.15	**3.819**	**569**	**22.7**	**643.0000**	**3.0900**	**190**	**10.3**	**26.9**						
-3.00	3.834													
-2.00	3.984													
-1.00	4.137													
0.00	4.296													
1.00	4.459													
2.00	4.626													
3.00	4.799													
4.00	4.977													
5.00	5.159													
6.00	5.347													
7.00	5.540													
8.00	5.739													
9.00	5.942													
10.00	6.152													
11.00	6.367													
12.00	6.588													
13.00	6.815													
14.00	7.047													
15.00	7.286													
16.00	7.531													
16.85	**7.753**	**501**	**25.2**	**615.0000**	**6.0800**	**152**	**11.05**	**22.4**						
17.00	7.783													
18.00	8.040													

Temperature T (°C)	Saturation Pressure P_s (bar abs)	Liquid Thermal Conductivity k_l (mW/mK)	Vapour Thermal Conductivity k_v (mW/mK)	Liquid Density ρ_l (kgm^{-3})	Vapour Density ρ_v (kgm^{-3})	Liquid Dynamic Viscosity μ_l (μNsm^{-2})	Vapour Dynamic Viscosity μ_v (μNsm^{-2})	Surface Tension σ (mN/m)	Latent Heat λ (kJ/kg)	Vapour Enthalpy h_v (kJ/kg)	Liquid Enthalpy h_l (kJ/kg)	Enthalpy Difference h_{fg} (kJ/kg)	Vapor Specifc Heat Capacity C_{pv} (kJ/kgK)	Vapor Specifc Heat Capacity C_{pv} (kJ/kgK)
22.00	9.137													
23.00	9.428													
24.00	9.726													
25.00	10.030													
26.00	10.340													
27.00	10.660													
28.00	10.990													
29.00	11.330													
30.00	11.670													
31.00	12.020													
32.00	12.380													
33.00	12.750													
34.00	13.120													
35.00	13.500													
36.00	13.900													
36.85	**14.249**	**456**	**28.9**	**584.0000**	**11.0000**	**125**	**11.86**	**18**						
37.00	14.300													
38.00	14.700													
39.00	15.120													
40.00	15.550													
41.00	15.980													
42.00	16.430													
43.00	16.880													
44.00	17.350													
45.00	17.820													
46.00	18.300													
47.00	18.790													
48.00	19.300													

Temperature T (°C)	Saturation Pressure P_s (bar abs)	Liquid Thermal Conductivity k_l (mW/mK)	Vapour Thermal Conductivity k_v (mW/mK)	Liquid Density ρ_l (kgm^{-3})	Vapour Density ρ_v (kgm^{-3})	Liquid Dynamic Viscosity μ_l (μNsm^{-2})	Vapour Dynamic Viscosity μ_v (μNsm^{-2})	Surface Tension σ (mN/m)	Latent Heat λ (kJ/kg)	Vapour Enthalpy h_v (kJ/kg)	Liquid Enthalpy h_l (kJ/kg)	Enthalpy Difference h_{fg} (kJ/kg)	Vapor Specifc Heat Capacity C_{pv} (kJ/kgK)	Vapor Specifc Heat Capacity C_{pv} (kJ/kgK)
52.00	21.410													
53.00	21.960													
54.00	22.530													
55.00	23.100													
56.00	23.690													
56.85	**24.220**	**411**	**34.3**	**551.0000**	**18.9000**	**105**	**12.74**	**13.7**						
57.00	24.280													
58.00	24.890													
59.00	25.510													
60.00	26.140													
61.00	26.790													
62.00	27.440													
63.00	28.110													
64.00	28.790													
65.00	29.480													
66.00	30.180													
67.00	30.900													
68.00	31.620													
69.00	32.370													
70.00	33.120													
71.00	33.890													
72.00	34.670													
73.00	35.460													
74.00	36.270													
75.00	37.090													
76.00	37.920													
76.85	**38.700**	**365**	**39.5**	**512.0000**	**31.5000**	**88.5**	**13.75**	**9.6**						
77.00	38.770													

Temperature T (°C)	Saturation Pressure P_s (bar abs)	Liquid Thermal Conductivity k_l (mW/mK)	Vapour Thermal Conductivity k_v (mW/mK)	Liquid Density ρ_l (kgm^{-3})	Vapour Density ρ_v (kgm^{-3})	Liquid Dynamic Viscosity μ_l (μNsm^{-2})	Vapour Dynamic Viscosity μ_v (μNsm^{-2})	Surface Tension σ (mN/m)	Latent Heat λ (kJ/kg)	Vapour Enthalpy h_v (kJ/kg)	Liquid Enthalpy h_l (kJ/kg)	Enthalpy Difference h_{fg} (kJ/kg)	Vapor Specifc Heat Capacity C_{pv} (kJ/kgK)	Vapor Specifc Heat Capacity C_{pv} (kJ/kgK)
81.00	42.310													
82.00	43.230													
83.00	44.170													
84.00	45.120													
85.00	46.090													
86.00	47.070													
87.00	48.070													
88.00	49.080													
89.00	50.110													
90.00	51.150													
91.00	52.210													
92.00	53.290													
93.00	54.390													
94.00	55.500													
95.00	56.630													
96.00	57.780													
96.85	**58.910**	**320**	**50.4**	**466.0000**	**52.6000**	**70.2**	**15.06**	**5.74**						

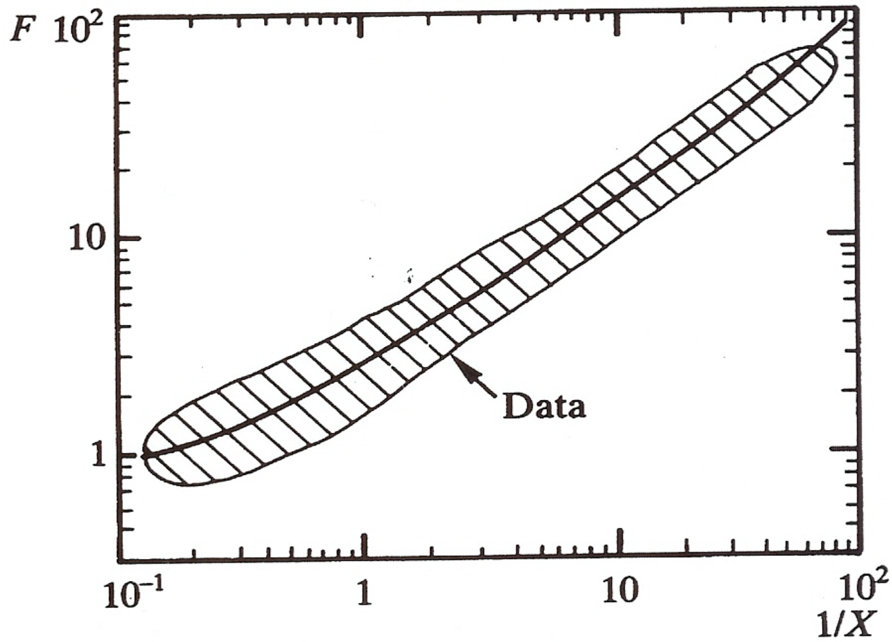

Figure E1 Chen correlation for F (courtesy of P.B. Whalley)

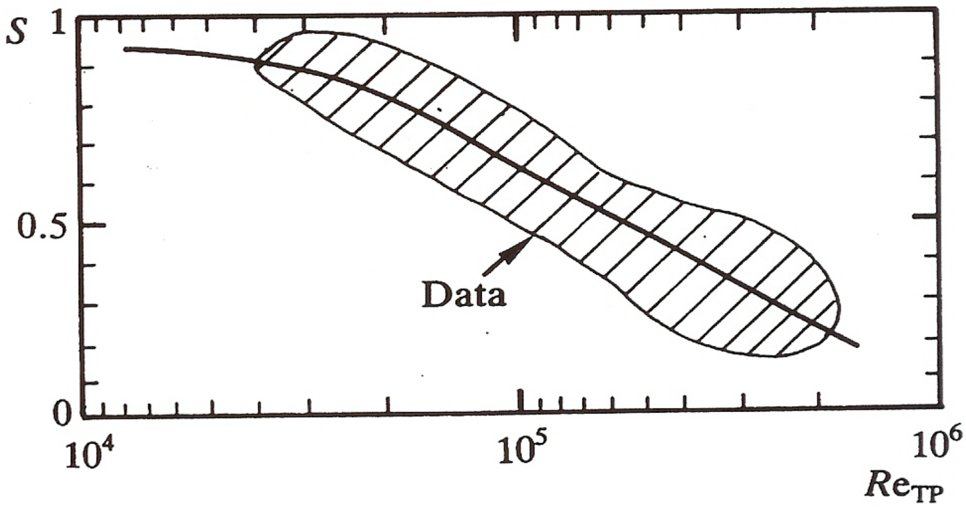

Figure E2 Chen correlation for S (courtesy of P.B. Whalley)

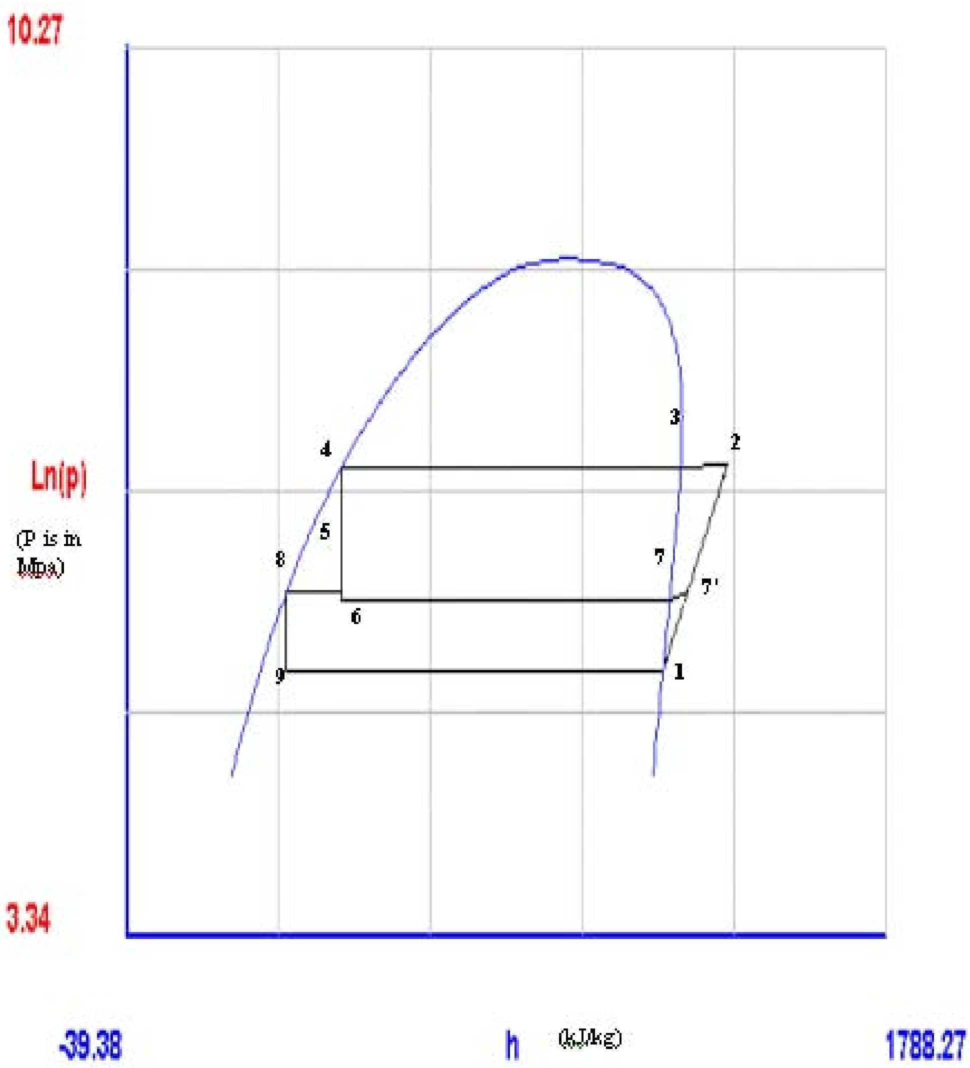

Figure 4.3.3 Pressure-enthalpy diagram for the chillers at design conditions

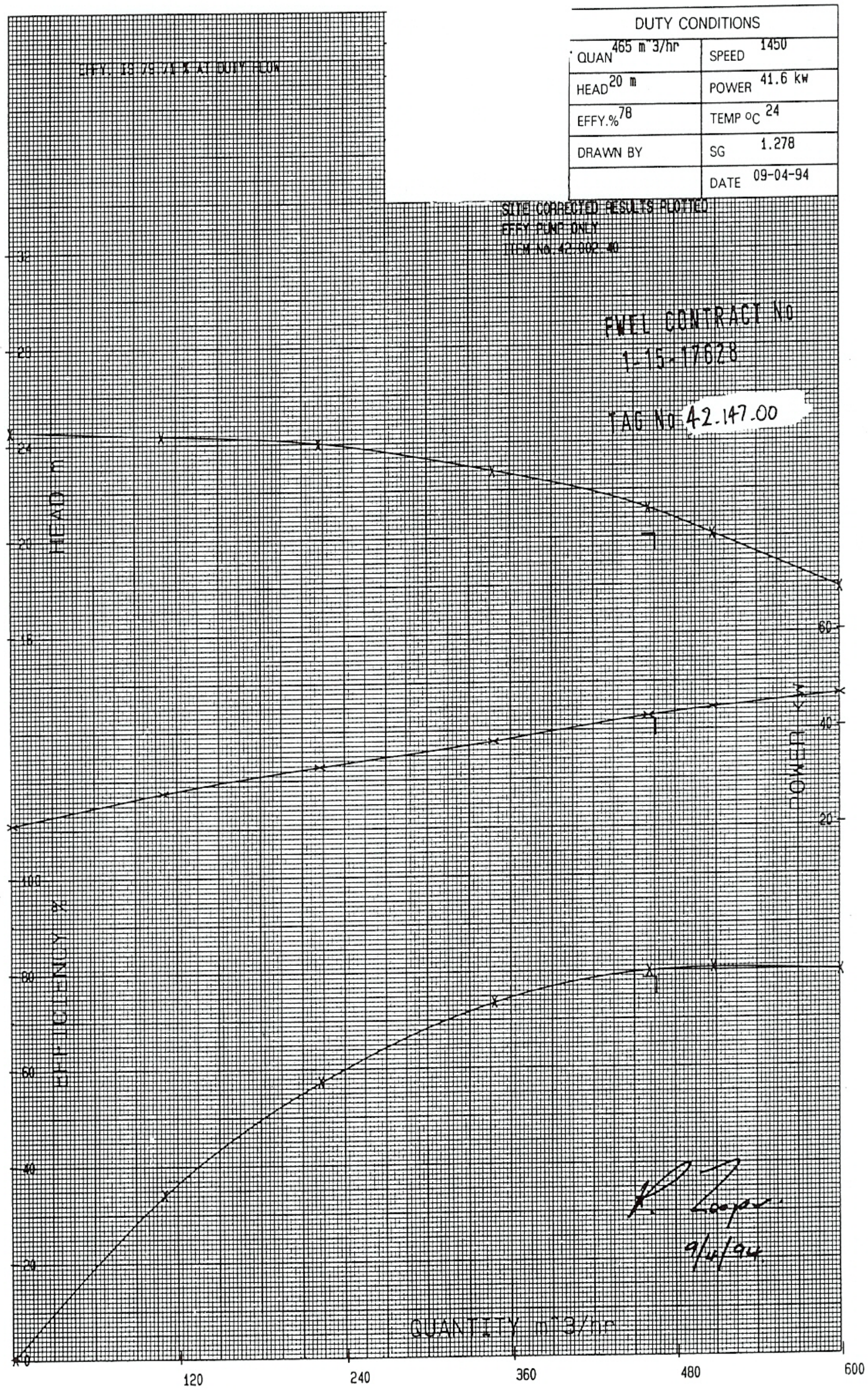

Figure G1 Pump performance curve (courtesy of Sulzer pumps)

Pump Flow Rates

The power input to each pump motor was measured and recorded during the test procedures. The following table was constructed from the pump curve shown in figure G-1.

Motor Power Input P_m (kW)	Motor Efficiency η_m	Pump Absorbed Shaft Power P (kW)	Pump Efficiency η_p (%)	Pump Flow Rate Q (m3/hr)
41	0.92	37.7	73.4	348.0
42	0.92	38.6	75.0	363.0
43	0.92	39.6	76.8	387.0
44	0.92	40.5	78.0	405.0
45	0.92	41.4	79.0	426.0
46	0.92	42.3	79.7	448.5
47	0.92	43.2	80.0	471.0
48	0.92	44.1	80.5	481.5
49	0.92	45.1	80.8	526.0
50	0.92	46.0	80.5	555.0
51	0.92	46.9	80.0	585.0
52	0.92	47.8	79.8	600.0

Note, the characteristics of the motor are given as 0.92 efficiency between 0.75 and full load.

Appendix H

Compressor load characteristics

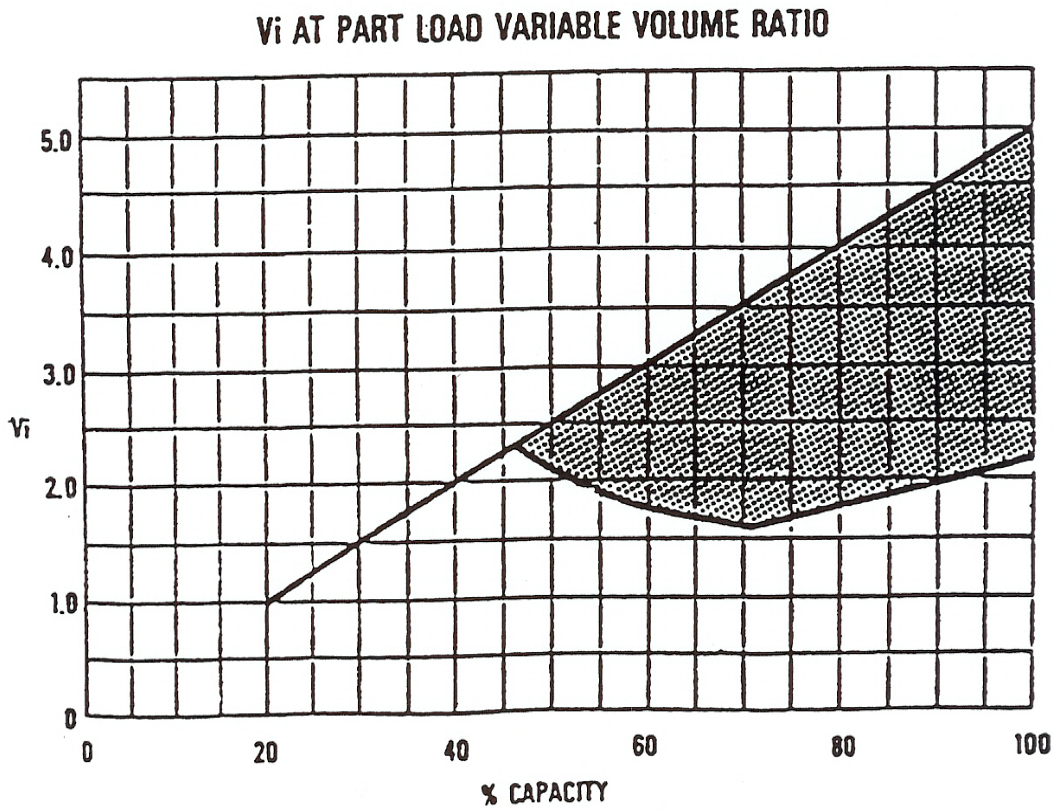

Figure H1 Compressor load versus volume ratio (courtesy of York International)